Numerical Analysis of Pile Groups in Multi-Layered Soil Subjected to Negative Skin Friction

Md Ahsan Habib

A Thesis

in

The Department

of

Building, Civil and Environmental Engineering

Presented in Partial Fulfillment of the Requirements

for the Degree of Master of Applied Science at

Concordia University

Montreal, Quebec, CANADA

January 2006

Your file Votre référence
ISBN: 0-494-14246-4
Our file Notre référence
ISBN: 0-494-14246-4

ABSTRACT

Nonlinear Analysis of Pile Groups in Multi-Layered Soil Subjected to Negative Skin Friction

Md Ahsan Habib

Several linear elastic and nonlinear slip models are reported in the literature for predicting negative skin friction on piles and pile groups in consolidating soils. They often produce significantly different results. Moreover, these models are either complex and unfeasible in practice or not capable of taking soil stratification into account, especially in pile groups. These make it difficult for practicing engineers to select appropriate method for predicting negative skin friction.

In this thesis, after critically reviewing the existing methods of analysis and examining the inherent mechanisms involved in pile-soil interaction process, a numerical method is proposed for analysis of the negative skin friction on piles and pile groups. The soil response along the depth of the pile is represented by a number of hyperbolic load transfer relationships, each of which relates the load mobilized to the pile at a particular depth and the corresponding relative soil displacement. The method uses conventional laboratory soil test data as input and incorporates nonlinear load transfer mechanism into an iterative finite element framework. A computer program is developed in "*Mathematica*" programming code to perform this analysis, based on the flowchart developed herein.

The results obtained by the proposed procedure compare well with the recent studies and available field data. It is concluded that an iterative finite element approach, coupled with the nonlinear load transfer model, provides a simplified and practical procedure which is capable of predicting the dragload on single or group piles with reasonable accuracy.

ACKNOWLEDGEMENTS

I would like to express my sincere gratitude to my supervisor, Professor Adel Hanna, for his valuable guidance, constant support and encouragement that he provided me throughout the course of this work, which made it possible to complete this research. I am honored to carry out the present investigation under his supervision.

The financial support from the Natural Science and Engineering Research Council of Canada (NSERC) and the department of Building, Civil and Environmental Engineering at Concordia University are gratefully acknowledged.

My deep gratitude is due to my wife Mahmuda, my son Alvi and my daughter Noshin, for their patience and support during preparation of this thesis.

TABLE OF CONTENTS

LIST OF TABLES

LIST OF FIGURES

LIST OF SYMBOLS

SYMBOL	REPRESENTS
A_e	Equivalent circular cross-sectional area having the same perimeter.
A_g	Gross cross-sectional area of the pile soil block
A_p	Cross-sectional area of pile
A_s	Shaft area associated with each node
α	A coefficient for bearing condition of pile
α_d	Dragload interaction factor
β	Shaft resistance coefficient in effective stress method
β_{nc}	Shaft resistance coefficient for normally consolidated soil
c_u	Undrained shear strength of soil
D_r	relative density
δ	Pile soil interface frictional angle
Δp	Surcharge load at the soil surface
E_b	Elastic modulus of the bearing stratum
E_{block}	Equivalent elastic modulus of the pile soil block
E_p	Elastic modulus of the pile
E_s	Elastic modulus of the soil
ε_z	Strain of soil at depth z
f	The flexibility coefficients

F^m	Maximum dragload
FS	Factor of safety
ϕ'	Effective angle of internal friction of soil
G	Shear modulus of elastic soil
G_b	Shear modulus of bearing layer
G_z	Soil shear modulus at depth z
γ'	Effective unit weight of soil
h	Thickness of the consolidating soil layer
η	Factor to account for stiffening effect of the soil above the pile toe
I_N	Downdrag influence factor
INCR	Increment number
k	Stiffness Coefficient
k_0	Initial tangent stiffness of soil
K_0	Coefficient of earth pressure at rest.
K_s	Lateral earth pressure coefficient
L	Length of the pile
l	Length of pile element
Layer	Layer number
L_{NP}	Depth of neutral plane
m	Number of nodes per pile
m_v	Coefficient of volume compressibility

n	Number of piles
N	Total number of nodes
N_{cor}	SPT blow counts corrected for overburden pressure
NINCR	Total number of increment
Nlayer	Total number of layer
ν_s	Poisson's ratio of soil
ν_b	Poisson's ratio of the soil at the base
OCR	Over Consolidation Ratio
p	Pile perimeter
P	Mobilized shear at pile nodes
P_f	Soil shear at failure
P_b	Load resistance at pile tip
P^b_f	Ultimate bearing capacity of the bearing stratum
q^b	Allowable bearing pressure of the bearing stratum
q_c	CPT value
Q_d	Allowable dead load
Q_s	Ultimate shaft resistance, and
ρ	Soil nonhomogeneity factor
r_0	Radius of the pile
R_f	Hyperbolic curve fitting constant
r_m	Radius of the influence zone around the pile

s	Centre to centre spacing of piles
S_c	Consolidation settlement of soil at pile nodes
S_0	Surface settlement of the soil
σ_v'	effective overburden pressure
σ_z'	Effective overburden pressure of soil at depth z
τ_f	Limiting skin friction at the pile soil interface
u_0	Excess pore pressure in the soil at the time of pile installation
u_t	Excess pore pressure in the soil at time t after pile installation
w	Relative soil displacement at a pile point
w_g	Soil displacement component at puile node caused by group interaction
w_p	Settlement of the pile node
w_s	Soil displacement component at pile node caused by pile soil interaction
W_t	Pile head settlement or downdrag
x	Number of soil layers
z	Depth below soil surface
$[F]$	Soil flexibility matrix
$[F_s]$	Flexibility matrix for pile soil interaction
$[F_g]$	Flexibility matrix for group interaction
$[K]$	Soil stiffness matrix
$[K_p]$	Pile stiffness matrix
$\{\Delta S_c\}$	Increment vector of soil settlement

CHAPTER 1
INTRODUCTION

1.1 PREFACE

Negative skin friction has progressively gained attentions of geotechnical engineers as substantial foundation mode of failure (Brand and Luangdilok 1975; Brackley and Steffen 1984; Hepworth 1993; Acar et al. 1984). It occurs when a pile is driven through a compressible soft soil layer, which settles faster than the pile under the direct loading. Negative skin friction develops as a result of the consolidation of soils surrounding the piles; generally it caused by:

1. Self weight of the unconsolidated fill, recently deposited
2. Surcharge load (Acar, et al 1984, Brand and Luangdilok 1975)
3. Dissipation of excess pore pressure induced by pile driving
4. Lowering of ground water table (Brand and Luangdilok 1975)
5. Wetting of unsaturated sub soil (Brackley and Steffen 1984; Hepworth 1993)

Negative skin friction will develop additional compressive force in end bearing piles or the excessive settlement in friction piles, which may leads to a loss in the integrity of the foundations and accordingly the superstructure.

Although the basic mechanism of negative skin friction phenomenon is well established, various researchers use different terminologies such as dragload (Briaud, 1991, Teh et al. 1995; Chow et al. 1996; Shen and Teh 2002), dragdown load (Walker et al. 1973), downdrag load (Polous et al. 1969; Polous and Davis 1972; Matyas et al. 1994), downdrag (Jeong et al. 1997) etc., which sometimes lead to confusion and misunderstanding (Lee and Xiao 2001; Lee et al. 2002). Hence, in this study the basic terms relating to the negative skin friction problem are mainly adopted according to the

definitions proposed by Fellenius (1999), which are used in most of the recent studies (e.g. Lee et al. 2002; Jeong et al. 2004 and Lee and Ng 2004).

1. Downdrag: The downward movement of a deep foundation unit due to negative skin friction and expressed in terms of soil settlement.
2. Dragload: The load transferred to a deep foundation unit from the negative skin friction acting on its shaft.
3. Neutral plane: the location where the relative movement between the pile and the soil is zero.

1.2 ORGANIZATION OF THE THESIS

A brief literature review of the subject of this thesis is presented in chapter 2. The analytical modeling adopting matrix operations and subsequent development of finite element framework for the case of negative skin friction acting on piles and pile groups are presented in chapter 3. Chapter 4 presents the validity of the proposed model through comparison between the predicted results with the available test and field results, followed by a detailed flow chart of the proposed procedure. Conclusions drawn from the present study and recommendations for future study appear in chapter 5.

CHAPTER 2
LITERATURE REVIEW

2.1 GENERAL

Although numerous studies have been reported in the literature over the years, foundation engineers still have to rely heavily on a few semi-empirical solutions in determining dragload of pile foundations in consolidating soil. Before any attempt to develop more rational solutions, it is prudent to have a full understanding of the negative skin friction which requires a theoretical assessment involving pile-soil interaction during the consolidation process.

Since the recognition of the phenomenon of negative skin friction in pile foundations, a considerable amount of research has been published on the subject. In this chapter, previous research activities dealing with negative skin friction and pile soil interaction mechanism in single piles and group piles are briefly reviewed with emphasis on the theories and assumptions employed therein. Finally a brief discussion is provided to outline the circumstances, which signify the present attempt to develop a practical computational framework for the analysis of negative skin friction on single piles and group piles.

2.2 NEGATIVE SKIN FRICTION ON SINGLE PILE

Terzaghi and Peck (1948) proposed an empirical solution for the higher bound of dragload on end-bearing piles. They suggested that the shear strength of the soil is mobilized along the full length of the single piles, assuming that the neutral plane is located at the bearing stratum. The maximum dragload is then given by the perimeter area of the pile multiplied by the shear strength of the surrounding soil.

Thus,

$$P_{max} = p\tau_f L \qquad \text{.....(2.1)}$$

Where, τ_f the soil shear strength, L depth of embedment of pile, and p the perimeter of the pile.

Zeevaert (1959) suggested a theoretical approach to evaluate the dragload on end-bearing piles subjected to negative skin friction. He included the reduction of the confining effective stresses caused by the hang-up tendency of the settling soil.

The reduced effective stress for a single pile was expressed by the following equation:

$$\sigma'_{vz} = (\gamma'/m)(1-e^{-mz}) + S\, e^{-mz} \qquad \text{.....(2.2)}$$

Where σ'_{vz} = the reduced effective stress at depth z

γ' = the effective unit weight of soil

S = the surcharge pressure

$m = p\beta$

$\beta = K_0 \tan\phi'$

p = pile perimeter

The dragload acting on the pile shaft was represented by:

$$F_n = \int_0^L p\beta\sigma'_{vz}\, dz \qquad \text{.....(2.3)}$$

Performing integration of equation (2.3) after substituting for σ_{vz} from equation (2.2):

$$F_n = (\gamma' L + S) - \sigma'_{vL} \qquad \text{.....(2.4)}$$

The assumption of the reduction in overburden pressure implicitly implies that the slippage between the pile and the soil will not occur. But, there is no compelling physical basis for this assumption.

Poorooshasb and Bozozuk (1967) introduced a closed form solution to an incompressible pile penetrating an upper clay layer to rest on bedrock. The clay layer was subject to a surcharge load and drainage was assumed to be permitted at both upper and lower surfaces of the layer. It was further assumed that the presence of the pile had no effect on the dissipation of the pore water pressure.

The solution was based on an upper bound plastic analysis, which utilizes a kinematically admissible displacement field that satisfies the overall equilibrium of the system. The displacement field considered was a product of two functions so that the separation of variables is possible. In addition, the soil was modeled with constitutive equation that indicates an increase in stiffness with depth. The solution is complex, involving infinite series and modified Bessel functions of the second kind, which makes it difficult to be utilized in practice.

Bjerrum et al (1969) presented a comprehensive study on negative skin friction on instrumented single piles. They have presented detailed results from a number of instrumented test piles, and concluded that the maximum negative friction on a single pile could be obtained by multiplying the effective overburden pressure by a constant, $\beta = K_0 \tan \phi'$. Thus,

$$\tau = \beta \sigma'_v = \sigma'_v K_0 \tan \phi' \qquad \text{.....(2.5)}$$

Where, τ = maximum negative skin friction

K_0 = earth pressure coefficient at rest

ϕ' = effective soil friction angle

In their experiments, the value of the constant β varied between 0.18 and 0.26 at the sites studied.

Endo et. al. (1969) measured the magnitude and the distributions of skin friction on four types of steel pipe pile. They confirmed the design procedure recommended by Bjerrum et al (1969). They found that the average values of β were about 0.35 in the closed point end-bearing piles, 0.3 for the friction piles and 0.2 in the open point piles. However, the data showed a considerable scatter.

Poulos and Mattes (1969) presented an analysis of dragload for end-bearing single compressible piles of circular cross-section using the boundary element method, which is also known as integral equation method. The tip of the pile was assumed to rest on perfectly rigid base, and the surrounding soil was assumed to be homogeneous isotropic elastic material. The relationship between the surface settlement of the soil and the dragload induced in the pile were determined by employing Mindlin equation for the vertical displacements of a point within a semi-finite mass. The influence of relative stiffness of the pile, the length to diameter ratio, and Poisson's ratio of the soil on this relationship was investigated.

The pile was divided into a number of equal cylindrical elements; each was subjected to a uniform vertical shear stress at the mid point. Furthermore, at each mid point, the displacement of the soil layer adjacent to the pile's shaft was equated to that of the pile itself. It was assumed that the consolidation settlement of the soil remote from the pile varies linearly with depth from S_0 at the ground surface to zero at the tip of the pile. A mirror-image technique was utilized in conjunction with Mindlin's equation (Mindlin, 1936) to enforce zero vertical displacement at the pile base, to simulate a rigid bearing stratum since Mindlin's solution is strictly valid for a homogeneous isotropic half-space. The expression presented to determine the maximum dragload is as follows:

$$F_n^m = I_N E_s S_o L \qquad \text{.....(2.6)}$$

Where F_n^m = the maximum dragload

I_N = the downdrag influence factor

E_s = the elastic modulus of the soil

S_o = the surface settlement of the soil

L = the length of the pile

Slippage between the pile and the surrounding soil was considered by modifying the analysis to take into account for the local yielding at the pile-soil interface defined by Coulomb equation. However, the linear relationship between the maximum dragload F_n^m and the surface settlement S_0 in the proposed model is likely to oversimplify the reality, especially in cases where slippage between the pile and the surrounding soil takes place.

Poulos and Davis (1972) extended the work of Poulos and Mattes (1969) to include the effect of the rate of development of dragload with time in an impermeable pile. The soil was assumed to be fully saturated and subjected to consolidation under the surcharge loading. In this analysis, possibilities of local yield between pile-soil interface and limited crushing of the pile due to overloading were considered.

The problem was solved in the same manner as of Poulos and Mattes (1969), except that the consolidation settlement in this analysis was obtained from a simple one-dimensional analysis. The consolidation settlement at the mid point of the i-th element counted from the bottom was expressed as follows:

$$S_i = \sum_{k=1}^{i} m_v F_k (u_{0k} - u_{tk}) L / x \qquad \text{.....(2.7)}$$

Where m_v = coefficient of volume compressibility

u_0, u_t = excess pore pressure at the point k in the soil at the time of installation of the pile, and at the time t after installation, respectively

F_k = 1 for k > i and 0.5 for k = i

L = the length of the pile

x = Number of pile elements

The solution for the maximum dragload in a pile was given by:

$$F_n^m = I_N \Delta P L^2 \qquad \text{.....(2.8)}$$

Where F_n^m = the maximum dragload

I_N = the downdrag influence factor

ΔP = the surcharge pressure

Although, some factors such as partial slip, delayed pile installation and Poisson's ratio etc are intended to address in the procedure, the method of analysis is elastic and is limited to end-bearing piles only.

Poulos and Davis (1975) presented an analysis based on the elastic theory for the development of dragload and axial movement of an end bearing pile in soil subjected to surface loading. The analysis considered the pile-soil slip and the rate of development of the dragload. Solution was presented for the magnitude and rate of the maximum dragload and the pile settlement with time. The solution enabled the transition from the case of full slip to the fully elastic case. Comparisons were made between predicted dragload and pile shortening and those measured in full-scale field tests.

Randolph and Wroth (1978) presented a closed form solution for single vertically loaded pile. The method was based on the load transfer approach, which considers the pile to be surrounded by concentric soil cylinders having shear stresses decreases inversely with the surface area of the cylinders. This leads to a logarithmic variation of the soil displacement *w* with the radius *r* as follows:

$$w(r) = \frac{\tau_0 r_0}{G} \ln\left(\frac{r_m}{r}\right) \qquad \text{.....(2.9)}$$

Where, $r_m = 2.5\rho(1-\nu')L$

r_m = the limiting radius of influence of the pile

ν' = Poisson's ratio of soil

ρ = soil homogeneity factor given by the ratio of the soil shear moduli at mid depth and at the pile toe ($G_{L/2}/G_L$).

τ_0 = shear stress on the pile shaft

r_0 = radius of the pile

G = shear modulus of soil

Since no slippage was considered, the soil displacement w_s at the pile interface was basically the same as the pile deflection, which is given by:

$$w_s = \frac{\tau_0 r_0}{G} \ln\left(\frac{r_m}{r_0}\right) \qquad \text{.....(2.10)}$$

The pile base acts as a rigid punch on the surface of the bearing soil layer. The deformation of the pile base as given by the Boussinesq solution was adopted from Timoshenko and Goodier, (1970)

$$w_b = \frac{P_b(1-\nu_s)}{4r_0 G_b}\eta \qquad \text{.....(2.11)}$$

Where, P_b = the load carried by the pile tip

ν_s = Poisson's ratio of the soil

The factor η has been introduced to allow for the depth of the pile toe from the ground surface, i.e., the interaction of the upper soil layer with the bearing layer (Randolph et al, 1978). For the analysis of pile capacities, they suggested a value of 1.0 for η, unless the shaft friction is fully mobilized in which η will be reduced to a value of about 0.85.

Alonso, et al. (1984) presented a numerical solution procedure for negative skin friction on single piles using load transfer model. The produced equations were

formulated in dimensionless terms to facilitate the analysis for arbitrary soil profiles, consolidation conditions and load histories. In this model, the non-linear plastic character of the shear stress acting on the pile shaft and the unloading and cyclic behavior were incorporated. From the summary of the measured and predicted loads, it was concluded that the theory overestimates the values of predicted dragload.

Fellenius (1989) indicated that eventually all piles will experience negative skin friction during their life span. This conclusion was based on the fact that a movement of 1-2 mm is sufficiently enough to mobilize the skin friction; considering the deference in rigidity between the pile and the soil in which such a small relative movement may occur.

A unified design approach was therefore proposed in which bearing capacity, pile's structural capacity and pile settlement were taken into consideration. The design steps involved locating first the neutral point, then checking the structural capacity of the pile followed by determining the settlement by applying the concept of an equivalent footing placed at the neutral plane, and finally verifying the bearing capacity.

Each design step has a combination of loads that should be used in its computation. The structural capacity of pile at the cap level is checked by a combination of dead and live loads, whereas at the neutral level was determined based on the combination of the dead loads and the dragload without the live load. For bearing capacity computation, dead and live loads are considered, but the dragload was omitted. Neither live load nor dragload, only dead load is considered in settlement calculation.

The neutral plane was determined by constructing two load distribution curves. The first, combining both the dead and the dragloads, is drawn starting from the pile head and being considered as acting on the entire length of the pile. Then starting from the pile tip, the second curve is drawn with the values of the tip resistance and the positive skin friction. Thus the neutral point is located at the intersection of the two curves.

Leung et al. (1991) studied the load-transfer behavior of precast reinforced concrete piles driven through soft marine clay and founded in residual soil and weathered rock of sedimentary origin. Strain gages were installed along the pile shafts and were monitored frequently during the static loading tests and at regular intervals during and after the construction of the superstructure. Piezometers were installed in proximity to one of the piles. The dissipation of excess pore water pressures indicated that setup in the marine clay was highly significant. Hence, pile capacities calculated using wave-equation models based on stress-wave measurements during initial pile driving gave consistently lower values than those of static loading tests one week later. Long-term instrument readings indicated development of negative skin friction when the piles were in service. Observing the increase of downdrag with time, they suggested that this additional loading should be accounted for in the pile design as part of the service load on the pile.

Indraratna et al. (1992) described the results of short-term pullout tests and long-term full-scale measurements of negative skin friction on driven piles in Bangkok subsoil. The two piles were hollow cylindrical prestressed concrete piles instrumented with two independent load-measurement systems, load cells, and telltale rods. Pore pressures and ground movements in the vicinity of the piles were monitored throughout the period of investigation. The effect of bitumen coating on negative skin friction was also studied. The long-term behavior of driven piles was compared with the estimated values obtained from short-term pullout tests and soil strength data. It was found that the negative skin friction can be predicted well by the effective stress approach using values of β between 0.1 and 0.2. The load-settlement and load-transfer behavior were numerically modeled to acquire a more comprehensive understanding of negative skin friction developed on driven piles. A settlement-controlled concept was also introduced for piles subjected to negative skin friction, on the basis of these findings.

Hepworth (1993) depicted a case history of pile failure due to negative skin friction. As he reported, a steel building at a cement plant in Utah was originally supported by spread footings. Shallow wetting of the coarse granular soils supporting the footings resulted in over three inches of settlement. Piles were used to underpin the

building. The northeast corner column was supported by two 12 × 54 WF piles driven to a depth of 98 feet. About two years after the underpinning a deep wetting of the soils at the northeast corner occurred. The result was several inches of additional settlement of the building on this corner and twelve inches of ground subsidence adjacent to it. Excavation around the pile cap revealed that one of the piles was eight inches below the pile cap. A pull out test performed on the failed pile indicated that the skin friction force was at least 182 tons. The building corner was underpinned again with three BP 12 × 74 piles driven to a depth of 145 feet. The upper 50 feet of each new pile was sleeved with an outer casing. Performance has been satisfactory since.

Lim et al. (1993) described a simple discrete element approach utilizing the subgrade reaction method to analyze negative skin friction on single piles. The pile was assumed to be embedded in a two-layer soil where the upper soil layer undergoes consolidation while the lower layer performs as a stiff bearing stratum. The analysis takes into account the effect of the socketed piles in the bearing layer. Galerkin method was applied to transform the following governing equation into discrete element formulation.

$$-E_p A \frac{\partial^2 w}{\partial z^2} + k(w - w_s) = 0 \qquad \text{.....(2.12)}$$

Where, E_p = the elastic modulus of the pile material

A = the cross-sectional area of the pile

w = the axial deformation of the pile

w_s = the soil consolidation settlement of soil

k = the stiffness per unit pile length

The soil stiffness, k, was determined based on the assumption that the deformation modes of the soil along the pile shaft and at the pile tip are uncoupled. The deformation modes were estimated according to the solution provided by Randolph and Wroth (1978). Thus, the expression adopted for the soil stiffness at the pile shaft, k, and at the pile tip, k_{base}, were as follows:

$$k = 2\pi \frac{G}{\ln\left(\frac{r_m}{r_0}\right)} \qquad \text{.....(2.13)}$$

And $$k_{base} = \frac{4G_b r_0}{(1 - \nu_b)} \qquad \text{.....(2.14)}$$

Where, G = shear modulus of the compressive layer

G_b = shear modulus of bearing layer

ν_b = Poisson's ratio of the soil at the base

r_0 = pile radius

r_m = radius of influence beyond which shear stresses become negligible.

The influence radius, r_m, was considered to vary linearly with depth. Based on a comparison study with other methods, empirical solution was developed for r_m. For practical purposes, r_m was recommended to be taken as a stepwise constant. It should be pointed out that the analysis described here provides an elastic solution; therefore, this method should be used with caution when excessive consolidation settlement is expected.

Matyas and Santamarina (1994) developed two closed-form solutions for determining the dragload and the location of neutral point. The first solution was based on modeling the soil-pile interface as a single rigid-plastic material, whereas in the second solution the interface was modeled as elastic-plastic material. The pile was assumed to be rigid and embedded in a medium with linearly increasing shaft resistance. By comparing the two solutions, it was found that the rigid-plastic solution may overestimate the dragload by as much as 50% or more, and over predict the location of neutral depth by about 30%.

In the rigid-plastic model, the negative skin friction, the positive shaft resistance, and the tip resistance were assumed fully mobilized. It was further assumed that the unit

negative skin friction, q_n, is equal to the unit positive skin friction, r_s. To preserve generally, two dimensionless ratios were introduced: $\alpha = Q_u/Q_s$ and $FS = Q_u/Q_d$, where Q_u is the ultimate bearing capacity, Q_s is the ultimate shaft resistance, and Q_d is the allowable dead load. Thus for equilibrium requirements:

$$Q_d + \int_0^{L_{NP}} A_s q_n dz = \int_{L_{NP}}^{L} A_s r_s dz + Q_t \qquad \text{.....(2.15)}$$

Where, A_s = area of the shaft surface

L = length of pile

L_{NP} = depth of neutral plane

Q_t = ultimate resistance of the pile tip

By integrating and rearranging equation (2.15), the following expressions were obtained:

$$\frac{L_{NP}}{L} = \sqrt{\frac{\alpha}{2}\left(\frac{FS-1}{FS}\right)} \qquad \text{.....(2.16)}$$

$$\frac{Q_{NP}}{Q_u} = \frac{(1+FS)}{2FS} \qquad \text{.....(2.17)}$$

Where, Q_{NP} = total load at the neutral plane depth.

For elastic-plastic method, the relative displacement profile was assumed linear, with maximum value at the ground surface and decreasing with depth. Three additional dimensionless ratios were introduced: $\psi = \delta_{ty}/S_t$, $\omega = \delta_{sy}/S_t$, and $\lambda = \delta_h/S_t$, where δ_{sy} is the relative displacement between the pile and the soil required for yielding the shaft resistance, δ_{ty} is the relative displacement that yields the tip resistance, δ_h is the settlement of the pile head, and S_t is the total relative settlement. By equating the forces above and below the neutral plane, the following expressions were obtained:

$$\frac{L_{NP}}{L} = \frac{\sqrt{(\alpha-1)^2 + 8\psi(\alpha-1) + 8\psi^2\left(1 - \frac{\alpha}{FS} - \frac{2\omega^2}{3}\right)} - (\alpha-1)}{4\psi} \quad \text{.....(2.18)}$$

$$\frac{Q_{NP}}{Q_u} = \frac{1}{\alpha}\left(\lambda^2 - \lambda\omega + \frac{1}{3}\omega\right) + \frac{1}{FS} \quad \text{.....(2.19)}$$

During the comparison of the two solutions, the elastic-plastic method was used to estimate the neutral depth values for rigid and deformable end-bearing layers, which contradict the physical evidences. Considering that both produce identical values of the neutral depths for both the cases, the later equation was not recommended for practical purpose.

Wong and Teh (1995) proposed a simplified numerical procedure for the analysis of the negative skin friction on single pile in layered soil deposits. The pile-soil interface behavior was modeled by a series of nonlinear soil springs governed by the following hyperbolic equation:

$$P_i = \frac{w_i}{\left(\frac{1}{k_{si}} + \frac{w_i}{P_{ui}}\right)} \quad \text{.....(2.20)}$$

Where, $P_{ui} = f_{si}.A_{si}$

P_{ui} = maximum allowable nodal load

f_{si} = limiting unit shaft friction

A_{si} = shaft area associated with the node i.

P_i = nodal force

k_{si} = initial tangent of the hyperbolic curve

w_i = relative pile-soil settlement

The elastic soil stiffness, derived from the load displacement relationship given by Randolph and Wroth, (1978) for a single pile, was adopted as the initial tangent modulus of the hyperbolic curve.

Thus,

$$k_{si} = \frac{2\pi G_i l_i}{\ln\left(\frac{r_m}{r_0}\right)} \qquad \text{.....(2.21)}$$

Where, G_i = soil shear modulus

l_i = pile segment length

r_m = radius of the influence zone

r_0 = pile radius

A hybrid incremental-iterative procedure was employed to allow for large incremental steps without compromising on the accuracy of the predicted values. It is intended to establish a procedure to estimate the input parameters of the proposed model from the conventional soil test data.

The procedure was used in back-analysis of five well-documented test piles in different soil deposits. The results of the analysis showed that the numerical approach is capable of predicting single pile dragload with reasonable accuracy.

Esmail (1996) conducted a parametric study on single piles subjected to negative skin friction due to surcharge loading. The numerical modeling was based on finite element technique utilizing two soil constitutive models, Modified Cam-Clay model and elastic-plastic model with Mohr-Coulomb yielding criterion. The soil was allowed to consolidate under the effect of surcharge loading. In the Mohr-Coulomb model, the strength parameter was introduced in terms of the undrained condition. Based on the parametric study, design charts for Modified Cam-Clay and Mohr-Coulomb models were developed to determine the neutral depth.

Goh et al. (1997) described a simplified numerical procedure based on the finite-element method for analyzing the response of single piles to lateral soil movements. The flexural bending of the pile was modeled by beam elements. The complex phenomenon of the pile-soil interaction was modeled by hyperbolic soil springs as used by Wong et al (1995). A framework for determining the soil parameters for use in the analysis was summarized. Based on parametric studies, empirical design solutions for pile foundation systems at the base of a sloped embankment were presented.

Hanna and Sharif (2006) developed a numerical model employing the finite element technique to analyze the negative skin friction induced in single floating piles subject to direct and indirect loading. The soil was assumed to behave as a linearly elastic perfectly plastic material with yield function defined by the Mohr-Coulomb equation. Based on the results of parametric study, a designed formula together with design charts were also presented for determining the allowable bearing capacity of coated and uncoated single piles.

2.3 NEGATIVE SKIN FRICTIONS ON PILE GROUPS

Terzaghi and Peck (1948) suggested a modification for their theory for the dragload on end-bearing single piles for predicting the dragloads on group piles. They further assumed that the pile group acts as a block and that the shear strength of the soil is mobilized along the full length of the perimeter of the group. The maximum dragload for each pile in the group is thus given by

$$P_{max} = p\tau_f L / n \qquad \text{.....(2.22)}$$

Where, n is the number of piles in the group, τ_f the soil shear strength, L depth of embedment of pile, and p the enclosing perimeter of the group. This method considers that the soil within the group of piles is an integral part of the pile foundation.

The interaction of soil with individual piles is not taken into account in this method, which, is beyond the actual situation unless the piles are very closely spaced.

Randolph and Wroth (1979) have developed an approximate method for analysis of pile group capacity, which was an extension of the approach they developed earlier (1978) for the analysis of single pile. This method was based on the superposition of individual pile displacement fields at the pile shaft as well as at the pile toe. Although the model considered linear variation of shear modulus along the depth, it is limited to rigid pile groups in elastic soil.

Kuwabara and Poulos (1989) presented a boundary element method to analyze the behavior of a pile group subjected to negative skin friction. The model was an extension of the procedure proposed by Poulos and Davis (1975) to analyze negative skin friction in a single pile. The analysis was used to determine the distribution of shear stress and dragload on pile groups arranged in a square configuration. The surrounding soil was assumed to be either homogeneous or Gibson soil with elastic modulus varying linearly with depth.

The study revealed that the dragload on individual piles in the group decreases significantly as pile spacing decreases. However, the reduction does not depend greatly on the number of piles unless there are less than nine piles in the group. The inner piles experience less dragload then the outer piles. As the pile spacing increases, the inner piles tend to perform in a similar manner to the outer piles.

They investigated the development of negative skin friction on pile groups for both rigid and flexible pile caps. The results showed that, shear stress distribution along the pile's shaft was almost unaffected by the cap rigidity. The only noted difference between the dragload distributions was observed near the pile head.

The method presented is not only limited to end-bearing piles, but it also considers linear variation of soil shear modulus only. It can not model a layered soil

deposit with changing soil parameters. Another limitation of the method is that it is an elastic approach and it excludes the important slip effect at the pile soil interface. Although, Kuwabara and Poulos (1989) proposed an interaction factor to incorporate pile-pile interaction, nonetheless, these may not provide a realistic solution. Above all, the proposed method is cumbersome and relatively time consuming.

Chin and Lee (1990) presented a numerical procedure for the downdrag analysis of group piles which penetrate a consolidating upper soil layer to socket into a firm bearing stratum of finite stiffness. The settlement of the consolidating upper soil layer under a surcharge load was estimated using Terzaghi's one-dimensional consolidation theory. Parametric solutions were presented to show the influence of various parameters such as the socketed length, the relative stiffness of the bearing stratum and the upper soil layer and the stiffness ratio of the pile and the soil, on the performance of the pile groups in terms of associated dragload and pile head settlements.

Chow et al (1990) presented a numerical procedure for analysis of negative skin friction on group piles socketed into a firm bearing stratum of finite stiffness. The settlement of the consolidating soil layer under a surcharge load is estimated using Terzaghi's one dimensional consolidation theory. They also investigated the influence of relative stiffness of the bearing stratum and the upper soil layer (E_b/E_s) and the stiffness ratio of the pile and the soil (E_p/E_s) on dragload and downdrag of single piles and group piles. For single piles, the maximum dragload and the pile head settlement were found to increase and decrease, respectively, for increasing values of E_p/E_s and E_b/E_s. The interaction between the group piles caused reduction of dragload and pile head settlement in comparison with isolated single pile solutions.

Briaud et al (1991) reviewed various techniques available to calculate dragloads on pile groups. Based on an analysis of the various methods and on the very limited available experimental data, they recommended a simplified method. They indicated that at spacing larger than 5 diameters there is very little group effect and the group should be designed as a cluster of single piles. At spacing smaller than 2.5 diameters, however,

there is a definite group effect and the dragloads for different position of piles in the group are proposed as follows:

$$F_{corner} = 0.75\ F_{single}$$
$$F_{side} = 0.50\ F_{single}$$
$$F_{interior} = S_0\ s^2$$

Where S_0 is the surcharge applied to the ground surface and s is the centre to centre spacing.

Lee (1993) presented a simplified hybrid load-transfer approach for analyzing the response of pile groups under negative skin friction. The response of single pile is evaluated by a discrete-element approach. The interaction between piles in a group bearing on a stiffer stratum is considered using the modified form of Mindlin's (Mindlin, 1936) analytical point-load solution. The nonlinear pile behavior is represented by a simple hyperbolic pile-soil model. The consolidation settlement is estimated by using Terzaghi's one-dimensional consolidation theory. The results of the proposed approach were in good agreement with those computed by elastic continuum approaches. Although the proposed approach was claimed to be simple, practical and suitable, the use of complicated and relatively ambiguous load transfer functions for single piles and modified Mindlin's solution for group piles made the approach clumsy and relatively complex for practical purpose.

Teh and Wong (1995) proposed an iterative procedure for the analysis of the dragloads in end bearing pile groups. The soil around the pile was assumed to be homogeneous and linearly elastic. The piles were connected at the top by a pile cap modeled as either perfectly rigid or perfectly flexible. Pile-soil-pile interaction was modeled using Mindlin's elastic solution for a point load in an elastic half-space. Pile-soil slip was taken into account by proposing a modification to the elastic analysis. The governing stiffness equation for the elastic analysis of the whole system was expressed using a partitioned matrix notation for the slipped and non-slipped nodes as:

$$\begin{bmatrix} [K^p_{11}] & [K^p_{12}] \\ [K^p_{21}] & [K^p_{22}]+[K^s_{22}] \end{bmatrix} \begin{Bmatrix} w_{p1} \\ w_{p2} \end{Bmatrix} = \begin{Bmatrix} P_{p1} \\ [K^s_{22}]\{\delta_2\} \end{Bmatrix} \quad \text{.....(2.23)}$$

$$\{\delta_2\} = \{S_0\} - [K^s_{21}]^{-1}\{P_{p1}\} \quad \text{.....(2.24)}$$

where, $[K_p]$ and $[K_s]$ are the pile and soil stiffness matrices respectively, $\{w_p\}$ and $\{P_p\}$ are the nodal displacement and force vectors, subscript 1 denotes the nodes where slip has taken place, subscript 2 denotes where the interface shear stresses are still smaller than the limiting values, δ_2 represents the soil displacements at the nodes that have slipped and $\{S_0\}$ is the free field soil settlement.

Parametric studies were conducted to elucidate the parameters that govern the relationship between free field soil settlement and dragloads induced in a pile group. Results indicated that interior piles of a large pile group experience relatively small dragloads, especially when the pile spacing is small. The validity of the proposed method was demonstrated by back-analyzing two model studies of negative skin friction on pile groups. The proposed method was also validated against the field test results of a 38-pile group. The computed results show an encouraging degree of agreement with the experimental data.

Ergun and Sonmez (1995) described a model experimental test of negative skin friction from surface settlement measurements. Groups of model wood piles were driven through dense sand over soft clay to rest on a thin sand layer at the bottom of the circular tank. A rubber membrane was placed on the sand to make it possible to stress the soil layer by air pressure. The relative settlement of the soil surface inside and outside the groups were determined in the test as the soil was compressed by air pressure. Square 30 mm piles at spacing of 2 to 6 times the pile width were used in groups of 3 × 3, 4 × 4, and 5 × 5. The results indicated that pile group effects were negligible at pile spacing of 5 to 6 pile widths.

Chow et al. (1996) reported simplified methods for the analysis of socketed pile groups subject to negative skin friction. In these methods, the piles were modeled using discrete elements with an axial mode of deformation. The soil behavior was modeled using a hybrid approach in which the soil response at the individual piles was represented by the subgrade reaction method while pile-soil-pile interaction was determined using elastic theory. The interaction effects were considered via two models namely, a layer model and a continuum model. In the layer model, the soil was assumed to be represented by independent horizontal layers, which permit interaction between piles to take place within the same soil layer only; the continuity of the soil in the depth direction was discontinued. In the continuum model, the theory of elasticity for a point force in the interior of an elastic medium was used to determine pile-soil-pile interaction.

The accuracy of the methods was assessed by comprehensive comparisons with theoretical solutions available. The study showed that: (a) for practical pile groups, the layer model can give reasonable solutions provided that the socket is not too deep, (b) the solutions obtained by the continuum model using Chan et al.'s solution (Chan et al. 1974) are in close agreement with the theoretical solutions, and (c) the continuum model using Mindlin's solution predicts reasonable dragloads but seriously under predict the downdrag.

Poorooshasb et al. (1996) presented a numerical scheme that can be used to evaluate the magnitude and distribution of the negative skin friction on both rigid and deformable piles and pile groups. An integro-differential equation in polar coordinates is developed in terms of vertical displacement, w, by substituting the stress components in the associated incremental equilibrium equation.

$$\frac{\partial w}{\partial z} + f(z)\int_0^z \left[g(\xi)\frac{\partial^2 w(r,\xi)}{\partial r^2} + \frac{1}{r}\frac{\partial w(r,\xi)}{\partial r} \right] d\xi - f(z)P_0 = 0 \qquad \text{.....(2.25)}$$

Where, f(z) = a soil parameter similar to the inverse of modulus of elasticity

g(z) = a soil parameter similar to the shear modulus

This equation serves as the governing equation, which is solved numerically by introducing finite difference method. It should be noted that the equilibrium is satisfied only globally, and hence the analysis yields an upper bound solution. Although it is claimed that the proposed method can handle material non-linearity, time dependency, and both end-bearing and floating piles, it is very complex to be used for practical purpose even for a Gibson soil.

As a demonstration to the capacity of the numerical procedure, a study on the behavior of negative skin friction for both floating and end bearing piles and pile groups were conducted. The study showed that the neutral depth was not prominently influenced by the height of the fill as suggested by Bowles (1982), rather, the presence of a strong layer at the pile tip would have the major effect. Based on limited parametric study, it was stated that in the case of pile groups or deformable piles extended to bedrock a good portion of the pile sustains little or no skin friction at all.

Jeong et al. (1997) investigated the downdrag on friction and end bearing pile groups on the basis of numerical analysis. The emphasis was on quantifying the reduction of dragload due to group effects on pile groups with a flexible pile cap. The case of a single pile and, subsequently, the response of group piles were analyzed by developing interaction factors obtained from a three-dimensional nonlinear finite element study. The extended Drucker-Prager model was adopted in the study in order to allow control of change in volume. It was controlled by using a non-associated flow rule by taking into account different values of dilation and friction angle and by intending the yield surface to occur in the deviatoric plane based on the third stress invariant.

The study suggested a great reduction in pile-soil-pile interaction by nonlinear analysis compared to that by a linear analysis. In other words, the model postulated that the dragload calculated by linear analysis can substantially overestimate the degree of interaction in realistic situations. Based on a limited parametric study, it was also shown that the downdrag on piles in a group is highly influenced by the group spacing, total

number of piles, and the relative position of the piles in the group. In light of all these influencing parameters, a simple method is recommended for square groups of 9-25 piles with spacing-to-diameter ratios of 2.5 and 5.0 for dragloads.

For spacing-to-diameter ratios of 2.5

$$F_{corner} = 0.50\ F_{single}$$
$$F_{side} = 0.40\ F_{single}$$
$$F_{interior} = 0.15\ F_{single}$$

For spacing-to-diameter ratios of 5.0

$$F_{corner} = 0.90\ F_{single}$$
$$F_{side} = 0.80\ F_{single}$$
$$F_{interior} = 0.5\ F_{single}$$

According to the study, the pile groups that have more than 25 piles show almost the same group effects as those with 25 piles. Further, at spacing larger than 5 times the diameter, there is very little group effect implying that the interaction factor is almost 1.0 like as a cluster of single piles.

Lee et al. (2002) described negative skin friction on pile foundations, predicted from the results of numerical analyses. The authors found the soil slip at the pile-soil interface to be the most important factor in governing pile behavior in consolidating ground. Reduction in dragload is predicted for piles in a group due to the interaction between soil and pile. It was demonstrated that the group effect depends not only on the configuration of the pile group, but also on soil along the pile-soil interface, governed mainly by the interface friction coefficient and the soil settlement. Various factors were suggested to be included in an evaluation of the group effect, including the pile spacing, the number of piles in a group, the relative location of piles in a group, the pile type, the pile installation method, the surface loading and the stiffness of the soil. Back-analyzed

dragloads and group effects considering soil slip were compared with a number of case histories.

Shen and Teh (2002) presented an approach for the analysis of dragloads of pile groups undergoing downward movement of soil. The variation of stiffness of surrounding soil with depth and the stiffness of end-bearing stratum at the pile toe were also taken into account. The theoretical load-transfer curves proposed by Randolph and Wroth (1978) were employed to describe the soil load-displacement relationship. The principle of minimum potential energy was applied to determine the response of pile groups. The slip at the pile-soil interface was taken into account through the use of the initial stress technique. The solution procedure was conducted in an iterative manner. First, purely elastic solution was solved. Second, the excess soil shear stresses above the limiting soil shear stress were transferred into additional external loads to give a new round solution. The process was repeated until the computed shear stresses along the pile shaft do not exceed the soil limiting shear stress.

The validity of the proposed method was demonstrated through comparison with existing theoretical solutions and field measurements. However, the method appears to be very tedious and complex for practical purposes especially when soil movement distribution and shear modulus don't follow specified pattern.

Jeong et al. (2004) conducted two and three dimensional elasto-plastic numerical analyses by using ABAQUS finite element package to investigate the pile behavior in consolidating ground for single pile and group piles. Conventional no-slip continuum analysis and slip analysis were carried out in a drained condition to examine the effects of soil yielding at the pile-soil interface on dragload and group effect. The piles were modeled as free-headed piles in a group, which may be considered similar to piles in a perfectly flexible pile cap. A non-associated Mohr-Coulomb model was used for the soil, which allowed control of the change in volume by using a non-associated flow rule as well as a yield surface in the deviatoric plane.

The numerical analyses showed that the dragload is heavily depended on the slip, which in turn, is mainly governed by the interface friction angle and the surface loading. The smaller the interface friction coefficient and the higher the surface loading, the more is the soil slip at the interface. It also proved that the dragload for single piles and their reductions in pile groups are substantially over-estimated by the continuum analyses. The computed group effects from the continuum analysis predicted maximum group effects of 57-85%, whereas the slip analysis showed smaller reductions in dragload with a maximum group effect of 39-72%. Affirmed with experimental observations, it was concluded that more realistic and plastic yielding behavior of the soil at the interface must be introduced if analyses are to be at all accurate.

The numerical analysis also demonstrated reduction in dragload with gradual increase in the external axial load after full development of dragload. An overall axial loading of about 125-325% of the maximum dragload was required to eliminate dragload, depending on the stiffness of the bearing layer. The application of axial load on pile head reduced also the group effects substantially.

Lee and Ng (2004) conducted two-dimensional axisymmetric and three-dimensional numerical parametric analyses to study the behavior of single pile and group piles respectively. For single pile, the downdrag computed from the no-slip elastic analysis and from the analytical elastic solution was about 8 to 14 times larger than that computed from the elasto-plastic slip analysis. The softer the consolidating clay, the greater was the difference between the no-slip and slip analyses. It suggested that an elasto-plastic slip analysis may be considered to achieve an economical design. For group piles, the relative reduction in downdrag increases with an increase in the relative bearing stiffness ratio, which is the ratio of Young's modulus of bearing layer to that of the consolidating soil. However, compared with the relative reduction in dragload, the relative reduction in downdrag was found less affected by the group interaction for a given surcharge load. Based on three case studies, it was concluded that the downdrag is more sensitive to the total number of piles than to the pile spacing within the group.

2.4 DISCUSSION

Based on the available literature, it can be reported that there is no practical solution available for single or pile groups embedded in a multi-layered soils. Although, finite element technique is capable to model soil-structure interaction in layered soil, the available no-slip approach employs linear elastic load transfer functions and can not be used to model cases of non-linear soil behavior. Currently, dragload and downdrag on pile groups are determined based on an average modulus for the soil layers. The slip model, on the other hand, considers sophisticated constitutive models, but, either they are very complex for practical purpose, or they use soil parameters which are often not easily available. Moreover, the pile soil slip is taken into account indirectly by curtailing the interface stresses to some limiting values that are not well recognized yet. The situation turned to complete uncertainty, because a large difference in calculated dragloads exists between the non-slip elastic model and the slip model as reported in the literature. Accordingly, comprehensive research on negative skin friction on piles and pile groups in multilayered soil is needed.

2.6 RESEARCH OBJECTIVES

After completing the literature review and based on the discussion given above, it is intended:

1. To examine various interaction mechanisms involved in the pile-soil system for single and group piles due to soil consolidation.

2. To constitute the analytical models which are representatives of the interaction mechanisms involved in cases of negative skin friction, so that sophisticated finite element technique can be employed.

3. To establish a consistent correlation among the model parameters and the conventional laboratory soil test data by investigating the advanced literature on soil behavior and testing.

4. To validate the proposed model by comparing the predicted values with the available full scale field test, centrifuge model test and other experimental test data.

5. To prepare a flow chart of finite element analysis involving nonlinear pile soil interaction for evaluating dragloads and downdrags on piles and pile groups.

6. To develop an iterative computer program for pile designer to predict negative skin friction acting on the piles or pile groups installed in consolidating soil.

7. To demonstrate the use of the software by solving an example problem of negative skin friction on group piles.

CHAPTER 3

DEVELOPMENT OF FINITE ELEMENT MODEL

3.1 GENERAL

Finite element method provides a powerful tool for analysis of complex geotechnical problems such as pile group analysis where complicated soil structure interaction prevails. The success of finite element technique is due to the proper identification, idealization and simplification of the problem by proper discretization of the physical model into finite elements, and the formulation of appropriate elemental properties. Taking this into consideration, it is intended to develop a finite element model for nonlinear analysis of the negative skin friction on group piles in consolidating soil. The proposed model is dedicated to preserve simplicity without compromising on the results.

3.2 DEFINING THE PROBLEM

The problem considered in this investigation is a pile group installed in soft soil as shown in the figure 3.1. The soil mass is subjected to consolidation settlement caused by surcharge load Δp acting on the ground surface. The downward movement of the soil induces negative skin friction $\{\tau_z\}$ along the pile shafts. $\{\sigma_b\}$ represents the resistances developed at the pile toe. The load vector acting at the pile heads from the superstructure is $\{P_t\}$.

The state of stresses in the soil around the pile depending on nature of soil consolidation, processes of pile installation, dissipation of pore water following pile installation, subsequent loading of the piles, etc. Since these complexities are as yet not well understood, some degree of idealization is necessary to make the problem more amenable to theoretical study. Assumptions on specific features will be discussed with justification in the relevant sections.

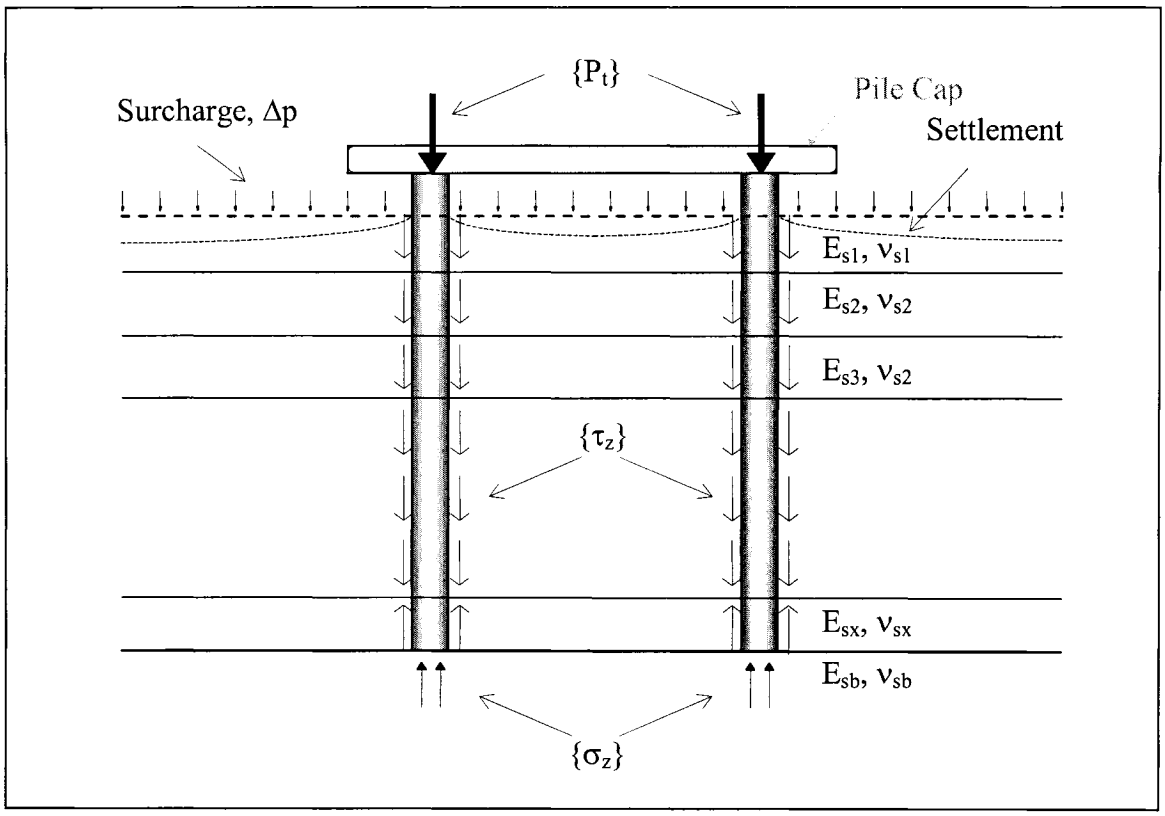

Figure 3.1: Pile Group Subject to Negative Skin Friction

The piles are assumed to be linear elastic and isotropic with constant Young's modulus E_p. The piles are considered vertical and impermeable having solid circular profile with radius r_0. For piles with other cross-sectional geometry, an equivalent circular pile that gives the same perimeter area is used. The corresponding stiffness of the actual pile is preserved by using an equivalent Young's modulus E_e. Thus,

$$\mathbf{E_e A_e = E_p A_p}$$

Or,
$$\mathbf{E_e = \frac{A_p}{A_e} E_p} \qquad \text{.....(3.1)}$$

Where E_p = Young's modulus of the pile material,

A_p = actual pile cross-sectional area, and

A_e = equivalent circular cross-sectional area having the same perimeter.

In this analysis, the pile cap in the group is assumed to be standing free from the ground surface. This assumption is considered reasonable because a gap is expected during the settlement of the soil. The stiffness of the pile cap is assumed to be perfectly flexible. This may be attained by considering each pile top to share equally the total external loads exerted from the superstructure to the pile cap.

The external or direct load on the pile cap exerted from the superstructure is not considered in this study, since the main intention of this study is to predict the maximum dragload. It is not uncommon that soil consolidation occurs after installation of piles but well ahead of the construction of the superstructure. The dragload due to consolidation of soil will have higher value when the direct load on the pile is relatively small. In other words, application of direct load causes piles to settle more resulting in reduction of relative pile soil displacement in consolidating soil and hence the impact of negative skin friction. Nevertheless, if such load would have been considered, there is no field test data available for comparison of negative skin friction on piles subject to direct load.

The soil surrounding the piles is represented by a finite number of independent horizontal layers. The soil properties may vary layer to layer, but in either layer it is homogeneous and isotropic. The layers are assumed to permit the pile soil pile interaction to take place within the same layer only. In other words, in a particular soil layer the response of surrounding soil settlement and the response of other piles in the group are coupled, but the interaction between the layers are not.

3.3 MODELING SOIL SETTLEMENT

In this investigation, the consolidation settlement will be evaluated by using Terzaghi's one dimensional consolidation theory, assuming a constant elastic modulus E_s, for simplicity. The validity of this assumption was confirmed in many case studies of negative skin friction by comparing the computed surface settlement and/or excess pore water pressure with the measured data (Teh et al, 1995, Chow et al, 1990, Jeong, 2004).

It is intended to determine the negative skin friction at drained condition. Consolidation settlement at a depth of z at fully drained condition is given by

$$S_c(z) = m_v \Delta p(h - z) \qquad \text{.....(3.2)}$$

Where, Sc = consolidation settlement at drained condition

z = depth at which the settlement is being calculated

Δp = uniform surcharge load

h = thickness of the consolidating soil layer

m_v = average coefficient of volume compressibility

Thus, the surface settlement of the soil layer (at z = 0) caused by primary consolidation is:

$$S_c = m_v h \Delta p \qquad \text{.....(3.3)}$$

For multilayered soil and/or soil subject to surcharge over a finite area, the settlement should be calculated for each layer preferably of up to 2 m thickness (Budhu, 2000) for better accuracy. The total soil settlement at particular layer will be the sum of settlements of each layer starting from the bottom layer to the layer for which the total settlement is being computed. Thus, if the lowest layer which experience consolidation is designated as 1, then the soil settlement at the top of layer i will be

$$S_{ci} = \sum_{k=1}^{i} m_{vi} h_i \Delta p_i \qquad \text{.....(3.4)}$$

Where, m_{vi}, h_i and Δp_i are the coefficient of volume compressibility, layer thickness and the increase of overburden pressure for different layers.

The coefficient of volume compressibility m_v may be obtained in the laboratory from the plot of ε_z versus σ_z' using the following relationship

$$m_v = \Delta\varepsilon(z) / \Delta\sigma'(z) \qquad \text{.....(3.5)}$$

Alternatively, it may be determined from the following relationship derived from the generalized Hook's Law assuming that the concerned soil layer is isotropic with Poisson's ratio ν_s, and the strain in horizontal direction is negligible.

$$m_v = \frac{(1+\nu_s)(1-2\nu_s)}{(1-\nu_s)E_s} \qquad \text{.....(3.6)}$$

However, the above equation can also be used to determine the Young's modulus of soil once the coefficient of volume compressibility is known.

Consolidation settlement can also be determined from the compression index C_c and swell index C_r, which are obtained from the plot of e versus log σ_z' curves. The detailed methods can be found in any standard books on Soil Mechanics (viz. Budhu, 2000; Poulos and Davis, 1980; Terzaghi and Peck, 1948).

3.4 ANALYTICAL MODELING OF PILE-SOIL INTERACTION

The problem of negative skin friction on piles driven through soft clay involves a complex interaction between pile and soil. The interaction process depends upon various factors such as physical properties of pile, pile material, number and spacing of piles, physical and mechanical properties of soil, pile driving procedure, hydrostatic conditions of subsoil etc. However, the total interaction process involved in the pile-soil system may be categorized as shown in the Figure 3.2 depending on load transfer mechanism.

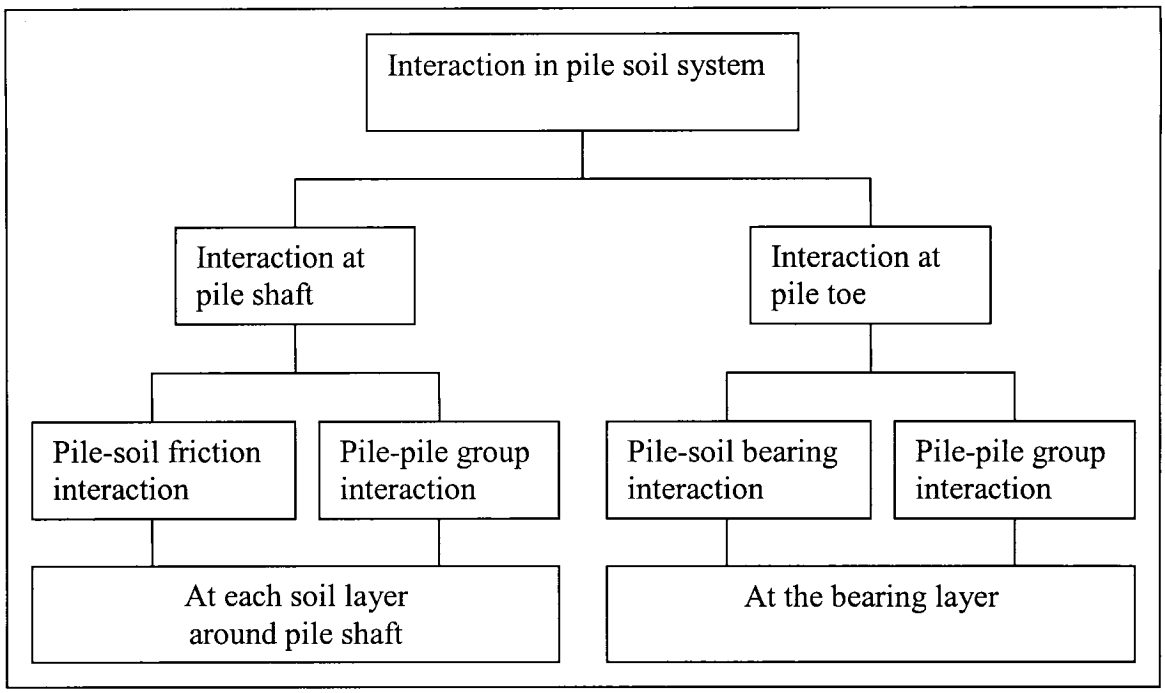

Figure 3.2: Categories of Interaction Mechanism in a Pile-Soil System

However, there are instances where pile-pile interaction are absent at the pile group, especially when laboratory test experiment (Ito and Matsui 1976, Ergun and Sonmez 1995) is performed for group piles at lower pile spacing. In other words the pile soil block appears to interact with surrounding soil as a single composite pile of radius equal to the gross radius of the pile group. In practice, for a given physical or mechanical properties of soil and pile material, the pile spacing may be closed enough for the pile soil system to act or move together as a block leading to a block interaction. Hence the block interaction is also investigated to determine the limiting value of pile spacing in the pile group.

3.4.1 Pile-Soil Friction Interaction

In order to develop an analytical model for pile-soil interaction at the pile shaft, the case of an individual pile element j in a soft consolidating soil layer is considered; Figure 3.3.

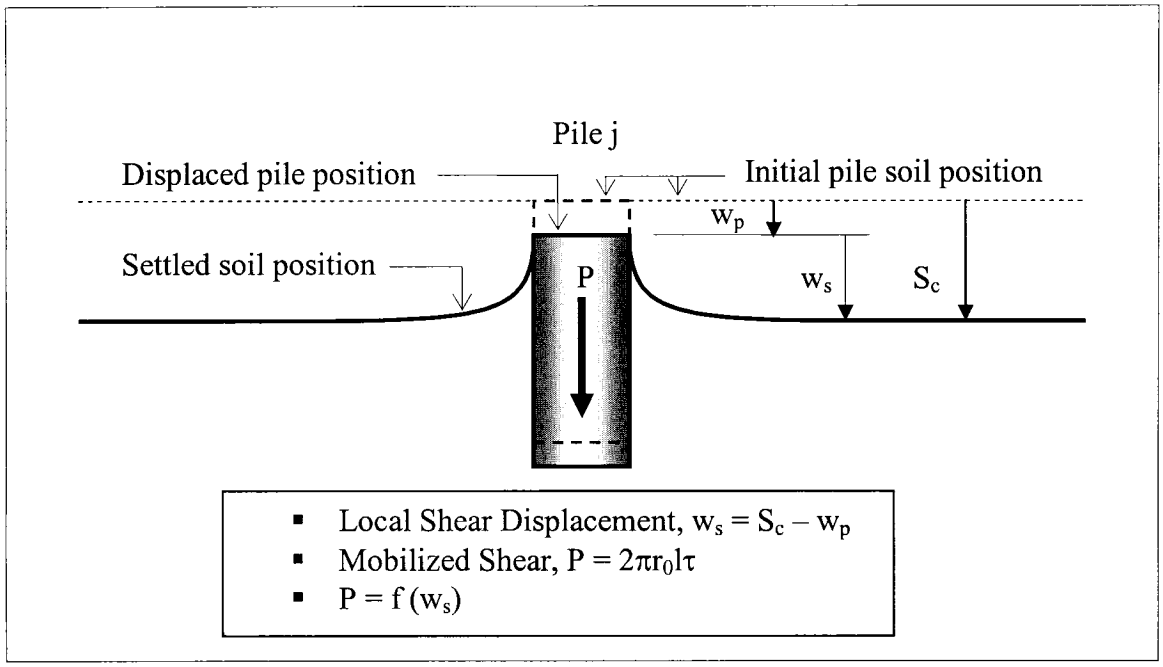

Figure 3.3: Pile-Soil Interaction at Pile Shaft

Due to the consolidation settlement S_c, of the soil layer, the shear stress will be acting downward in the form of negative skin friction along the pile shaft. The pile will tend to settle as a result of negative skin friction and the direct load (if there any) applied on the top of the pile. Assume that, w_p is the settlement of the pile element and w is the relative soil displacement with respect to pile element, then

$$w = S_c - w_p \qquad \text{.....(3.7)}$$

The equation (3.7) holds for both single and group piles. Indeed, the relative soil displacement w consists of all the displacement fields. However, in case of single piles it consists only the shear displacement w_s of soil inducing mobilized load P to the pile element as shown in the Figure 3.3. The shear displacement w_s developed in the pile element is referred to as local shear displacement in this study to distinguish it from the relative soil displacement, because the former is related to the mobilized load at the same pile element.

Thus,

$$w_s = S_c - w_p - w_g \quad (w_g = 0 \text{ for single pile}) \qquad \text{.....(3.8)}$$

If τ is the frictional shear stress at the pile shaft, l and r_0 the length and radius of pile segment, then the mobilized shear P is given by

$$P = 2\pi r_0 l \tau \qquad \text{.....(3.9)}$$

The relation between the mobilized load, P, and the local shear displacement, w_s, is investigated theoretically to adopt a rational model for load transfer characteristics involved in negative skin friction. Generally speaking, at low shear stress level, the mobilized shear is linearly related to the local shear displacement induced by soil consolidation. But, as the shaft shear stress level is increased by continuing soil consolidation, the shear displacement relationship is no longer linear. Load tests on instrumented piles (Chan et al. 1977, Acar, et al, 1984, Caputo and Viggiani 1984, Carrubba, 1997, Comodromos, et al 2003) and centrifugal model piles (Ko, et al., 1984) show that the load displacement behaviors is nonlinear and is very similar to hyperbolic relationship. Hence, a hyperbolic load-transfer model can be introduced constructively to simulate the complex nonlinear relationship between the mobilized shear and the local shear displacement. The main intention to adopt the hyperbolic model is to capture the complex phenomenon of pile-soil interaction with a simplistic approach. Emphasis is focused on how to correlate the available and relevant soil parameters to the model parameters for the analysis to be a success. Many researchers (Goh, et. al., 1997, Rajeshree, et. al. 2001, Castelli, et al 2002) found it suitable and simple to represent nonlinear pile response to soil displacement. Wong, et. al. (1995) used this approach successfully for analysis of negative skin friction on single piles.

A simple geometric hyperbolic nonlinear model is shown in Fig 3.4, which may be conveniently adopted to describe load transfer, P, and the local shear displacement, w_s.

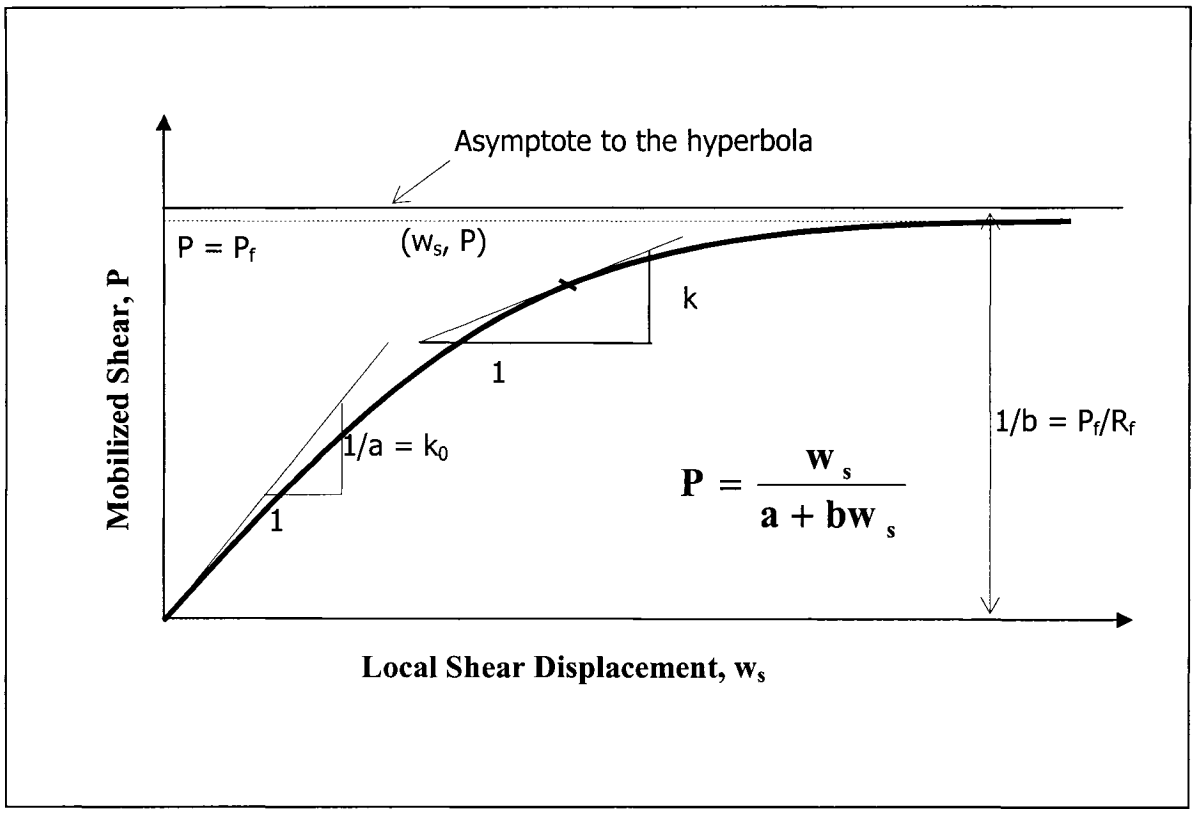

Figure 3.4: Generalized Hyperbolic Load Displacement Relationship

Thus, from Geometry,

$$P = \frac{w_s}{a + bw_s} \qquad \text{(P and } w_s \text{ act along same direction)} \qquad \text{...(3.10)}$$

The parameters 'a' and 'b' represent the reciprocals of initial slope and the limit shear of the hyperbolic curve, respectively:

$$\lim_{w \to 0} \frac{dP}{dw} = \frac{1}{a} = k_0 \qquad \text{.....(3.11)}$$

$$\lim_{w \to \infty} P = \frac{1}{b} = P_u \qquad \text{.....(3.12)}$$

Where, P_u represents the asymptotic value of the shear and k_0 the initial tangent stiffness. In hyperbolic relation, it is quite often customary to introduce a hyperbolic constant R_f such that

$$\mathbf{R_f = \frac{P_f}{P_u}} \qquad \text{.....(3.13)}$$

where, P_f represents shear at failure given by

$$\mathbf{P_f = 2\pi r_0 l\tau} \qquad \text{.....(3.14)}$$

Where, l is the length of pile segment, r_0 is the pile radius and τ is the limiting skin friction at the pile soil interface.

Conceptually, R_f symbolizes the degree of nonlinearity of the hyperbolic curve. Although, from the definition it is obvious that the value of R_f should be less than unity, some researchers (Wong et al, 1995) intend to assume it as unity for simplicity. Generally, the values R_f is found in the range between 0.8 and 0.95 for load transfer nonlinearity of soil structure interactions (Clough and Duncan 1971). In the present study, it is assumed to have a value of 0.90, as taken by many researchers (Kraft et al, 1981, Lee, 1993, Castelli, et al, 2002) in pile soil interaction problems.

Combining equation (3.10) through (3.13) and applying those at pile j in layer i, the load displacement relationship takes the following form,

$$\mathbf{P_j^i = \frac{w_{jj}^i}{\frac{1}{k_0^i} + R_f \frac{|w_{jj}^i|}{P_f^i}}} \qquad \text{.....(3.15)}$$

The term w_s is replaced by w_{jj} because it represents the displacement components at a node at pile j caused by its won mobilized load P_j. It is also important to note that, a

positive value of shear displacement w_{jj}, refers to development of negative skin friction. However, the model is generalized by using the absolute term for w_{ij} in the denominator of equation (3.15) in order to assimilate negative value of w_{jj}, which eventually means positive skin friction. The limiting shaft friction is considered the same for both the negative and the positive skin friction.

The hyperbolic relationship between the mobilized shear (P) and local shear displacement (w_s) leads to a continuing reduction in the soil stiffness with the increase of load level. At any load level, the tangent soil stiffness ($k = dP/dw_s$) is to be determined so that load mobilizing mechanism can be captured more realistically in the modeling.

Differentiating equation (3.15) with respect to w_{jj}, the general expression for tangent stiffness of soil in layer i at the pile j can be obtained as

$$k_{jj}^{i} = \frac{k_0^i}{\left(1 + R_f k_0^i \frac{\left|w_{jj}^i\right|}{P_f^i}\right)^2} \qquad \text{.....(3.16)}$$

Where, k_0 is the initial tangent stiffness

Although, the relationship between mobilized shear and local shear displacement is hyperbolic, it may reasonably be assumed that the initial tangent modulus is analogous to the elastic soil stiffness, because at low stress level, the soil behaves elastically. The load-transfer model proposed by Randolph and Wroth (1978, 1979) is adopted to describe the initial load transfer behavior in the present study. This is due to the fact that this model incorporates the interactive effects of soil movements surrounding the pile. Accordingly, initial tangent stiffness of each soil layer is given by,

$$k_0^i = \frac{2\pi G^i l^i}{\ln\left(\frac{r_m}{r_0}\right)} \qquad \text{.....(3.17)}$$

Where, r_0 = pile radius

l_i = length of pile segment at corresponding soil layer

G_i = Shear modulus of soil

L = Pile length

i = Suffix to represent each layer

It is to be noted that, r_m is some empirical distance beyond which the shear stress in the soil becomes negligible. For soil in which shear modulus increases linearly with depth, Randolph and Wroth (1978) proposed the following expression for r_m

$$r_m = 2.5\rho(1-\nu')L \qquad \text{.....(3.18)}$$

where, ν' is the Poisson's ratio of soil and ρ is the soil non-homogeneity factor given by the ratio of the soil shear moduli at mid depth and at the pile toe ($G_{L/2}/G_L$).

In the present study, which deals with multilayered soil, the non-homogeneity factor ρ may be expressed as

$$\rho = \alpha \frac{\sum G_i l_i}{G_L L} \qquad \text{.....(3.19)}$$

The term α is introduced as a coefficient for bearing condition of pile. It is given by

$$\alpha = \frac{1}{1+\frac{G_L}{G_b}} \qquad \text{.....(3.20)}$$

Where, G_L is the soil shear modulus at depth L and G_b, the soil shear modulus below pile base.

Note that, for a floating pile with $G_L/G_b = 1$, $\alpha = 0.5$, and

for end-bearing pile with $G_L/G_b = 0$, $\alpha = 1$

3.4.2 Pile-Pile Group Interaction at Pile Shaft

In group piles, relative soil displacement at a pile point involves two components: primary displacement components w_s causing mobilized shear at the same pile point, and the secondary displacement component w_g due to the displacement fields of mobilized shear at neighboring piles in the group. If w is the relative soil displacement at a pile point, then

$$w = w_s + w_g \qquad \text{.....(3.21)}$$

The shear displacement w_s causing transfer of load on the same pile involves single pile soil interaction and is modeled as a hyperbolic functions as described earlier. The displacement component w_g at a pile point is the sum of the displacements due to the displacement fields at the corresponding layer of all other piles in the group.

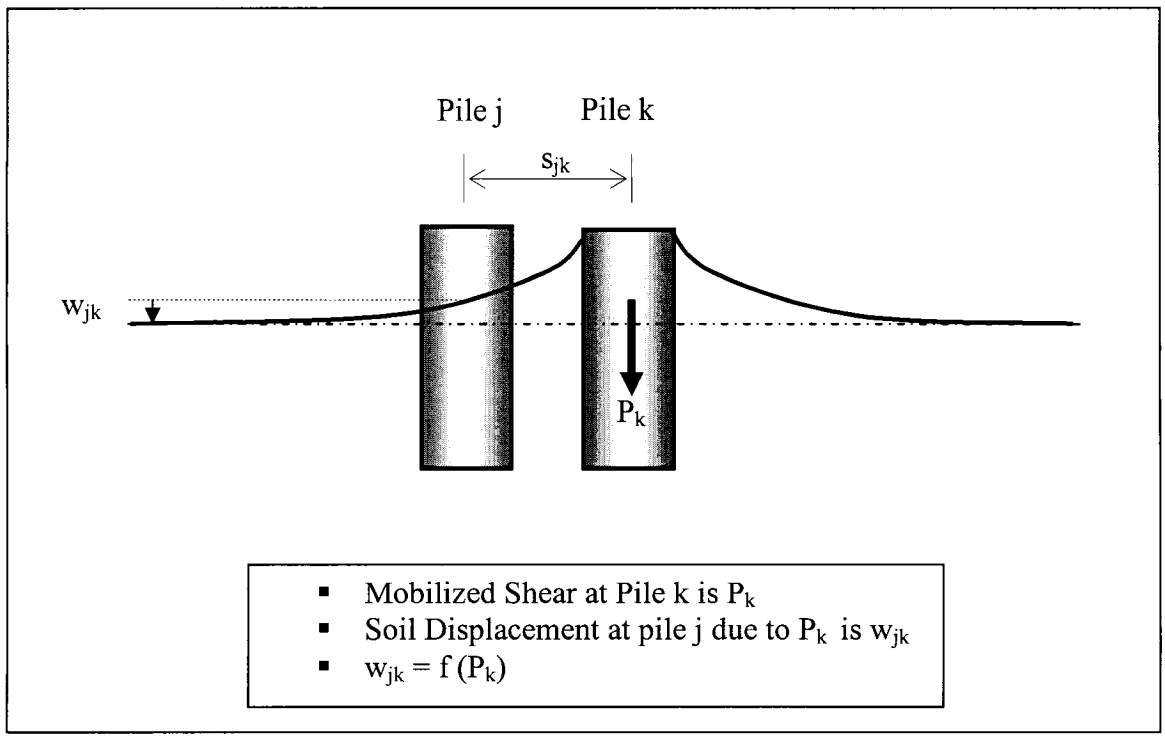

Figure 3.5: Displacement Component of Pile j due to Displacement Field of Pile k

Figure 3.5 shows the displacement field of a pile k at a certain soil layer while the mobilized shear is P_k. The displacement field of the pile j is not shown, because our focus is the secondary soil displacement at pile j induced due to the interaction of pile k. In the figure, w_{jk} represents this displacement. The relationship between the mobilized load at pile k (i.e., P_k) and the induced displacement at pile j (i.e., w_{jk}), is investigated to adopt a realistic mathematical model to represent pile-pile interaction in the pile group.

Experimental data on the interactions between adjacent piles are quite limited. Nevertheless, Lee and Xian (2001) described a well-documented case history on the interaction of two adjacent identical piles originally illustrated by Caputo and Viggiani (1984). It was observed that the interaction effect in pile-pile system is linearly elastic, although the pile soil interaction showed nonlinear behavior. From a theoretical point of view, this finding is consistent with the concept of the load-displacement relationship for a pair of piles as proposed by Randolph and Wroth (1979).

Adopting the formulation presented by Randolph and Wroth (1979), the elastic displacement of pile j due to the interaction of pile k, at the soil layer i, can be written as

$$w_{jk}^{i} = \frac{P_k^i \ln\left(\frac{r_m}{s_{jk}}\right)}{2\pi G^i l^i} \qquad (j \neq k) \qquad \text{.....(3.22)}$$

Where, P_{ik} is shaft shear stresses developed at i-th node of pile k, s_{jk} is the centre to centre distance between pile j and pile k, l_i is the length of pile element corresponding to i-th node and G_i is the corresponding shear modulus of the elastic soils. The value of r_m is assumed to be identical to the value adopted for a single pile. This is because r_m is only used to calculate the potential influence of soil displacement induced by each individual pile on the nearby piles within the influence zone. Outside r_m, no pile interaction is considered.

The equation (3.22) can be written in the following form by expressing the load at pile k for unit displacement at pile j,

$$k^{i}_{jk} = \frac{2\pi G^{i} l^{i}}{\ln\left(\frac{r_m}{s_{jk}}\right)} \qquad (j \neq k) \qquad \text{.....(3.23)}$$

3.4.3 Pile Soil Bearing Interaction

Consider the toe of a pile on the bearing layer as shown in the figure 3.6. Consolidation settlement at the pile toe is S_c and the displacement of pile toe is w_p. The transfer of bearing load at the pile toe is represented by tip resistance P_j and the corresponding relative soil displacement is w_{jj}. Thus,

$$w^{b}_{jj} = S_c{}^{b} - w^{b}_{jp} - w^{b}_{jg} \quad (S_c \text{ will be zero for end bearing pile}) \qquad \text{.....(3.24)}$$

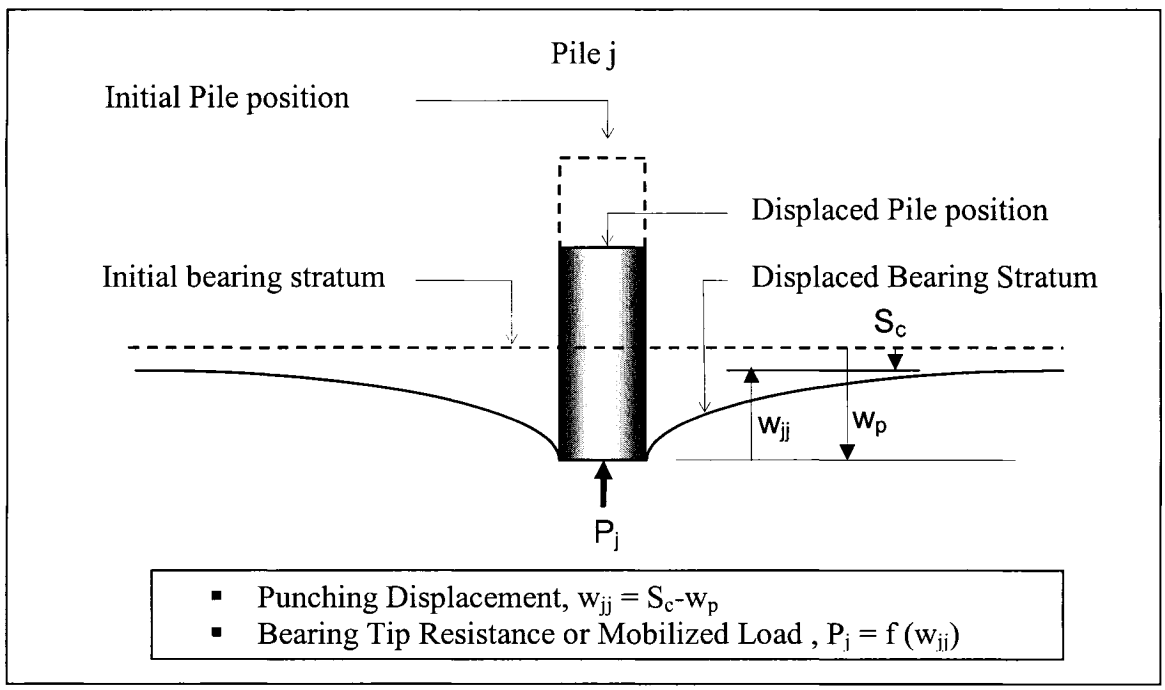

Figure 3.6: Pile-Soil Bearing Interaction at Pile Toe

If q^b is the allowable bearing pressure of the soil below pile toe, then

$$P^b_f = \pi r_0^2 q^b \qquad \text{.....(3.25)}$$

In the same manner as in the case of pile shaft, the load displacement relationship at the pile toe is also assumed to follow the hyperbolic relationship. Hence,

$$P^b_j = \frac{w^b_{jj}}{\frac{1}{k^b_0} + R_f \frac{|w^b_{jj}|}{P^b_f}} \qquad (P^b_j \text{ and } w^b_j \text{ acts in same direction}) \qquad \text{.....(3.26)}$$

Where $S_c{}^b$= consolidation settlement at pile toe; zero for the end bearing pile

$w_p{}^b{}_j$ = settlement of pile j at the toe

$k^b{}_0$ = initial tangent stiffness of the soil below the pile toe

R_f = a hyperbolic curve fitting constant.

$P^b{}_f$= allowable maximum bearing capacity

The pile base acts as a rigid punch on the surface of the lower layer of the soil. Since, at low level of stress, load displacement relationship may be considered elastic, Boussinesq solution for a rigid punch on the surface of a homogeneous elastic half-space is adopted which may be expressed as (Timoshenko and Goodier, 1970),

$$w^b_{jj} = \frac{P^b_j (1 - \nu_b'^2)}{2 r_0 E_b} \eta \qquad \text{.....(3.27)}$$

Where η is a factor introduced (Randolph and Wroth, 1978) to modify the original solution that applies to a punch at the surface of an elastic half space, in order to take account of the stiffening effect of the soil above the pile toe. Randolph and Wroth (1978) suggested a value of unity for η, unless full friction is mobilized in which case it will be reduced to 0.85. They considered that soil above pile base deforms solely by the shear stress along the pile shaft and hence have negligible effect on the bearing layer.

However, if the bearing layer is not sufficiently rigid, it is likely that the deformation of upper soil layer will have interaction effect to the bearing layer and the bearing layer involves consolidation settlement as well. Fox (1948) studied the influence of loaded area embedded in a soil mass and proposed a factor of 0.5.

In the present study an attempt is intended to assign a value of η depending on the relative rigidity of the bearing layer, with a consideration of 1.0 and 0.5 to be the limiting values.

Thus,

$$\eta = \frac{1}{1 + \frac{G_L}{G_b}} \qquad \text{.....(3.28)}$$

Note that, for $G_b >>> G_L = 0$, $\eta = 1$, and

for $G_b = G_L$, $\eta = 0.5$

From equation (3.27), the initial tangent stiffness of the soil below the pile toe may be written as

$$k_0^b = \frac{4 r_0 G_b}{\eta\ (1 - \nu_b')} \qquad \text{.....(3.29)}$$

where G_b represents the shear modulus of soil below pile toe

In the similar manner as in the case of pile shaft, the bearing stiffness for the soil below pile toe at any load level can be obtained as

$$k_{jj}^b = \frac{k_0^b}{\left(1 + R_f k_0^b \frac{|w_{jj}^b|}{P_f^b}\right)^2} \qquad \text{.....(3.30)}$$

3.4.4 Pile-Pile group Interaction at Pile Toe

The displacement at each pile toe is also composed of two parts in case of a pile group. The first part w_{jj} is the punching displacement induced by its won load mobilized as bearing tip resistance and is modeled in the last subsection. The second part w_{jg} is the additional pile base displacement induced by the interactive effects of neighboring piles in the group.

The Figure 3.7 shows the displacement field of the base of pile k induced by the tip resistance P_k at its own toe. This displacement field causes pile j to experience a displacement w_{jk}. Consequently, the interaction of pile k to pile j at the toe can be modeled by the relation between P_k and w_{jk}. Finally, the total group interaction at the toe of pile j can be determined by superimposing the iterative effects of all the neighboring piles in the pile group.

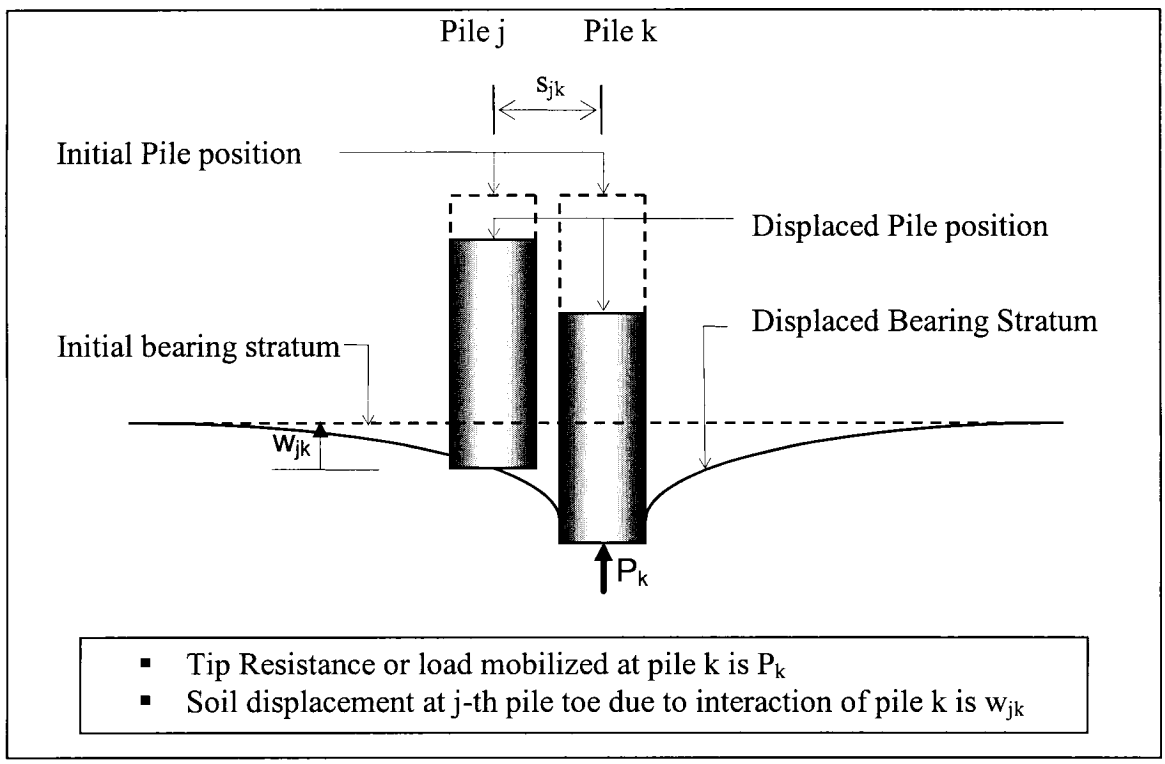

Figure 3.7: Interaction at Pile j due to Pile k at the Toe

According to Randolph and Wroth (1979) and Caputo and Viggiani (1984), the settlement of pile toe induced by the interaction of neighboring piles is largely elastic. Hence, the group interaction at pile toe is considered linear as in the case of pile shaft and is determined from closed form elastic solution.

At some distance from the pile toe, the toe load will appear as a point load, and the displacement at a distance from the point load is given by Boussinesq's solution (Timoshenko and Goodier, 1970). Thus, the elastic soil displacement induced on the toe of the pile j due to the interaction of the pile k is

$$w_{jk}^{b} = \frac{P_k^b(1-\nu_b)}{2\pi G_b s_{jk}}\eta \qquad (j \neq k) \qquad \text{.....(3.31)}$$

Where, P^b_k = vertical load developed at the toe of the pile k

G_b = shear modulus of the soil below the pile toe

ν_b = Poisson's ratio of the soil below the pile toe

s_{jk} = the centre to centre distance between pile j and pile k

η = factor to account for the interaction of upper soil layer

The above equation may be written in the following form in terms of stiffness

$$k_{jk}^{i} = \frac{2\pi G_b s_{jk}}{\eta\ (1-\nu_b')} \qquad (j \neq k) \qquad \text{.....(3.32)}$$

3.4.5 Block Interaction

In case of densely spaced group piles the pile soil block may appear to act as a single composite pile as discussed before. The block interaction may be modeled in the following manner.

The cross-sectional area of the pile soil block is the area covered by the perimeter of the pile group. Since the block is a composite of pile and soil, an equivalent elastic modulus has to be determined. This can be derived from the consideration of equal rigidity.

Hence, $$\mathbf{A_{block}E_{block} = nA_pE_p + (A_{block} - nA_p)E_s}$$

Or, $$\mathbf{E_{block} = E_s + \frac{nA_p}{A_{block}}(E_p - E_s)} \qquad \textbf{.....(3.33)}$$

where, E_{block} = equivalent elastic modulus of the block

E_p = elastic modulus of the pile material

Es = elastic modulus of soil

A_g = cross-sectional area of the block

A_p = cross-sectional area of each pile

n = number of piles

Considering the block as a single pile, the model proposed can readily be applied to investigate the negative skin friction developed around the block. Investigating the results of block soil interaction and the so called pile-soil-pile interaction, it can be determined whether block soil interaction controls the development of negative skin friction.

3.4.6 Model Parameters Vs Conventional Soil Test Data

An accurate evaluation of the soil parameters is crucial for validity of any load transfer model. According to Maugeri, et al (1996), the influence on the results due to different soil models is less than the influence due to different evaluation of model parameters particularly, the initial tangent stiffness and limit shearing stress of the soil. These parameters may be determined analytically, experimentally or by back-analysis of field

pile-load test results. Indeed, the model proposed in this research uses readily available soil test data as its input. The initial tangent stiffness requires soil shear modulus and the Poisson's ratio of the soil. These soil parameters are also involved in group pile interaction. A framework for determining these parameters from available soil test data is established to enable a rational analysis to be carried out.

The shear modulus G is the most important parameter for initial tangent stiffness of soil. It is the slope of the initial straight portion of the shear stress-shear strain response of soil as determined in the laboratory. This can also be determined from Young's modulus. Since, at low stress level, soil behaves elastically, the following relation may be adopted from the theory of elasticity

$$G = \frac{E'}{2(1+\nu_s')} = \frac{E}{2(1+\nu_s)} \qquad \text{.....(3.34)}$$

Where E' and E are drained and undrained elastic or Young's moduli; and ν_s' and ν_s are drained and undrained Poisson's ratios, respectively.

It is to be noted that the Young's modulus referred to here is its tangent value which is relevant at the initial or low stress level. Table 3.1 summarizes some recommended relations to determine Young's initial tangent modulus from available soil test data.

Table 3.1: Initial Tangent Modulus from Available Soil Test Data

Soil Type	Available Data	Correlation	Remarks	Reference
Clays	N	E' = 14N MPa	N = SPT value	Hirayama 1991
	c_u	E' = 1500c_u	c_u = undrained shear strength	Hirayama 1991
	q_c	E' = 21q_c MPa	q_c = CPT value	Poulos 1989, Poulos, 1994
Silica Sand	N	E'=16.9$N^{0.9}$ MPa		Ohsaki, et al, 1973
	q_c	E'=53 $q_c^{0.61}$ MPa		Imai et al, 1982

The Poisson's ratio is frequently estimated from empirical relationships for soils since is not easy to determine (Budhu, 2000). For undrained condition, Poisson's ratio may be assumed as 0.5 (Poulos, 1989). For drained condition it can be obtained from any standard books on soil mechanics. In general, it ranges between 0.15 to 0.35 for loose to dense sand and 0.30 to 0.10 for soft to stiff clay respectively.

Allowable frictional stress or limiting skin friction τ_f of soil at the pile interface is another important parameter in the proposed model. It is, indeed, a function of the effective stress or overburden pressure of the soil. For piles installed in consolidating soil, the effective stress changes until excess pore pressure has dissipated completely. In the evaluation of τ_f, the appropriate effective stresses are those prevalent at the time when down drag is being computed. At any time during the consolidation process, the effective stress can be obtained by subtracting the pore pressure from the total stress at that particular time. However, for most practical problems, it corresponds to the final effective stresses at the end of primary consolidation.

In the present study, the effective stress approach or β-method (Burland, 1973) is adopted, because this approach is fundamentally sound for all type of soil (Poulos, 1989).

Thus,

$$\tau_f = \beta \sigma_v' \qquad \text{.....(3.35)}$$

Where, σ_v' is the effective overburden pressure adjacent to the pile shaft at the time when the dragload is being computed. The coefficient β is a function of the soil type, pile material and the method of pile installation.

For cohesionless soil such as sand, β is a function of the lateral earth pressure coefficient K_s and the interface angle δ, and may be expressed as follows:

$$\beta = K_s \tan \delta \qquad \text{.....(3.36)}$$

Different values of β, K_s and δ have been reported in the literature (Poulos, 1989; Poulos and Davis, 1980; Budhu, 2000; Kulhawy, 1984). In the present study simple correlations are employed for sand because sand is not often encountered in downdrag problems.

The value of lateral earth pressure coefficient K_s is influenced by the in situ density and angle of shearing resistance of the soil and the amount of displacement. It is higher for displacement type of piles than for low displacement type piles such as H-piles. According to Canadian Foundation Engineering Manual (1992), K_s is usually assumed as

$$\mathbf{K_s = K_0} \qquad \text{For bored piles} \qquad \textbf{.....(3.37a)}$$

$$\mathbf{K_s = 2K_0} \qquad \text{For driven displacement type piles} \qquad \textbf{.....(3.37b)}$$

Where, K_0 is the coefficient of earth pressure at rest. Following a review of laboratory test data of 170 different types of soil, Mayne and Kulhawy (1982) suggested an empirical equation for determination of K_0 which is common to clays, silts and sands.

$$\mathbf{K_0 = (1 - \sin\phi')OCR^{\sin\phi'}} \qquad \textbf{.....(3.38)}$$

The interface friction angle δ may be assumed as recommended by Kulhawy, (1984) as shown in Table 3.2.

Table 3.2: Recommended Interface Friction Angle δ for Sand

Pile material	Interface Friction Angle, δ	Typical Field Analogy
Rough concrete	ϕ'	Cast-in-place
Smooth concrete	0.8ϕ' – ϕ'	Precast
Rough steel	0.7ϕ' – 0.9ϕ'	Corrugated
Smooth steel	0.5ϕ' – 0.7ϕ	Coated
Timber	0.8ϕ' – 0.9ϕ'	Pressure-treated
Kulhawy (1984)		

There are other empirical methods for determination of limiting skin friction from SPT or CPT values for different soil conditions and pile types (Poulos, 1989), but considerable variations occur in these correlations, particularly for bored and cast-in-place piles.

For cohesive soil, the coefficient β may be determined from the empirical correlation similar to that proposed by Ladd et al (1977)

$$\beta = \beta_{nc} OCR^{0.5} \qquad \text{.....(3.39)}$$

Where the subscript nc denotes normally consolidated clay and OCR represents overconsolidation ratio. Mesri, (1989) found that at normally consolidated state, the ratio of undrained shear strength and the effective overburden pressure is approximately a constant 0.22.

Hence,

$$\beta_{nc} = 0.22 \qquad \text{.....(3.40)}$$

The value of overconsolidation ratio may be determined by oedometer test on undisturbed soil sample. But the test is time consuming and sometimes may be difficult especially in very stiff to hard clays (Mayne and Mitchell 1988). In addition, sample disturbance tends to reduce the apparent value of pre-consolidation pressure (Ladd et al, 1977). Rather, the determination of undrained shear strength especially from the vane shear test, unconfined compression test, unconsolidated undrained test etc are common practices. Mayne and Mitchell (1988) suggested that these undrained shear strength can be used to estimate the overconsolidation ratio (OCR). This is also recommended in Canadian Foundation Engineering Manual (1992).

The value of OCR can be estimated from the following equation, which is derived from the correlations suggested by Jamiolkowski, et al (1985) and Mesri (1989).

$$OCR = 6.645\left(\frac{c_u}{\sigma_v'}\right)^{1.25} \qquad \text{.....(3.41)}$$

Further, in case of vane shear test data, $(c_u/\sigma_v')_{vane}$ is to be corrected for plasticity index as proposed by Bjerrum (1974)

$$\frac{c_u}{\sigma_v'} = \lambda\left(\frac{c_u}{\sigma_v'}\right)_{vane} \qquad \text{.....(3.42)}$$

Where, $\lambda = 1.7 - 0.54 \log (PI)$

If, however, the effective angle of internal friction ϕ' of the clay is available, then the value of β may be determined from the following equation

$$\beta = K_0\mu = K_0 \tan\delta \qquad \text{.....(3.43)}$$

Where, the coefficient of lateral earth pressure at rest K_0 is given by equation (3.38) and the interface coefficient μ can be estimated from effective angle of internal friction ϕ' as proposed by Randolph and Wroth (1981):

$$\mu = \frac{\sin\phi' \cos\phi'}{1 + \sin^2\phi'} \qquad \text{.....(3.44)}$$

The ultimate bearing capacity at the pile toe is determined using the following equation:

$$qb = c'N_c + \sigma_v'N_q \qquad \text{.....(3.45)}$$

Where N_c and N_q are the bearing capacity factors. The formulae recommended in the Canadian Foundation Engineering Manual (1992) are employed in this study.

$$N_q = e^{\pi \tan\phi'} \frac{1+\sin\phi'}{1-\sin\phi'} \qquad \text{.....(3.46)}$$

$$N_c = (N_q - 1)\cot\phi' \qquad \left(\phi' \to 0, \quad N_c \to 5.14\right) \qquad \text{.....(3.47)}$$

Effective angle of internal friction ϕ' can be determined in the laboratory. Alternatively, the internal friction angle may be estimated by using the correlation by Meyerhof (1956):

$$\phi' = 28 + 0.15\ D_r \qquad \text{.....(3.48)}$$

Where ϕ' is in degrees and relative density D_r is expressed as a percentage. The relative density may be estimated from SPT blow counts (N_{cor}) corrected for overburden pressure, using the correlations shown in Figure 3.8.

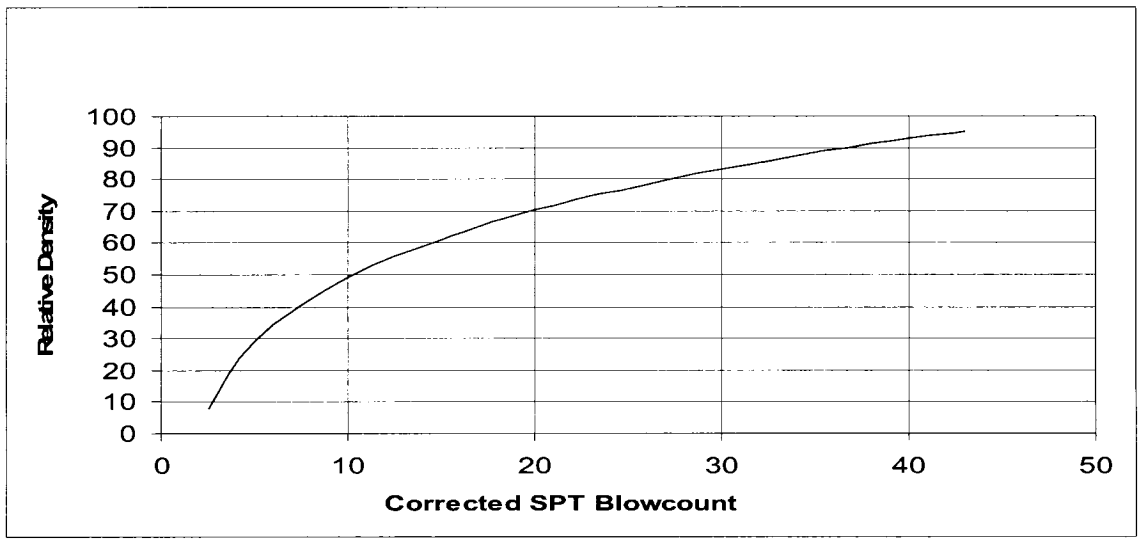

Figure 3.8: Correlation between D_r and N_{cor} (Holtze et al., 1979; Wong et al., 1995)

The correction of SPT blow count for overburden pressure is determined using the correlation recommended in the Canadian Foundation Engineering Manual (1992)

$$N_{cor} = 0.77N \log\left(\frac{1920}{\sigma_v'}\right) \qquad \sigma_v' > 24kPa \qquad \text{.....(3.49)}$$

Where, σ_v' is the effective overburden stress in kPa at the level of N-value.

3.5 FINITE ELEMENT ANALYSIS

Let us consider that there are 'n' numbers of vertical piles in the pile group. The soil surrounding the pile group is represented by 'x' number of soil layers excluding the bearing layer underlying the pile base. The piles are modeled using discrete rod elements.

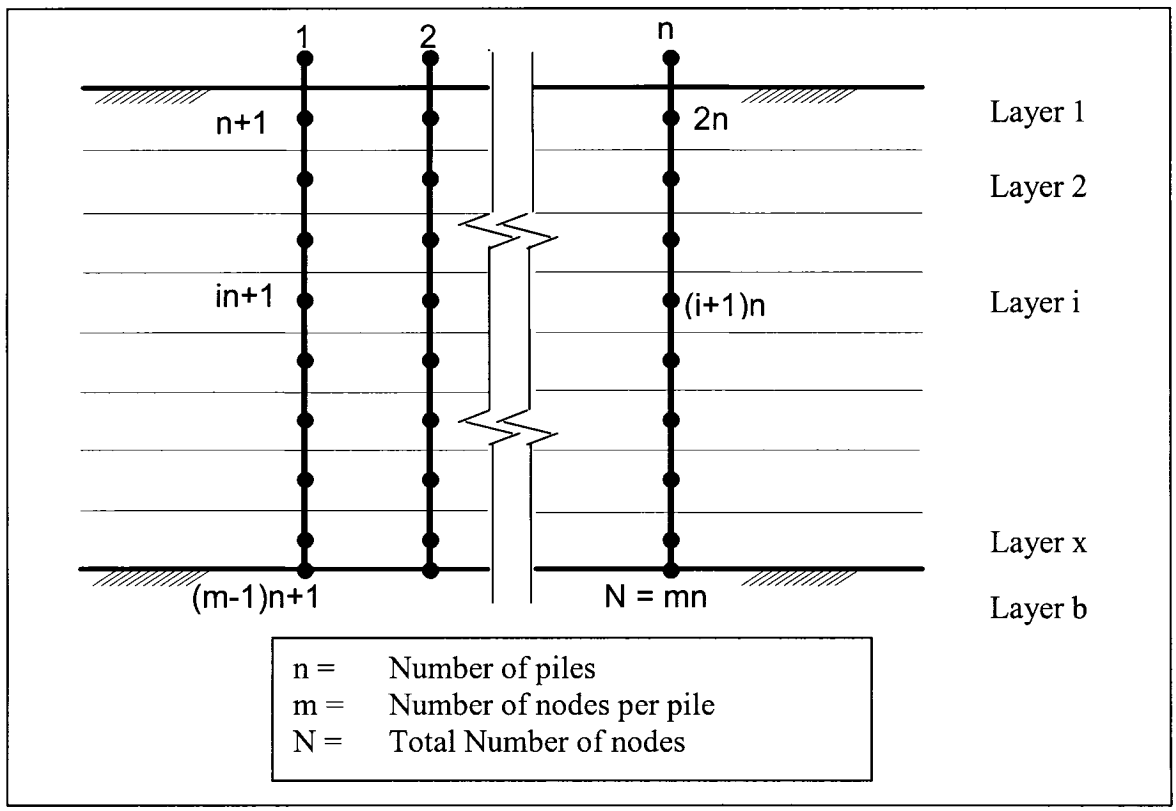

Figure 3.9: Nodal Scheme for a Pile Group

Each pile consists of a top node, a bottom node and nodes at the centre of each soil layer. Thus, in the pile group the nodes are maintaining 'm = x+2' number of

horizontal nodal planes each of which consists of 'n' nodes. The nodal scheme employed in the study is shown in the figure 3.9 for a pile group.

3.5.1 Formation of Stiffness Matrices

Each pile is discretized into rod elements as described above. The stiffness matrix for a rod element is standard and given by

$$\mathbf{k} = \frac{\mathbf{AE}}{\mathbf{l}}\begin{bmatrix} 1 & -1 \\ -1 & 1 \end{bmatrix} \qquad \text{(Cook et al, 2002)} \qquad \textbf{.....(3.50)}$$

Where, A is cross-sectional area of the pile, E the Young's modulus of the pile material, and l is the length of the pile element.

By assembling the stiffness matrices of all the pile elements in a consistent manner according to the employed nodal scheme, the global stiffness matrix for the pile system can be determined.

The interaction of soil layers and neighboring piles are attributed to act at the corresponding pile nodes and are described by a combined soil stiffness matrices associating two types of displacement fields, one from own mobilized load by soil interaction and the other from group interaction.

At each layer along the pile shaft, the pile-soil friction interaction and pile-pile group interaction are coupled to model load-displacement relationship. Similar relationship for the bearing layer will be obtained by coupling the pile-soil and pile-pile interaction at the pile toes. Combination of the load displacement relationships for all the soil layers and the bearing layer will provide complete load transfer mechanism to be employed for the analysis.

The vector of soil displacements along the shafts of the pile group at i-th layer can be expressed as

$$\{w^i\} = \{w_s^i\} + \{w_g^i\} \qquad \text{.....(3.51)}$$

Where, $\{w^i\}$ = Relative soil displacement

$\{w_s^i\}$ = Soil displacement caused by own mobilized load

$\{w_g^i\}$ = Soil displacement induced by group interaction

Hence, the flexibility matrix of the i-th soil layer can be obtained by assembling the two flexibility matrices, one from the soil interaction and the other from the group interaction,

$$[F^i] = [F_s^i] + [F_g^i] \qquad \text{.....(3.52)}$$

Where, $[F^i]$ = Assembled soil flexibility matrix for i-th layer

$[F_s^i]$ = Flexibility matrix for soil interaction

$[F_g^i]$ = Flexibility matrix for group interaction

Suffix i represents corresponding layer

The flexibility matrix $[F_s^i]$ represents the load displacement relationship between the mobilized load vector and the respective displacement vector at the same nodes. The flexibility matrix $[F_g^i]$ on the other hand represents displacement components induced by mobilized load at other piles in the group.

Consequently,

$$[F_s^i] = \begin{bmatrix} f_{11}^i & 0 & 0 & 0 & 0 \\ 0 & \ldots & 0 & 0 & 0 \\ 0 & 0 & f_{jj}^i & 0 & 0 \\ 0 & 0 & 0 & \ldots & 0 \\ 0 & 0 & 0 & 0 & f_{nn}^i \end{bmatrix} \qquad \ldots\ldots(3.53)$$

$$[F_g^i] = \begin{bmatrix} 0 & f_{12}^i & f_{13}^i & \ldots & f_{1n}^i \\ f_{21}^i & 0 & f_{23}^i & \ldots & 0 \\ f_{31}^i & f_{32}^i & 0 & \ldots & 0 \\ \ldots & \ldots & \ldots & 0 & 0 \\ f_{n1}^i & \ldots & \ldots & \ldots & f_{nn}^i \end{bmatrix} \qquad \ldots\ldots(3.54)$$

$$[F^i] = \begin{bmatrix} f_{11}^i & f_{12}^i & f_{13}^i & \ldots & f_{1n}^i \\ f_{21}^i & f_{22}^i & f_{23}^i & \ldots & \ldots \\ f_{31}^i & f_{32}^i & f_{33}^i & \ldots & \ldots \\ \ldots & \ldots & \ldots & \ldots & \ldots \\ f_{n1}^i & \ldots & \ldots & \ldots & f_{nn}^i \end{bmatrix} \qquad \ldots\ldots(3.55)$$

The flexibility coefficients of the flexibility matrix $[F^i]$ can be expressed as

$$f_{jk}^i = \frac{1}{k_{jk}^i} \qquad (j = 1,2,\ldots..n) \quad (k = 1,2,\ldots n) \qquad \ldots\ldots(3.56)$$

It is worthwhile mentioning that k_{jk} represents the stiffness or the slope of the load displacement curve for pile-soil or pile-pile interaction as described earlier in the section of analytical modeling. It is not however the coefficient of the soil stiffness matrix, which can be obtained once flexibility matrix is developed. For j = k, i.e., k_{jj}^i is given by equation (3.16) and for $j \neq k$, k_{jk}^i is given by equation (3.23). The value of k_{jj}^i is to be updated with changing values of w_{jj}, because k_{jj}^i is a function of w_{jj}^i.

The vector of displacements of group piles at the pile base can be expressed as

$$\{w^b\} = \{w_s^b\} + \{w_g^b\} \qquad \text{.....(3.57)}$$

where, $\{w^b\}$ = Relative soil displacement vector at pile toe

$\{w_s^b\}$ = Displacement component induced by single pile soil interaction

$\{w_g^b\}$ = Displacement component induced by group interaction

Hence, the flexibility matrix of the bearing layer can be obtained by

$$[F^b] = [F_s^b] + [F_g^b] \qquad \text{.....(3.58)}$$

where, $[F^b]$ = Assembled soil flexibility matrix

$[F_s^b]$ = Flexibility matrix for soil interaction

$[F_g^b]$ = Flexibility matrix for group interaction

Suffix b stands for bearing layer

More specifically,

$$[F^b] = \begin{bmatrix} f_{11}^b & f_{12}^b & f_{13}^b & \cdots & f_{1n}^b \\ f_{21}^b & f_{22}^b & f_{23}^b & \cdots & \cdots \\ f_{31}^b & f_{32}^b & f_{33}^b & \cdots & \cdots \\ \cdots & \cdots & \cdots & \cdots & \cdots \\ f_{n1}^b & \cdots & \cdots & \cdots & f_{nn}^b \end{bmatrix} \qquad \text{.....(3.59)}$$

The coefficients of the flexibility matrix can be obtained by inverting the corresponding stiffness values.

Thus, $$f_{jk}^b = \frac{1}{k_{jk}^b} \qquad (j = 1,2,\ldots..n) \quad (k = 1,2,\ldots n) \qquad \text{.....(3.60)}$$

For j = k, i.e., k^b_{jj} is given by equation (3.30) and for j ≠ k, k^b_{jk} is given by equation (3.32). The value of k^b_{jj} is to be updated with changing values of w^b_{jj}, because k^b_{jj} is a function of w^b_{jj}. As stated earlier, k_{jk} is not the coefficients of the soil stiffness matrix.

The individual soil layers are assumed to permit the pile soil interaction to take place within the same soil layer only, that means the interactive effects between the layers are not coupled. This assumption reduces the computational time and data storage space requirements substantially compared with those for the fully interactive approaches. Mathematically, the assumption interprets that the soil flexibility or stiffness matrices for different layers, which are essentially the sub-matrices of the global matrix, can be handled separately. Thus, for each soil layer the soil stiffness sub matrix may be obtained by inverting the corresponding flexibility matrix.

$$[K^i] = [F^i]^{-1} \qquad \text{.....(3.61)}$$

$$[K^b] = [F^b]^{-1} \qquad \text{.....(3.62)}$$

Assuming $[K^0]$ as the stiffness matrix corresponding to the nodes of pile heads, which essentially means a zero matrix, the global soil stiffness matrix for the total soil system can be assembled as

$$[K] = \begin{bmatrix} [K^0] & & & & & & \\ & [K^1] & & & & & \\ & & [K^2] & & & & \\ & & & \cdots & & & \\ & & & & [K^i] & & \\ & & & & & \cdots & \\ & & & & & & [K^b] \end{bmatrix} \qquad \text{.....(3.63)}$$

3.5.2 Formulation of Finite Element Equation

Once the stiffness matrices for piles and soil system are obtained, the finite element equation for the whole pile soil pile system can be devised from the compatibility of pile soil displacement. The stiffness equation for only the pile system can be written as (Cook, et al 2002)

$$[K_p]\ \{w_p\} = \{P\} \qquad \text{.....(3.64)}$$

where, $[K_p]$ is the assembled stiffness matrix of all elements of the group piles, $\{w_p\}$ is the vector of vertical deformations of the pile nodes, and $\{P\}$ is the mobilized load vector acting on the pile from pile soil interaction.

Similarly, the finite element equation of the soil system can be written as

$$[K]\ \{w\} = \{P\} \qquad \text{.....(3.65)}$$

where, $[K]$ is the assembled soil stiffness matrix, $\{w\}$ is the vector of relative vertical soil displacements at the nodes and $\{P\}$ is the vector of shear forces mobilized to the nodes. It is to be noted that the diagonal elements of the global soil stiffness matrix $[K]$ is to be updated on incremental basis as they are modeled with hyperbolic nonlinearity.

From the compatibility of pile soil displacement as explained earlier

$$\{w\} = \{S_c\} - \{w_p\} \qquad \text{.....(3.66)}$$

From equation (3.64) and (3.65) we get

$$[K_p]\ \{w_p\} = [K]\ \{w\} \qquad \text{.....(3.67)}$$

Equation (3.66) and (3.67) yields,

$$[K_p]\ \{w_p\} = [K]\ \{S_c - w_p\}$$

Or, $$[[K_p] + [K]]\{w_p\} = [K]\{S_c\} \qquad \text{.....(3.68)}$$

3.5.3 Iterative Nonlinear Analysis

Nonlinear load deformation relationship leads to change in stiffness of the soil with respect to relative soil displacement. In other words, the soil stiffness is a function of soil displacement, which in turn depends on soil consolidation settlement. Hence an iterative process is applied to satisfy the finite element equation. For this purpose several methods are available in literature. However, Newton-Raphson Method of iteration is adopted here which considers initial tangent stiffness for the initial state of settlement. This method is more likely to converge for hyperbolic load deformation model in which rate of increase of mobilized load decreases with the increase of relative soil displacement. Physically, for the hyperbolic nonlinear problem which is analogous to nonlinear spring problem, the hyperbolic relationship can be generated by displacement control, gradually increasing deformation on incremental basis and applying whatever load is needed (Cook et al, 2002). Consequently, by applying a sequence of increasing settlement, and iterating to converge for each, we can locate as many points as needed to construct an adequate representation of the load deformation curve. The likelihood of convergence to a correct solution at each deformation level can be enhanced by taking small settlement increments.

Thus, the total consolidation settlement will be applied on an incremental basis and at the end of each increment the stiffness matrix of soil will be updated in order to simulate the nonlinearity of the load transfer system. If $\{\Delta S_c\}$ is the increment vector of

the consolidation settlement $\{S_c\}$, the iterative finite element relationship can be expressed by the following equation analogous to equation (3.68)

$$[[K_p]+[K]]\{\Delta w_p\} = [K]\{\Delta S_c\} \qquad \text{.....(3.69)}$$

The above equation is the governing equation to compute the downdrag developed at the pile soil system. In other words, for a realistic solution of a negative skin friction problem, the equation (3.69) has to be satisfied at each iterative increments of consolidation settlement. At the end of each incremental soil settlement, the pile settlement and the relative soil displacement can be determined as

$$\{w_p\}_i = \{w_p\}_{i-1} + \{\Delta w_p\}_i \qquad \text{.....(3.70)}$$

And

$$\{w\}_i = i * \{\Delta S_c\} - \{w_p\}_i \qquad \text{.....(3.71)}$$

Where, i is the suffix for increment. In general, at the end of (i-1)-th increment, the equation (3.69) provides $\{\Delta w_p\}_i$. The vector $\{\Delta w_p\}_i$ updates vector $\{w_p\}_i$ by the equation (3.70), and the vector $\{w_p\}_i$ updates vector $\{w\}_i$ by the equation 3.71.

The iterative steps for the analysis are summarized below

a) For each incremental consolidation settlement vector $\{\Delta S_c\}$, the vector $\{\Delta w_p\}$ is determined from equation (3.69). The vector $\{w_p\}$ is updated by equation (3.70).

b) The new value of $\{w_p\}$ provides the mobilized load vector $\{P\}$ and relative soil displacement vector $\{w\}$ by equation (3.64) and (3.71), respectively.

c) The displacement vector $\{w_g\}$ is then obtained from the interaction of all neighboring piles in accordance with equations (3.22) and (3.27), which in turn provides the local displacement vector $\{w_s\}$ by using equation (3.21).

d) The next step is to use the new values of $\{w_s\}$ to update the diagonal elements of the soil stiffness matrix **[K]** according to the equations (3.16) and (3.30).

e) The updated soil stiffness matrix **[K]** will be used in equation (3.69) for the next increment of vector $\{S_c\}$.

f) Finally, the vector $\{w_p\}$ and the equation (3.64) can provide the downdrag and the dragload of the pile(s).

CHAPTER 4

MODEL VERIFICATION AND PROCEDURE OF ANALYSIS

4.1 GENERAL

A number of published theoretical and experimental results of single and group piles are reviewed and compared with the computed results for the purpose of verification of the proposed model. Furthermore, the proposed procedure is demonstrated by solving an example problem followed by providing a flow chart of analysis.

4.2 COMPARISON WITH THEORETICAL RESULTS

The accuracy of the present approach, which is applicable to both single and group piles, is validated by comparison with theoretical solutions.

4.2.1 Single Piles

Poulos and Mattes (1969) reported elastic solutions obtained by boundary element method for negative skin friction on end-bearing single piles in a homogeneous soil. The length to diameter ratio of the pile was 25. In the present study, a pile of length 25 m and diameter 1.0 m installed through a soil layer of Young's modulus 4.0 MPa to bear on a rigid layer is analyzed. The soil settlement profile is assumed to be decreasing linearly from ground surface to zero at the pile toe. The Poisson's ratio is taken zero as considered by Poulos and Mattes (1969). The surface settlement of 31 mm was assumed corresponding to a surcharge of 5kPa. The β-value is taken as 0.3.

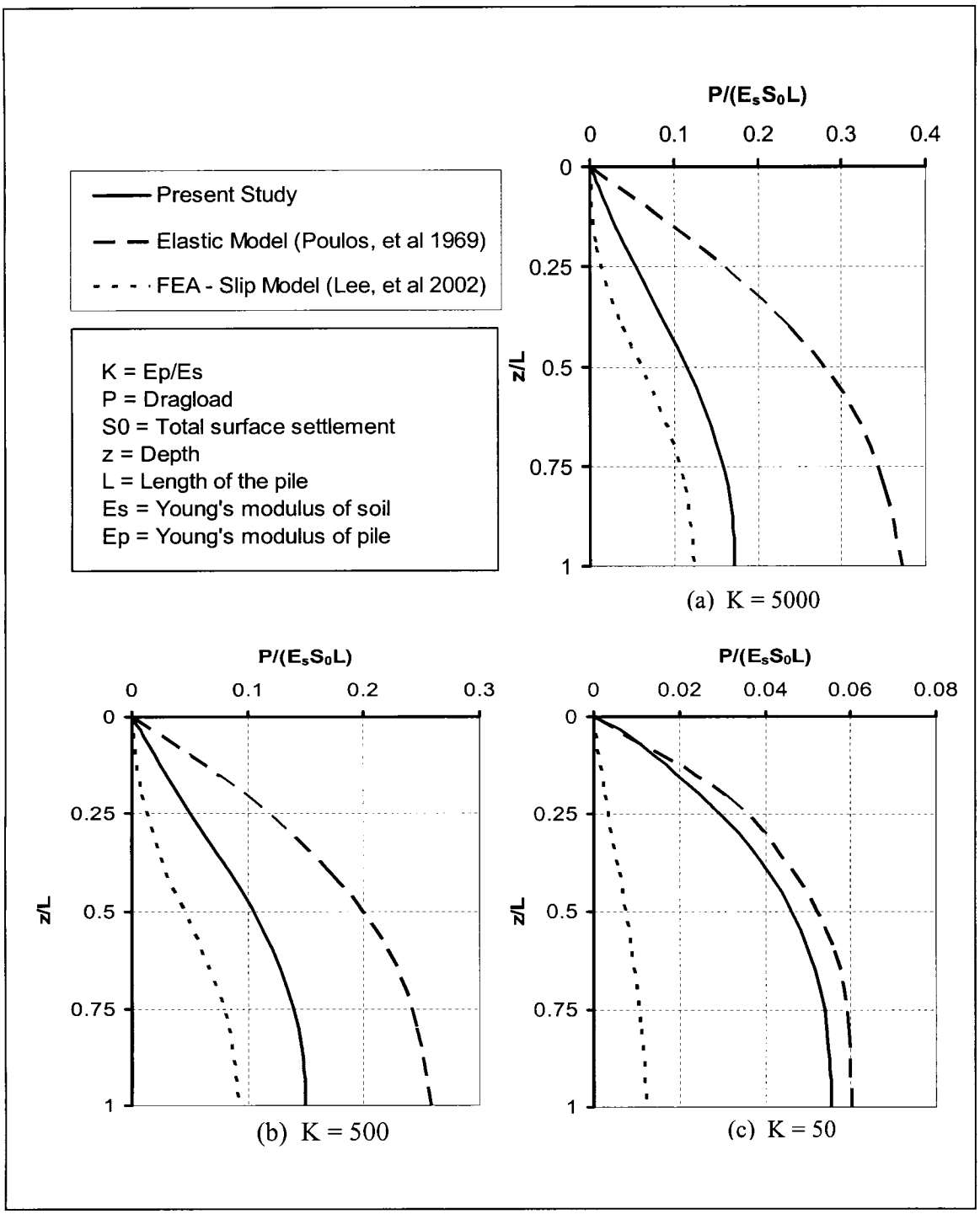

Figure 4.1: Comparison of Dragload Distribution on End-Bearing Single Pile

Figure 4.1 compares the dragload distribution in the pile computed by present approach and the solutions presented by Poulos and Mattes (1969). The solutions taking

pile soil slip into account by Lee, et al (2002) using commercial finite element software is also presented for comparison. The dragload in the figure is represented by a dimensionless term $P/(E_sS_0L)$, where P, S_0 and L are the dragload of the pile, the soil consolidation settlement at the ground surface and the length of the pile, respectively.

It can be seen from the Figure 4.1 that the normalized dragload from the finite element slip analysis is significantly smaller than that from the analytical elastic analysis, for any pile soil stiffness ratio. Although, the results of Poulos and Mattes (1969) were supported by many other analytical or finite element elastic analyses (Lim, et al 1993, Shen and Teh, 2002), Lee, et al (2002) showed that elastic solutions predict excessive large dragloads. The result of Lee et al. (2002) is substantiated by many later researchers (e.g., Jeong, et al 2004; Lee and Ng 2004) through finite element slip analysis. However, the general trend of dragload distribution is similar in both elastic and slip analysis. Interestingly, the dragloads computed by the present approach are smaller than that of elastic solutions as expected but relatively higher than the finite element slip analysis. In the finite element analysis load deformation curve is assumed linearly elastic perfectly plastic. Further, pile soil slip is assumed to occur at 5 mm of relative soil displacement irrespective of depth, which may be deemed to be an oversimplification of load displacement relationship to take into account the variation of soil modulus with depth.

It can be concluded that elastic analysis provides an upper bound of the dragload since it does not allow soil yielding to take place at the interface thereby developing substantially larger shear stress. The slip analysis, on the other hand, gives the lower bound of the dragload, because it curtails the shear stress at an assumed constant value of soil deformation (and hence the soil strain) irrespective of depth causing apparently a lower value of mobilized load. In consideration of these upper and lower limits of dragloads, the present approach provides reasonable results as computed for different pile soil stiffness ratios. The more the compressibility of piles (e.g., K = 5000 to K = 50), the less will be the difference between the results of present and the elastic solutions. Alternatively, for less compressible piles, present solution provides results similar to finite element slip analysis.

The Figure 4.2 shows the results of single pile analysis for different stiffness of bearing layer (Chow et al. 1990; Lee and Ng 2004). In the analysis, E_p and Δp are taken as 12.5 GPa and 50 kPa, respectively, and the interface coefficient and the coefficient of lateral earth pressure at rest are taken as 0.3 and 1.0, respectively, as assumed by Lee and Ng (2004). The pile radius r_0 is assumed as 25 mm.

The variation of the normalized downdrag, $W_t E_p A/(\Delta p L^3)$, with relative stiffness between the bearing stratum and the surrounding soil, E_b/E_s is presented, where W_t is the pile head settlement or downdrag, A is the cross-sectional area of the pile, Δp is the surcharge load at the soil surface and E_p, E_b and E_s are the Young's moduli of the pile, the bearing stratum and the surrounding soil, respectively. Results of the finite element elastic model by Chow et al. (1990) and the finite element slip model by Lee and Ng (2004) are plotted along with the computed result for comparison.

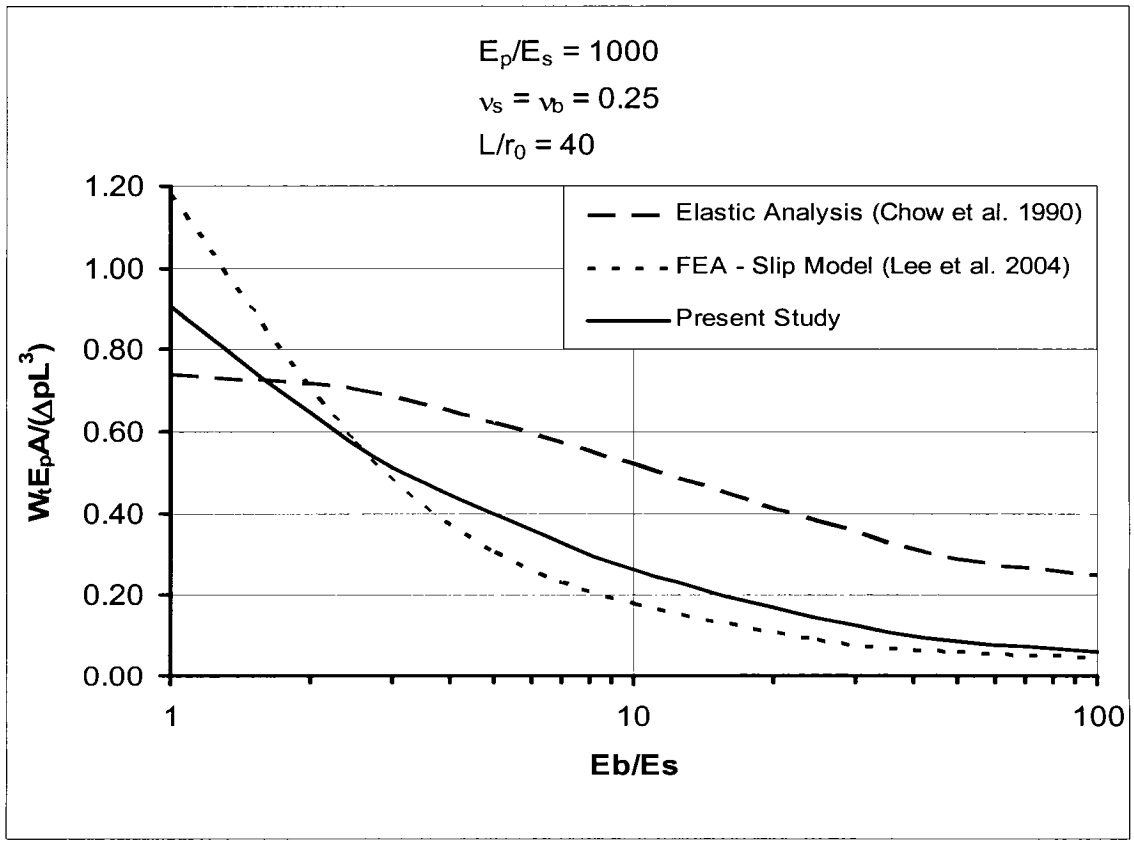

Figure 4.2: Variation of Normalized Downdrag with E_b/E_s

It is observed from the Figure 4.2 that the normalized downdrag decreases nonlinearly with the increase of relative stiffness ratio E_b/E_s. As expected, the pile head settlement decreases with increase in relative stiffness ratio because of the stiffer bearing stratum. In case of friction piles ($E_b/E_s = 1$), the computed downdrag is approximately the average of the values of elastic and slip analysis. However, as the stiffness ratio increases, the computed downdrag matches with the results of slip analysis. It is expected because stiffer bearing stratum induces higher relative soil displacement causing a load transfer behavior to approach towards plastic state as assumed in FEM slip model. The significantly smaller computed downdrag is due to the fact that at higher relative soil displacement the tangent stiffness of soil is reduced as per the hyperbolic load transfer relationship, thereby producing less shear stress than that computed by the elastic no slip analysis. The smaller the induced shear stress, the smaller is the pile settlement.

4.2.2 Group Piles

Figure 4.3 presents the distribution of dragload presented by Kuwabara and Poulos, (1989) and Lee et al. (2002) in a pile group of flexible pile cap. There were 25 end-bearing piles, which were arranged in a square configuration in a homogeneous soil. The pile spacing to diameter ratio, the pile length to diameter ratio, and the pile-soil stiffness ratio (E_p/E_s) were 5, 25 and 1000, respectively. The Poisson's ratio was 0.3. In the present analysis, pile length is assumed 20 m and the surcharge is taken as 25 kPa. The Young's modulus of the consolidating soil layer is assumed 20 MPa. The interface coefficient and the coefficient of lateral earth pressure at rest are taken as 0.3 and 1.0 as assumed by Lee, et al (2002).

The dragload is normalized with the maximum dragload on single pile. It can be seen from the Figure 4.3 that the dragload induced on individual piles in a group is much less than that on single pile. However, the corner and side piles attract significantly higher dragload than does the centre pile.

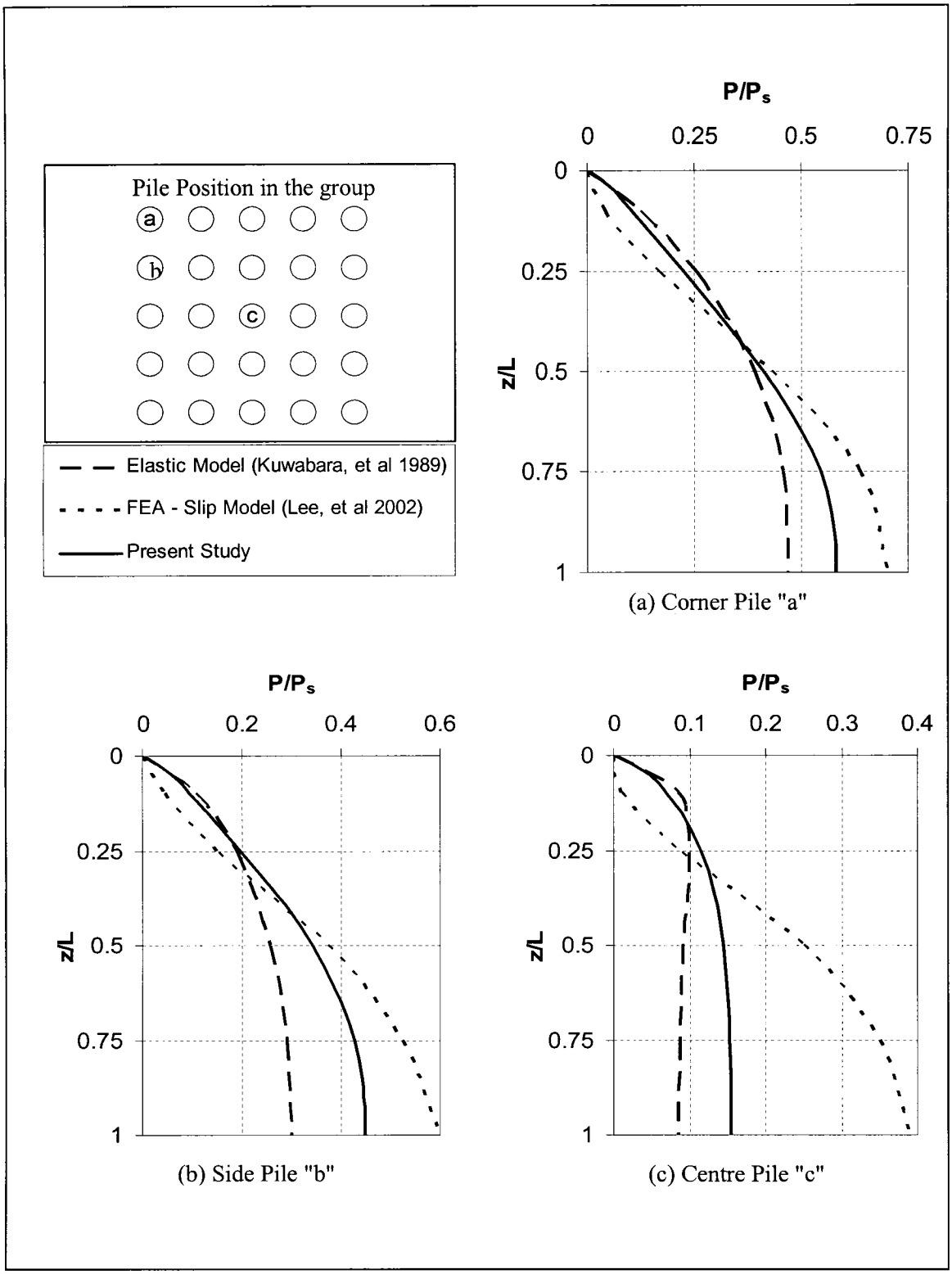

Figure 4.3: Comparison of Dragload Distribution in End-Bearing Pile Group (Normalized by the Maximum Dragload in Single Pile)

Although the trends for dragload distribution are very similar, different approaches provide results with significant difference. The analytical boundary element method of Kuwabara and Poulos (1989) predicted smaller dragloads, particularly at the pile toes, which amounted to only 9 to 46 % of that predicted for a single pile. Elastic finite element analysis (Jeong, et al 2004; Shen and Teh, 2002; Chow, et al 1990) also showed similar results. The elasto-plastic slip analysis using ABAQUS finite element package performed by of Lee, et al (2002), on the other hand, observed relatively higher dragloads of 40 to 70 % of that of single piles, which was substantiated by similar finite element slip analysis (Jeong, et al 2004). In the dilemma of deciding an acceptable value of dragload reduction from the upper bound value obtained by elastic analysis and the lower bound value obtained by finite element slip analysis, the present approach provides a reasonable reduction in the dragload. In the present study, the dragloads for centre, side and corner piles are computed as 16%, 45% and 58%, respectively.

Table 4.1: Comparison of Dragload Interaction Factor for Piles in a Group

Reference of Study	Dragload Interaction Factor, α_d		
	Centre Pile	Side Pile	Corner Pile
Kuwabara and Poulos (1989)	91	71	54
Lee, et al (2002)	60	40	30
Chow, et al (1996)	85	61	43
Present Approach	84	55	42

Table 4.1 shows the computed dragload interaction factor α_d for different approaches, where α_d is as defined by Poulos and Davis (1980) as follows;

$$\alpha_d = \frac{P_s - P_g}{P_s}$$

Where, P represents the maximum dragload and suffixes s and g stand for a single pile and piles in a group, respectively.

Table 4.1 shows that the present approach is capable of predicting the dragload on single and group piles with reasonable accuracy.

4.3 COMPARISON WITH EXPERIMENTAL RESULTS

Five case studies of field pile tests and centrifuge model pile tests of single and group piles from published literature are presented to validate the application of the present method for practical purpose. The required input parameters listed with each case study are determined from the soil test data using the framework developed in the previous chapter.

4.3.1 Case Study 1: Field Test on Single Pile (Walker and Darvall, 1973)

Walker and Darvell (1973) reported field measurements of dragload on an uncoated steel shell pile near the City of Melbourne, Australia. The pile was 31 m long, with an external diameter of 760 mm and a wall thickness of 11 mm. It was driven through 2 m existing fill, 7 m medium fine sand, 15.5 m firm silty clay and 3 m sandy silt, and was tipped into 3.5 m a layer of dense sand and gravel (Figure 4.4). After the pile was driven, a test embankment (200 m x 100 m x 3 m) was constructed. It took four months to complete primary consolidation. During this period, the ground settled about 29 mm at the surface presumably decreased linearly to zero at the pile toe. The maximum dragload was measured to be 1766 kN.

In the computation, the upper soil system is assumed to be composed of ten layers. The soil parameters were based on SPT blow counts for the fill and cohesionless soil and undrained shear strength for the clay layers. The N values were corrected for effective

overburden pressure while the vane data were corrected for average plasticity index. The unit weights of soils were back analyzed from the stress data provided in the original paper. The water table was deemed to be located at 2 m below the ground surface.

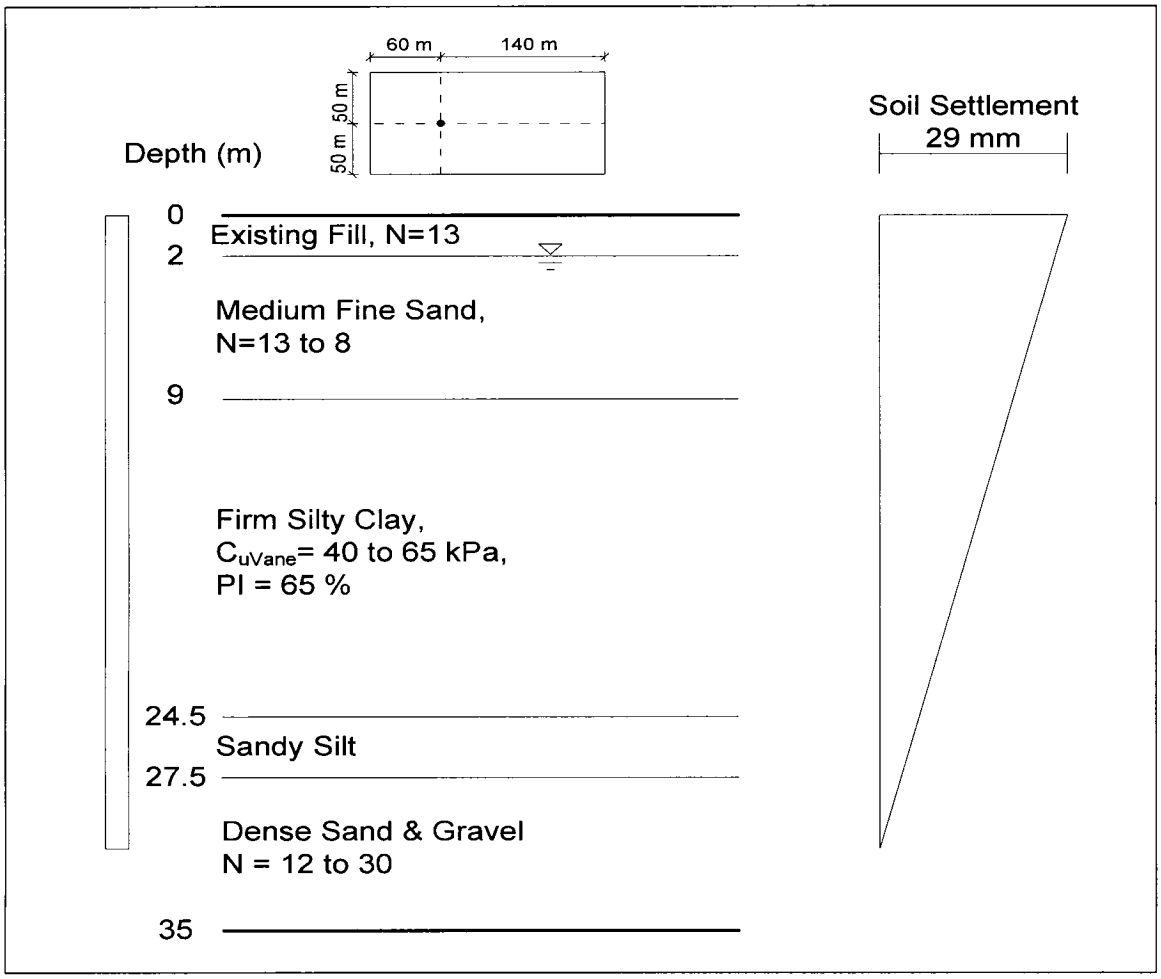

Figure 4.4: Case Study 1: Soil Profile and Settlement Profile (Walker and Darvall, 1973)

Walker and Darvall (1973) reported an OCR of 1.57 at a depth of 18.5 m based on consolidation test. Computed OCR from the corrected vane data matches this value. For sandy layers, OCR value was assumed 1.57. The stress increase due to the surcharge was determined using Boussinesq's solution. The OCR data were updated accordingly.

The computed and measured variation of dragload and shearing stress with depth are shown in the Figure 4.5. Generally good agreement has been obtained. About the peak value of measured skin friction at the top of the clay layer (at about a depth of 9 m), Walker and Darvall (1973) admitted that it even exceeded the in situ undrained shear strength unexpectedly. One possible explanation could be attributed to local variation of soil properties. However, the maximum computed dragload of 1725 kN compares reasonably with the measured value of 1766 kN.

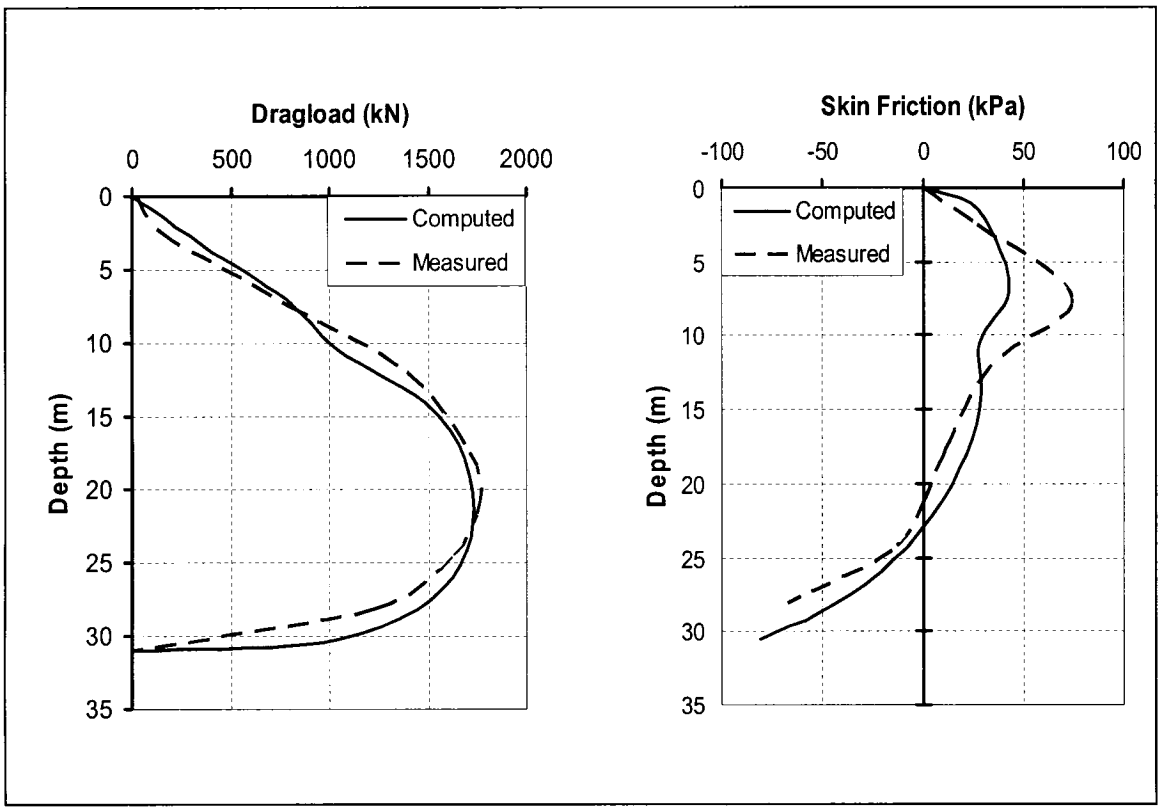

Figure 4.5: Case Study 1: Comparison of Dragload and Skin Friction Distribution

4.3.2 Case Study 2: Field Test on Single Pile (Fukuya et al, 1982)

Fukuya et al (1982) reported a field testing program to investigate the effect of negative skin friction on an uncoated steel pipe pile at a reclaimed land called Ohgishima

in Tokyo Bay. The data of this program are adopted here from Wong et al (1995) and Lim et al (1993). The reclamation work continued for three years since November 1971 to December 1974. The pile 37.5 m in length with an outside diameter of 610 mm and a wall thickness of 9.5 mm was driven with a diesel hammer during October-November 1973. The Young's modulus of steel is assumed as 210 GPa. The soil profile, SPT blow counts and the undrained shear strength data from unconfined compression tests are shown in Figure 4.6. The water table was assumed to be located at 2 m below the ground surface.

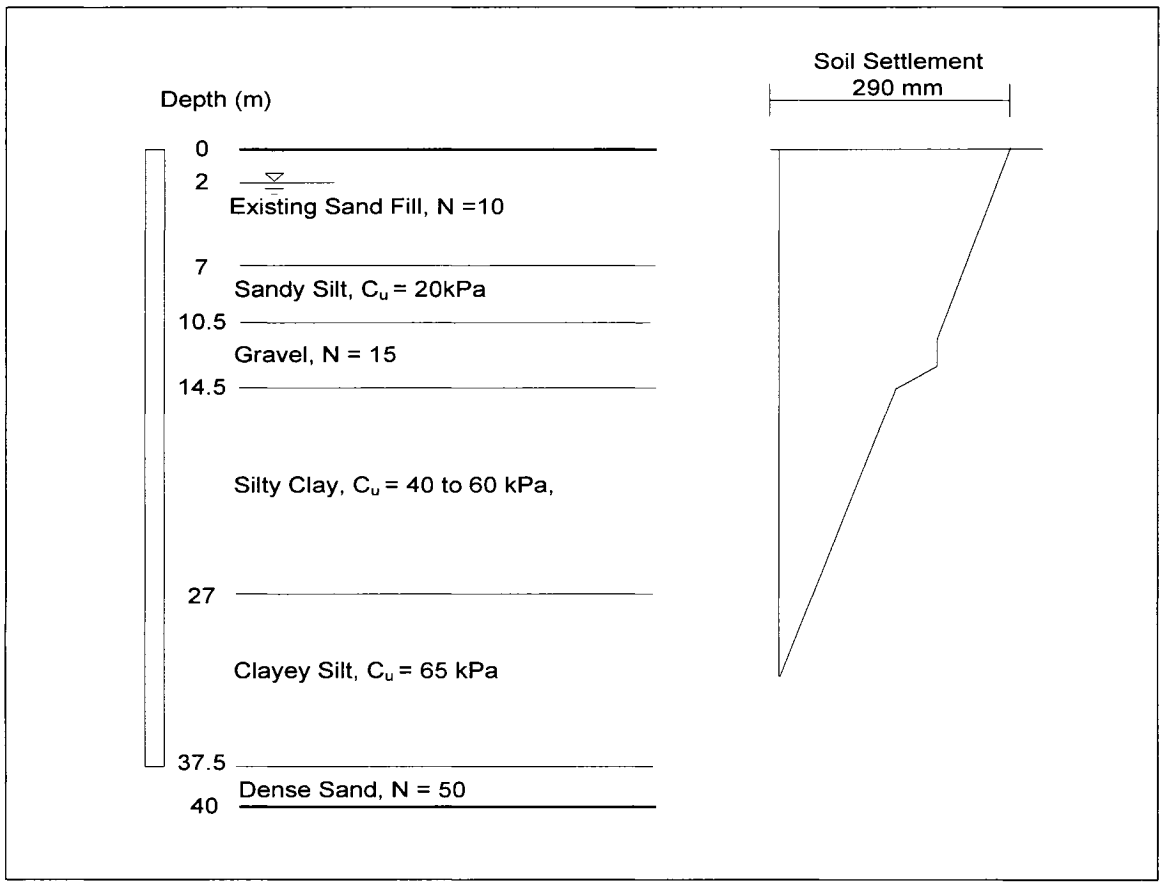

Figure 4.6: Case Study 2: Soil Profile and Settlement Profile (Fukuya et al, 1982)

Figure 4.6 also shows the ground settlement profile obtained in March 1976 a few years after the pile installation. Primary consolidation had nearly completed. With a

ground surface settlement of 290 mm, the maximum dragload of 2390 kN was measured at the neutral point located approximately at 82% of pile length below ground surface.

The upper soil layer was assumed to be divided into ten sub-layers. For non-cohesive layers, OCR was deemed as unity since the stress history was unknown. In the computation of cohesive layers, OCR values estimated from the undrained shear strength were assumed to remain the same during the test period.

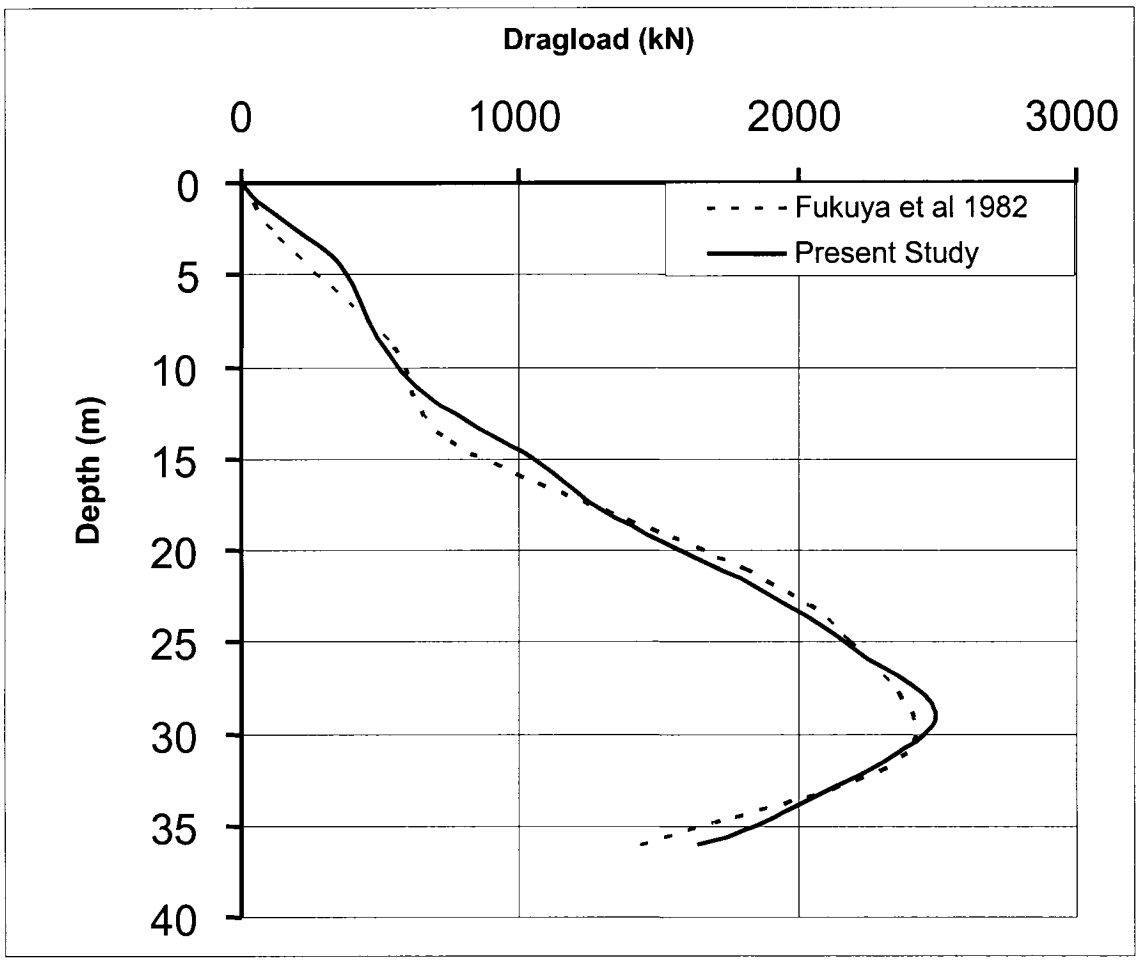

Figure 4.7: Case Study 2: Comparison of Computed and Measured Dragload

The computed and measured dragload profiles are shown in the Figure 4.7. Good agreement is observed between the present solution and the field measurements.

Computed dragload 2485 kN with neutral depth 80% of pile length compared well with field values 2390 kN and 82%, respectively.

4.3.3 Case Study 3: Field Test on Single Pile (Bjerrum et al, 1969)

Bjerrum et al (1969) reported a field study of negative skin friction on a series of piles including two test piles at Sorenga, in the harbor of Oslo. The pile without enlarged base denoted as G in the original paper is reviewed in the present study. It was a conventional uncoated steel tube pile having an external diameter of 500 mm and a wall thickness of 8 mm driven to bedrock at 40 m. The Young's modulus of the pile material was taken 210 GPa..

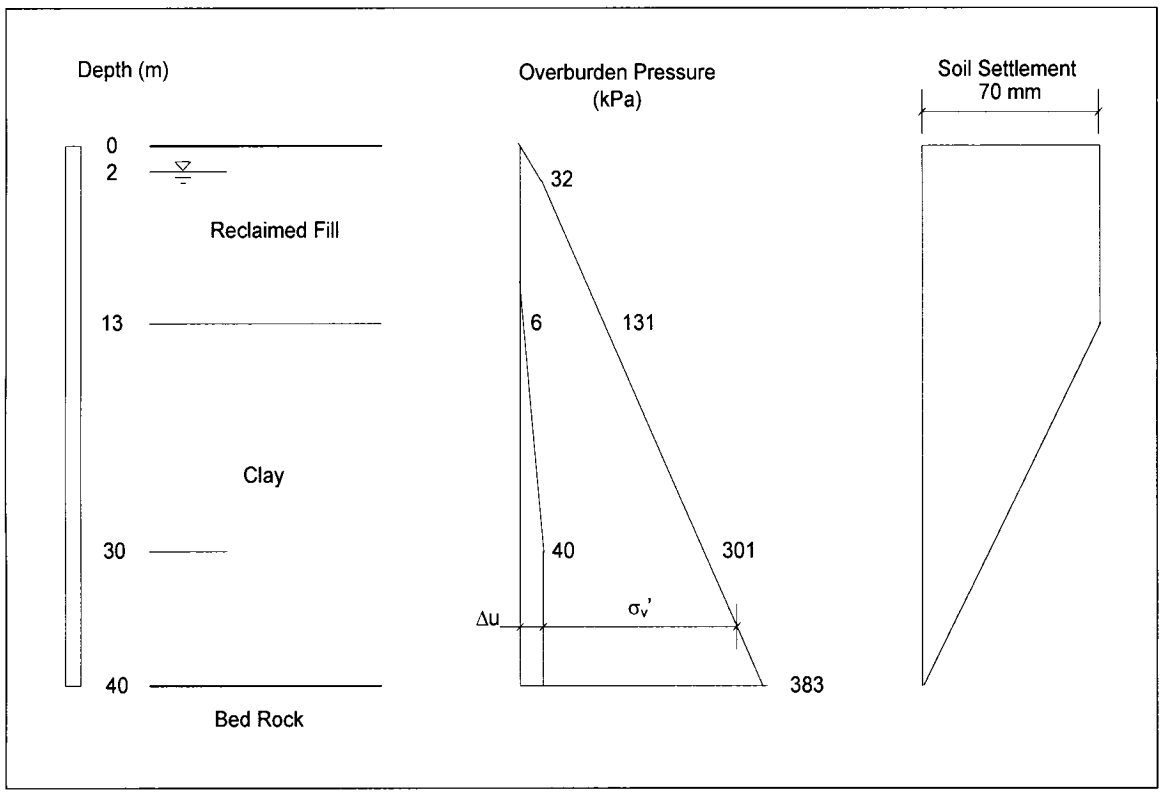

Figure 4.8: Case Study 3: Soil Profile, Effective Overburden Pressure, Excess Pore Pressure and Settlement Profile (Bjerrum et al, 1969)

The site was layered by 13 m of fill consisted of sawdust and sandy organic mud reclaimed more than 70 years ago followed by 27 m of soft clay overlaying bedrock (Figure 4.8). Small excess pore water pressure was recorded before piling. Two years after pile installation, remote ground surface was found to have settled about 70 mm (Figure 4.8). The measured values of maximum dragload and pile shortening were 2450 kN and 13.8 mm respectively

The unit weights of fill and clay were back analyzed from the overburden pressure distribution reported by Bjerrum et al (1969). The water table was assumed at 2 m below ground surface. The only known information on the fill was its composition. The β value of 0.35 was assumed for the fill. The clay layer was assumed to be normally consolidated with a β of 0.22. The excess pore pressure at the end of the test was not reported. Since the fill was placed more than 70 years ago, the change in excess pore water pressure was likely to be small. Hence the effective stress variation during the 2-year test period was neglected.

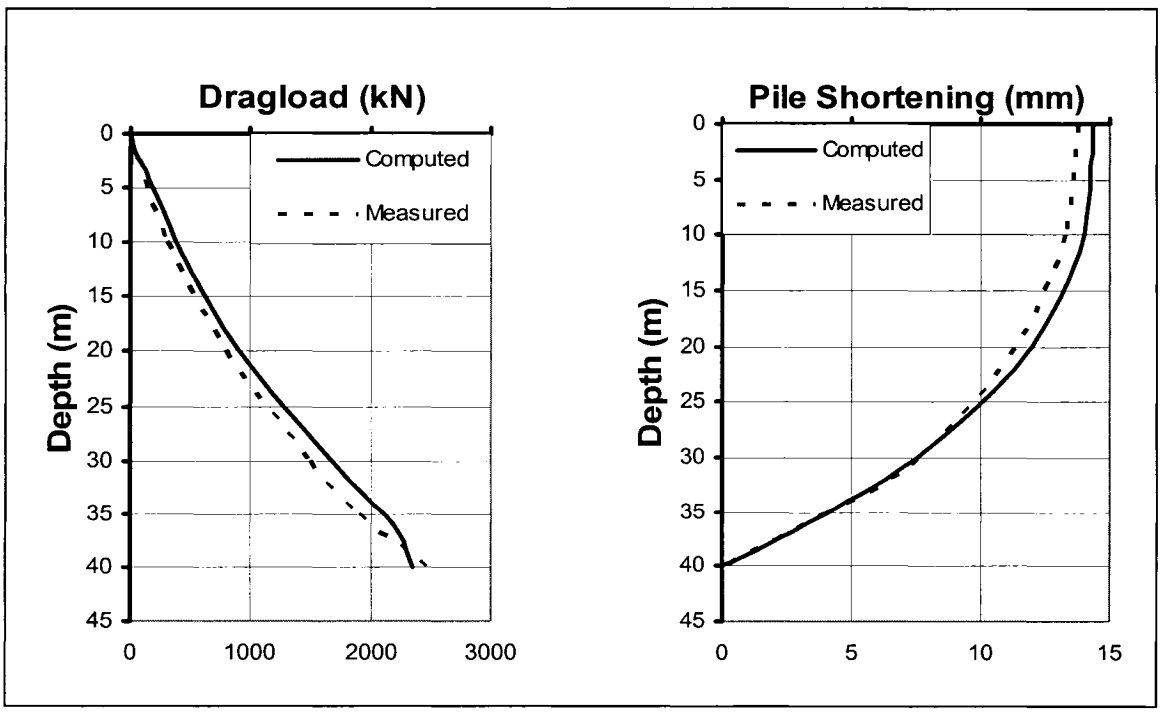

Figure 4.9: Case Study 3: Comparison of Dragload and Pile Shortening Distribution

The distribution of computed dragload and pile shortening are shown in Figure 4.9 along with the measured values. Generally good agreement has been obtained between the computed and measured data. The maximum computed dragload is 2350 kN, which compares well with the measured value of 2450 kN. The neutral point was located at the pile tip as expected for end bearing pile.

4.3.4 Case Study 4: Centrifuge Model Test on Pile Group (Shibata et al 1982)

Shibata et al (1982) conducted a series of laboratory tests to study the development of negative skin friction on vertical and battered piles and pile groups. The present study, however, confined to the case of uncoated vertical nine-pile group test. The instrumented model piles were steel tubes of length 700 mm with an outer diameter of 60 mm and a wall thickness of 1.2 mm. The piles were installed in a three by three square configuration at a centre to centre spacing of 2.5 times the pile diameter. All piles were end-bearing, installed in a testing chamber with an inner diameter of 1486 mm and a depth of 1000 mm. The 700 mm thick model ground was formed by kaolin slurry under self weight consolidation. A sand layer at the base of the chamber allowed downward drainage of water during consolidation. The index properties of the kaolin clay were liquid limit 52%, plastic limit 39%, clay fraction 39%, and specific gravity 2.61. After completion of the self weight consolidation, the model ground was subject to undergo settlement by a surface loading of 20 kPa applied by air pressure.

Table 4.2: Case Study 4: Parameters of Soil and Centrifuge Pile Group (Shibata et al, 1982)

L =	700 mm	E_s =	150 kPa
d =	60 mm	E_p =	210 GPa
s =	2.5 D	Δp =	20 kPa
t =	1.2 mm	S_0 =	65 mm

To perform the analysis, the model clay layer was assumed to be consisted of ten sub-layers, each having a set of model parameters. Several researchers had previously assumed a wide range (25 – 200 kPa) of Young's modulus E (Chow et al, 1996, Teh, 1995, Jeong et al, 2004). However, an average soil modulus of 150 kPa (Jeong et al, 2004) was found pertinent from the consideration of 65 mm of measured soil settlement under surface load of 20 kPa. Further, it was assumed appropriate to employ a linear increasing variation in soil modulus with depth along the pile shaft as suggested by Randolph, (1978), Kraft et al, (1981) and Guo (2000). Hence, in this research, the soil modulus was assumed to vary linearly from zero at the surface to 300 MPa at the bottom of the clay layer giving an average value of 150 kPa. Accordingly, the Shear modulus of soil for each apparent sub-layer was calculated by taking Poisson's ratio of soil $\nu_s = 0.3$. For the determination of limiting shear stress, the β value of 0.18, as reported by Shibata et al, (1982), was employed.

Table 4.3 summarizes dragloads and group effects computed from the present analysis, the numerical results reported by other researchers, and the experimental measurements of Shibata et al (1982). The computed dragloads compared well with the corresponding measured values with a scatter of only 2 to 7 %, depending on the position of the pile in the group (Table 4.8 a). But earlier researchers obtained a variation of as high as 21% from the measured values.

Shibata et al (1982) reported measured group effects of 13 – 28% for the piles in the group (Table 4.8 b). The present analysis predicted a group effect of 16 – 33 % offering a good agreement with the measurement. Jeong et al (2004) computed a group effect of only 7 – 15% from slip analysis by a commercial finite element package ABAQUS. Jeong et al (1997), on the other hand, reported very large group effects (50 – 85%) from the continuum analysis. Obviously, the present analysis offered a very reasonable prediction.

Table 4.3: Case Study 4: Comparison of Results of the Centrifuge Pile Group (Shibata et al, 1982)

(a) Comparison of Dragloads

References	Centre Pile		Perimeter pile		Corner Pile	
	Dragload (N)	Error (%)	Dragload (N)	Error (%)	Dragload (N)	Error (%)
Shibata et al 982:Measured	294	0	347	0	355	0
Shibata et al 1982: Predicted	242	-18	275	-21	303	-15
Chow et al 1990	317	8	356	3	378	6
Chow et al 1996	308	5	372	7	384	8
Teh et al 1995	245	-17	323	-7	323	-9
Jeong et al 2004	297	1	314	-10	325	-8
Present Study	278	-5	321	-7	349	-2

(b) Comparison of Group Effects

	Dragload single pile	Group effect (%) = (Psingle-P)/Psingle *100		
	N	Centre Pile	Perimeter Pile	Corner Pile
Shibata et al 1982:Measured	410	28	15	13
Shibata et al 1982: Predicted	410	41	33	26
Jeong et al 1997	-	85	60	50
Jeong et al 2004	349	15	10	7
Present Study	417	33	23	16

4.3.5 Case Study 5: Field Test on Full Scale Pile Group (Little, 1994)

Little (1994) reported field measurements of two pile groups (end-bearing and friction) driven in normally consolidated estuarine clay on the south side of the Fourth Estuary in Scotland. The parameters of pile and soil are given in Table 4.4. Each group consists of nine piles in 3 x 3 square fashions with a spacing of 4.0 times the pile diameter. The piles were concrete piles having a diameter of 406 mm. The end-bearing pile group of

length 20.8 m was driven to rest on a gravel layer, while the embedded length of the friction pile group was 20.4 m. After full dissipation of excess pore water pressure due to driving, an embankment loading of 40 kPa was applied on the top of the clay. The ground settlement at the end of primary consolidation was measured at 180 mm. The measured dragloads on the centre piles were 202 and 187 kN for end-bearing and friction piles, respectively.

Table 4.4: Case Study 5: Pile and Soil Parameters of Full Scale Concrete Pile Group (Little, 1994)

L =	20.4 m, friction pile	E_s =	3.35 MPa
	20.8 m, end-bearing pile	E_p =	10 GPa
d =	406 mm	Δp =	40 kPa
s =	4.0 D	S_0 =	180 mm

A β value of 0.2 was reported by Little (1994). An average value of Young's modulus E of 3.35 MPa for the clay layer was back-analyzed from the ground settlement of 180 mm under surface loading of 40 kPa. A linear distribution of Young's modulus was adopted with a zero value at the top of the soil surface to 6.70 MPa at the pile toe. The Young's modulus of concrete was assumed 10 GPa.

Table 4.5 shows both measured and computed dragloads for the centre pile and the normalized group effects [($dragload_{corner\ pile}$ – $dragload_{centre\ pile}$)/$dragload_{corner\ pile}$)], since the dragload for a single pile was not reported. The normalized group effects reported by Jeong et al (1997) through elastic analysis are interpolated for the present pile spacing. The larger normalized group effect and hence smaller dragload at centre pile was estimated from the elastic approach. The predictions from Shibata et al (1982) also over-estimated normalized group effects. However, smaller normalized group effects (14 – 16%) were computed from the present approach, which match reasonably with the field observations (18 – 14%) for end-bearing and friction pile group. Jeong et al (2004) predicted a group effect of 15% for both the cases.

Table 4.5: Case Study 5: Comparison of Results of Full Scale Concrete Pile Group with the Field Measurements (Little, 1994)

References	Dragload for centre pile (kN)		Normalized group effect (%)	
	Friction pile	End-bearing pile	Friction pile	End-bearing pile
Measured (Little 1994)	187	202	14	18
Shibata et al 1982*	-	-	24	26
Jeong et al 1997	-	-	35	24
Jeong, et al 2004	223	347	15	15
Present Study	184	219	16	14

* Adopted from Jeong et al 2004

Figure 4.10 and 4.11 show the measured and computed distribution of dragload on a centre pile for end-bearing and friction pile group, respectively.

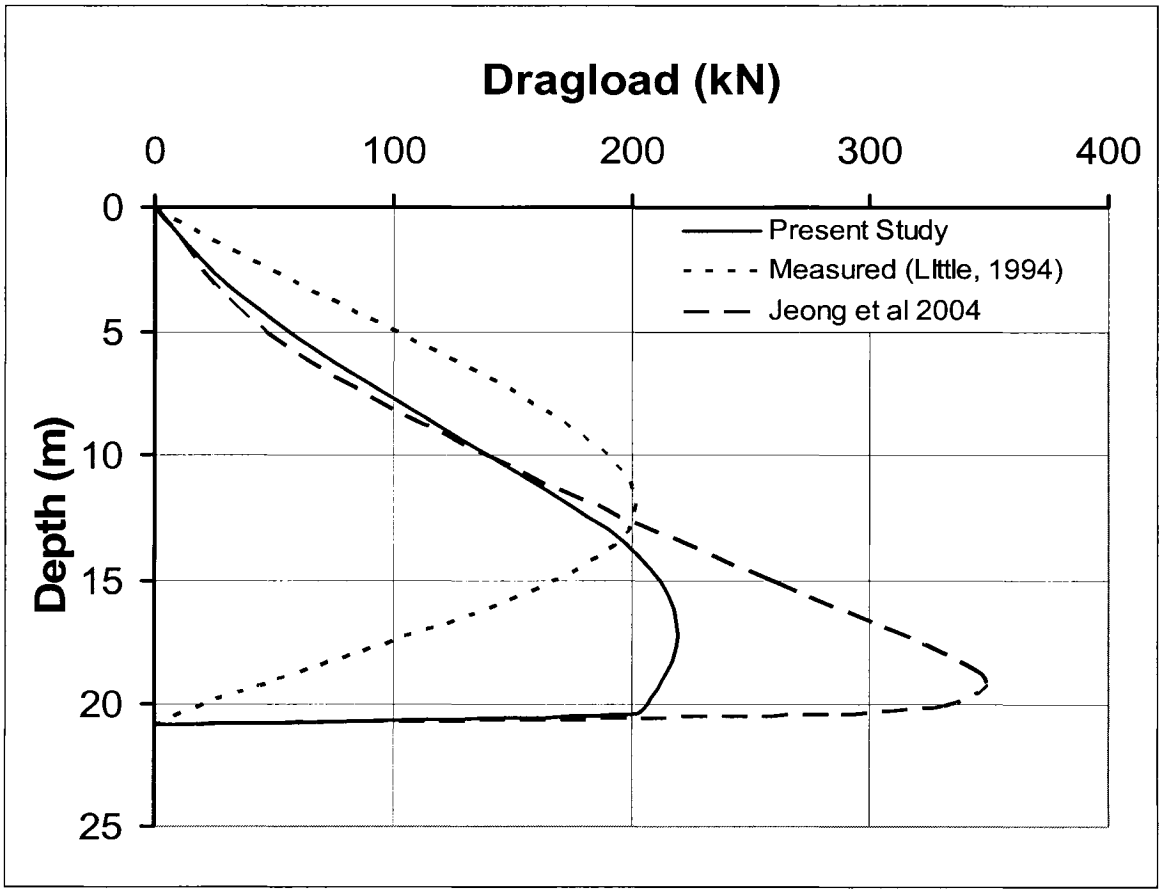

Figure 4.10: Comparison of Dragload on Centre Pile of the End-Bearing Pile Group (Little, 1994)

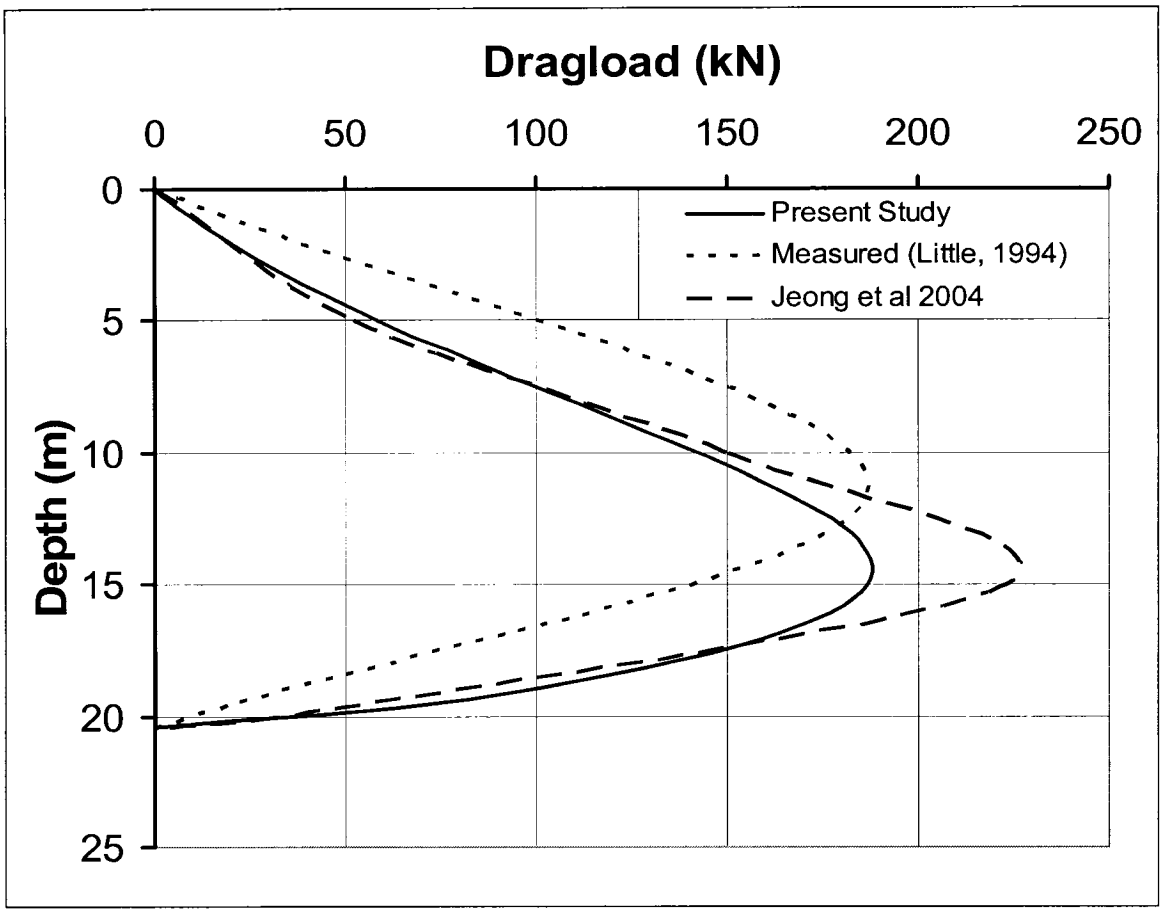

Figure 4.11: Comparison of Dragload on Centre Pile of a Frictional Pile Group (Little, 1994)

For the end-bearing pile, the measured neutral plane was not located near the pile toe, which was likely to be a reflection of significant penetration of the pile toe into the bearing layer. To compare the results for the end-bearing pile group, Young's modulus of the bearing layer was assumed ten times the value at the bottom of the clay layer. Since the so-called end-bearing pile group was not practically behaved as end bearing, the scatter is likely to be expected in the distribution of dragload between the measured value and the value computed from the theoretical end-bearing perspective. Jeong et al (2004) predicted even larger values from a finite element slip model.

For the friction pile group, the computed maximum dragload 184 kN on the centre pile compares well with the measured value 187 kN, while Jeong et al (2004) predicted

223 kN. The neutral plane was located at a depth of 55 % of pile length as per measurement for the friction pile. The computed neutral depth is 68 % showing a slight scatter. However, more variation was obtained from finite element slip model (Jeong, et al 2004). It appears from the distribution of the computed dragload (Little, 1994) that the higher position of measured neutral plane was obtained due to the fact that sufficient number of loading gauges was not installed along the pile depth, especially below the mid depth. Under these considerations, the predictions are reasonable for both end-bearing and friction piles.

4.4 RECOMMENDED PROCEDURE OF ANALYSIS

The detailed procedure of analysis of negative skin friction is intended to demonstrate by solving an example problem. Consider a pile group consisting of nine uncoated steel pipe piles driven into a stratified consolidating soil as shown in Figure 4.12.

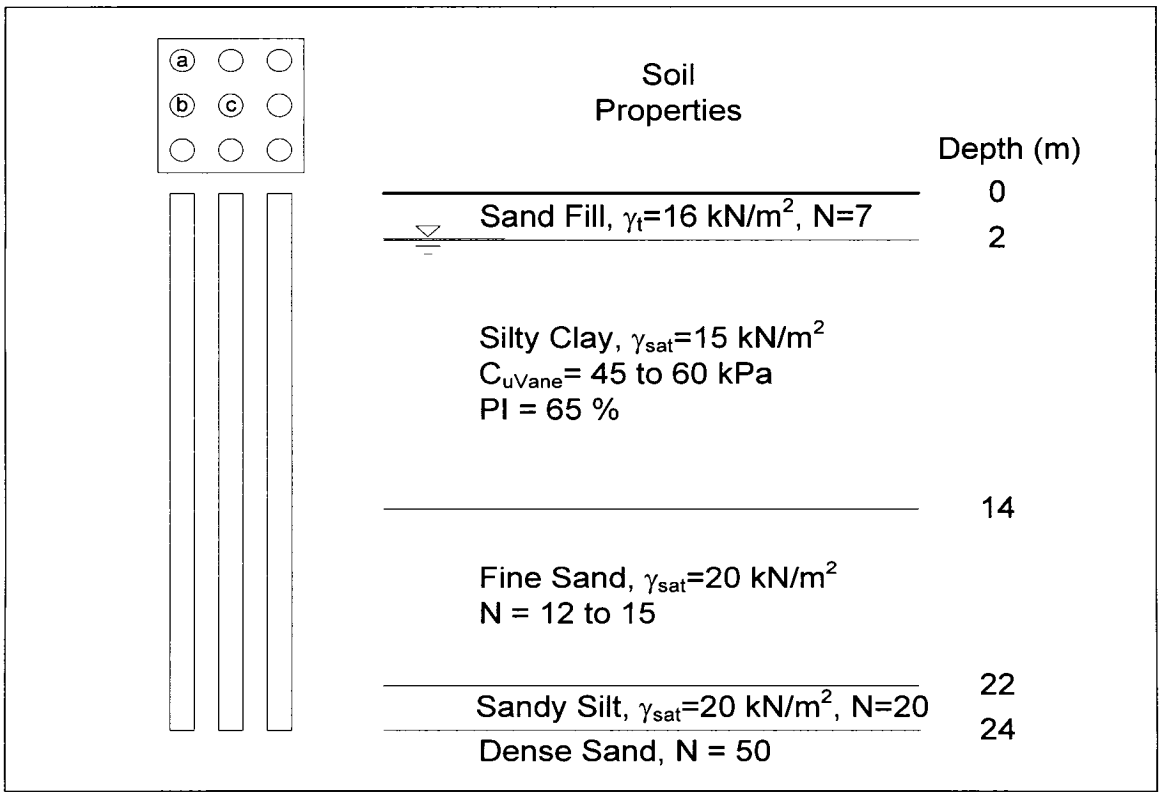

Figure 4.12: Example Problem: Pile and Soil Profile

Figure 4.12 presents also the soil profile with available soil test data such as unit weight, SPT blow count, undrained vane shear strength and plasticity index. The piles of outer diameter 610 mm with a wall thickness of 95 mm are installed in a 3 x 3 square configuration with a centre to centre spacing of three times the diameter. The water table is at 2 m from the surface. The distribution of the dragload, shear stress and pile shortening along the piles are to be determined for a surcharge of 100 kPa.

Let us consider that the soil surrounding the pile group is represented by 8 number of intermediate soil layers. Accordingly, the available soil properties are prepared in Table 4.6.

Table 4.6: Example Problem: Preparation of Available Soil Properties

Soil Type	Depth (m)		γ_t	γ_{sat}	N	δ/ϕ'	c_u	PI	ν'	σ'_v
	From	To	(kN/m^3)	(kN/m^3)			(kPa)	(%)		(kPa)
Existing Fill	0	2	16	-	7	0.7	-	-	0.25	0
Silty Clay	2	5	-	15	-	-	45	65	0.25	33
	5	8	-	15	-	-	50	65	0.25	58
	8	11	-	15	-	-	55	65	0.25	90
	11	14	-	15	-	-	60	65	0.25	106
Fine Sand	14	18	-	20	12	0.7	-	-	0.25	127
	18	22	-	20	15	0.7	-	-	0.25	147
Sandy silt	22	24	-	20	20	0.7	-	-	0.25	171
Dense sand	24	-	-	20	50	0.7	-	-	0.25	201

For each soil layer, the limiting skin friction of soil τ_f, and the soil shear modulus G are computed in Table 4.7 and 4.8 as explained in section 3.6.4. The consolidation settlement at each layer is also calculated in these tables as explained in section 3.3.

Table 4.7: Example Problem: Determination of Parameters of Non-Cohesive Layers

Depth	σ'_v	N_{cor}	D_r	ϕ'	Δp	$\sigma'_{v(final)}$	K_s	tan δ	β	τ_f	G	S
(m)	(kPa)		(%)	(deg)	(kPa)	(kPa)				(kPa)	(MPa)	(mm)
1.0	16	7	40	34.0	100	116	0.88	0.44	0.39	45	39	24
16.0	115	11	50	35.5	100	215	0.84	0.46	0.39	83	60	4
20.0	155	13	58	36.7	100	255	0.80	0.48	0.39	99	66	2
23.0	186	16	61	37.2	100	286	0.79	0.49	0.39	111	80	0
24.0	196	38	90	41.5	100	296	-	-	-	-	179	0

Note: Ultimate bearing capacity of dense sand & gravel = 24 MPa (Equation 3.45).

Table 4.8: Example Problem: Determination of Parameters of Cohesive Layers

Depth	σ'_v	$c_{u(cor)}$	OCR	P_c'	Δp	$\sigma'_{v(final)}$	OCR_{final}	β	τ_f	G	S
(m)	(kPa)	(kPa)		(kPa)	(kPa)	(kPa)			(kPa)	(MPa)	(mm)
3.5	40	32.45	4.87	194	100	140	1.38	0.26	36	19	20
6.5	55	36.05	3.67	203	100	155	1.31	0.25	39	22	15
9.5	71	39.66	3.04	215	100	171	1.26	0.25	42	24	11
12.5	86	43.26	2.64	228	100	186	1.22	0.24	45	26	7

A computer program is developed in *Mathematica* programming code to perform the analysis of negative skin friction. The analysis method is based on nonlinear finite element technique since hyperbolic load transfer approach is incorporated. The non linear finite element analysis is performed using the Newton-Raphson method to implement the incremental iterative procedure. A typical flowchart of the analysis of negative skin friction is shown in Figure 4.13.

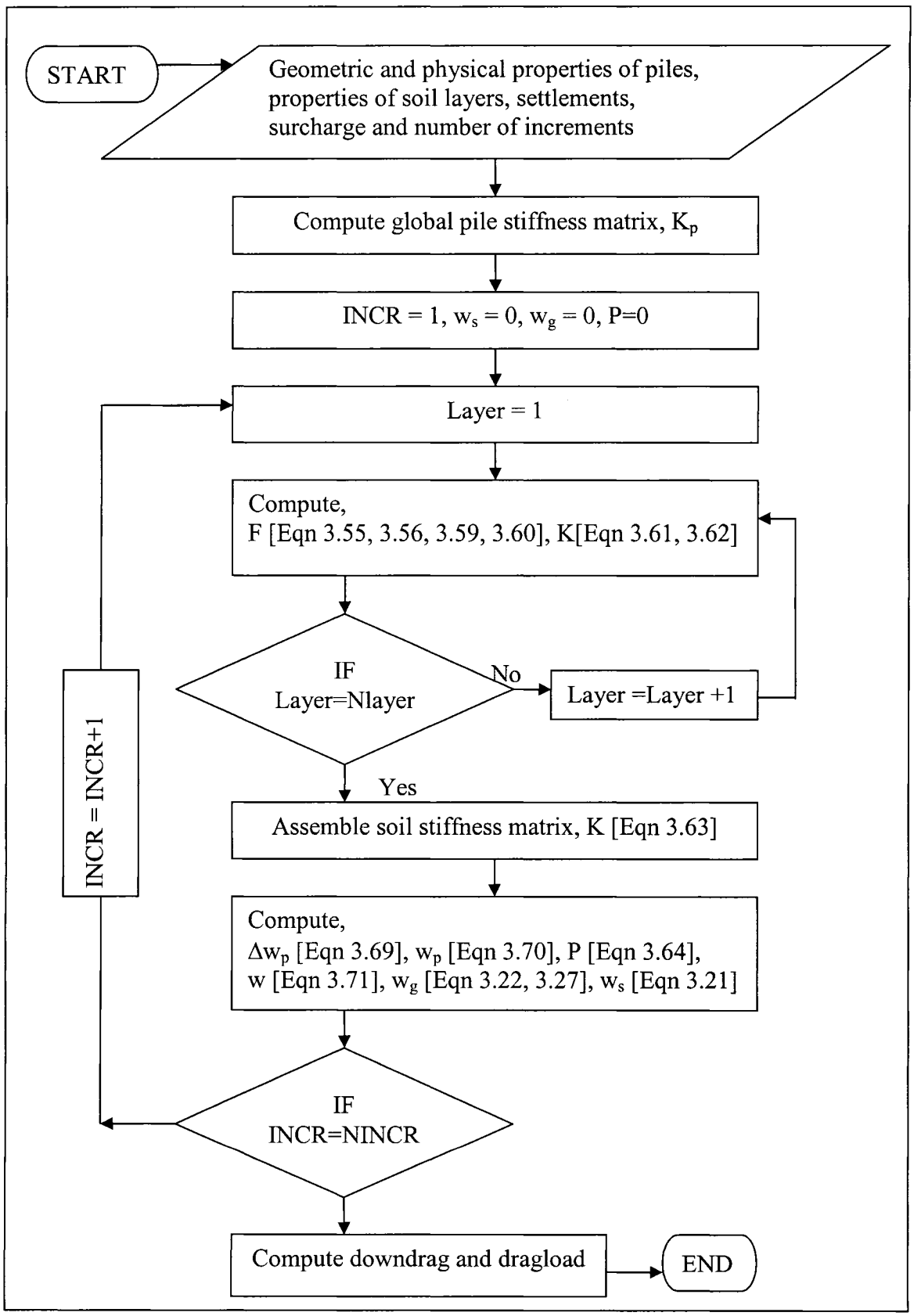

Figure 4.13: Flow Chart for Simplified Nonlinear Analysis of Negative Skin Friction

The results of the analysis as obtained from the computer program are graphically represented in Figure 4.14 to Figure 4.15. The result of a single pile is also presented with the results of group piles for the purpose of comparison. Thus demonstrated how the proposed procedure can be used for practical analysis of negative skin friction on piles in consolidating soil.

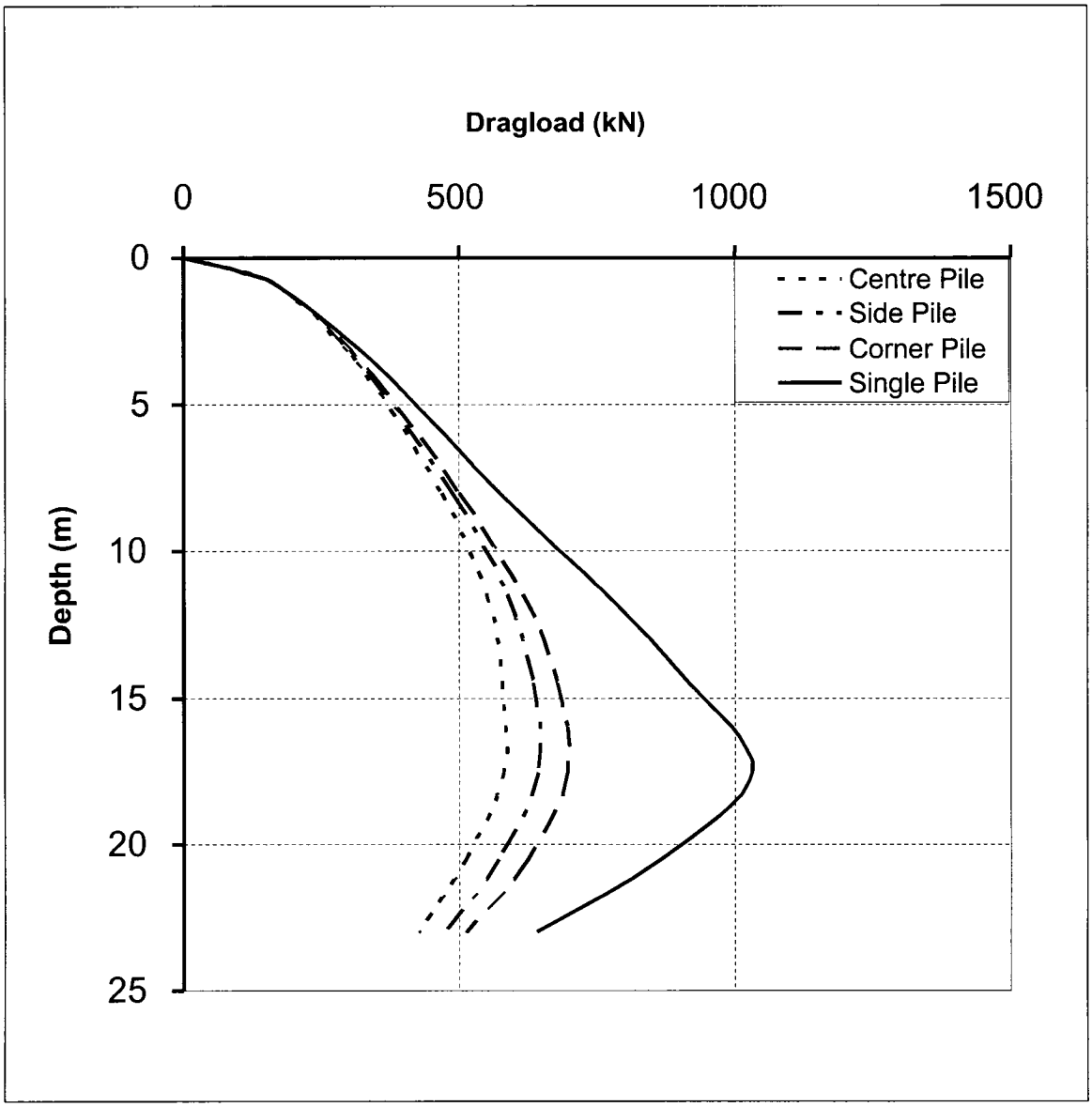

Figure 4.14: Example Problem: Distribution of Dragload in Single and Group Piles

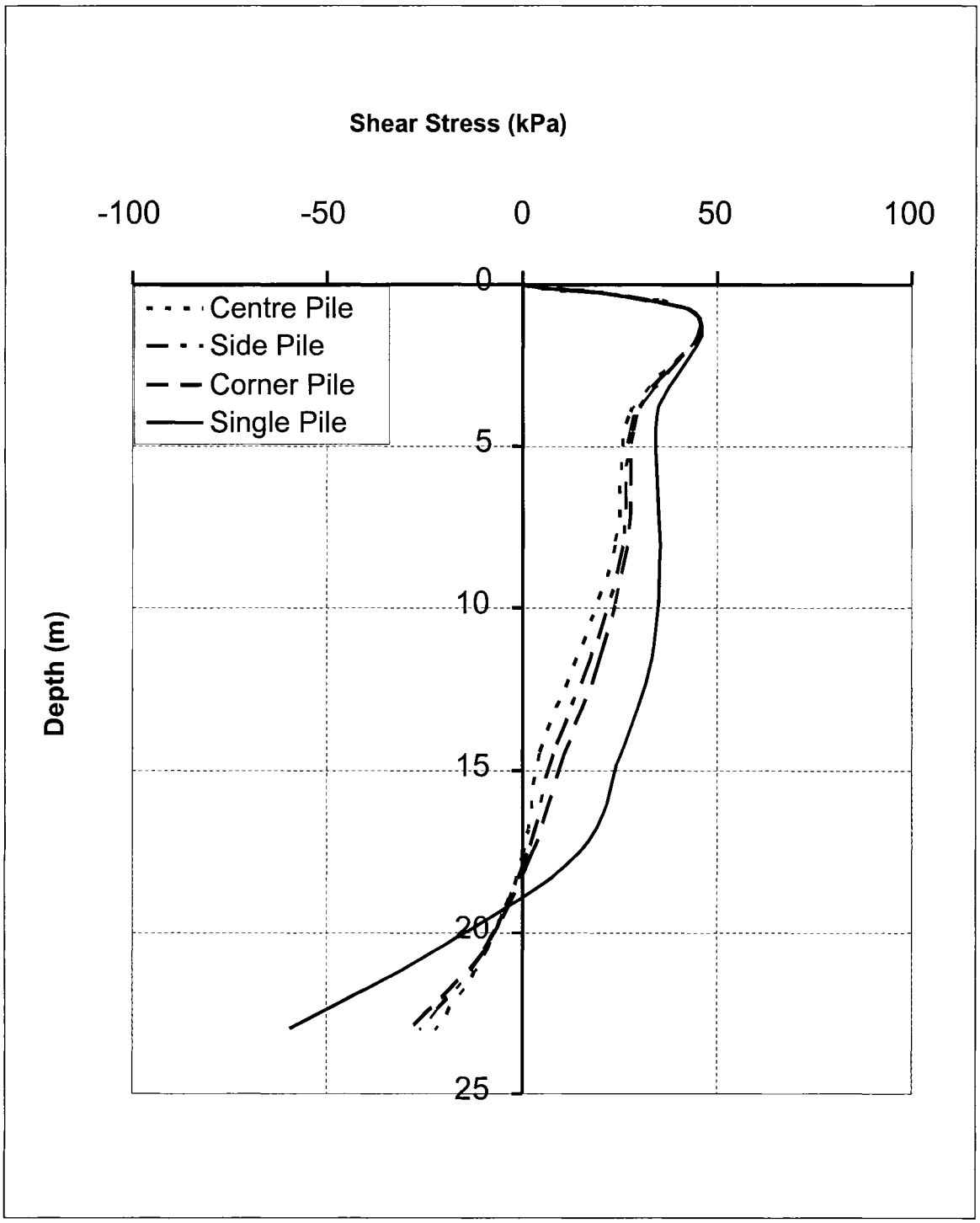

Figure 4.15: Example Problem: Distribution of Shear Stress in Single and Group Piles

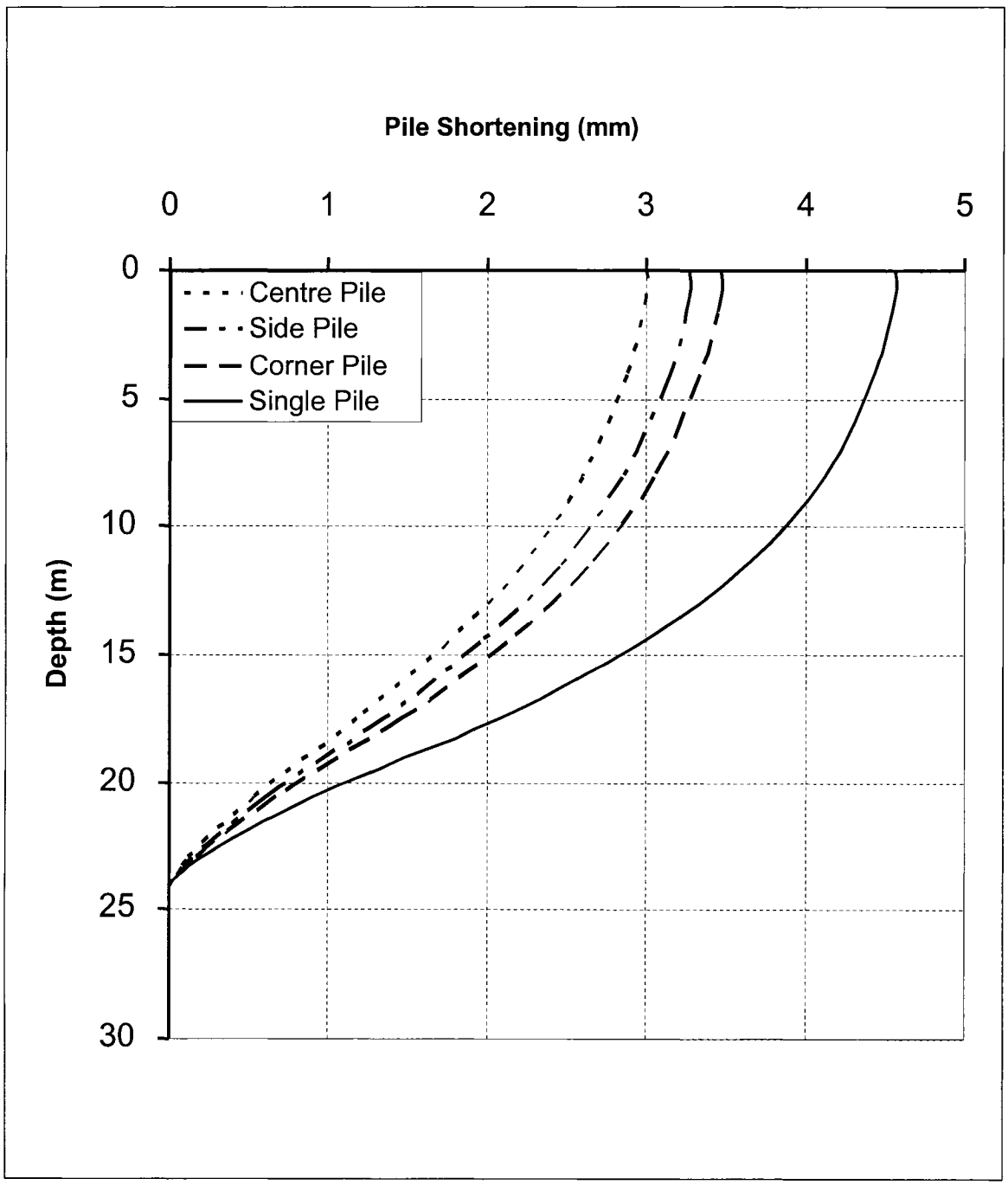

Figure 4.16: Example Problem: Distribution of Pile Shortening in Single and Group Piles

CHAPTER 5
CONCLUSIONS AND RECOMMENDATIONS

4.1 GENERAL

Literature review has demonstrated a large scatter among the results of analysis of piles under negative skin friction. These may be attributed to the use of different assumptions of soil properties and the load transfer mechanism employed in different methods. Besides, the methods are either complex and impractical or not capable of predicting solutions for multilayered soil. The present study is vested with the aim of achieving a simple and fundamentally consistent nonlinear analysis and developing a finite element procedure for negative skin friction. Finally, computer software is developed for analysis of negative skin friction on single or group piles using conventional soil test data as input.

4.2 CONCLUSIONS

Based on the results of the present investigation, the following conclusions can be drawn:

1. The finite element technique in conjunction with hyperbolic load transfer mechanism has been proved to be an acceptable numerical model to analyze the negative skin friction on single and group piles.

2. A nonlinear hyperbolic approach as proposed in the present study predicts a reasonably accurate dragload, whereas it is normally overestimated from analytical or finite element elastic analysis and underestimated from finite element slip analysis.

3. While the elastic analytical or finite element analysis computes extremely large group effects for pile groups and the slip finite element analysis shows extremely smaller group effects, the present hyperbolic approach provides a balanced and reasonable group effects.

4. The proposed procedure of analysis is rigorous as it simulates nonlinear soil behavior, although, it preserves simplicity by using elastic soil properties and laboratory soil test data as input.

5. The iterative finite element computer program developed to perform the analysis will assist the designer to predict negative skin friction on piles and pile groups in homogeneous and multilayered soil deposits with reasonable accuracy. The flowchart of the analysis is also presented for the computer programmers to develop software in any programming language.

6. The results of the proposed procedure compared well with full scale pile test, centrifuge model test and other theoretical and experimental studies for single piles and group piles.

7. The proposed approach is proved to be equally suitable to predict negative skin friction on single or group piles, friction or end bearing piles, in cases of both homogeneous and stratified soil.

4.3 RECOMMENDATIONS FOR FURTHER RESEARCH

1. The present study can be extended to investigate the development of negative skin friction with time for different sequence of the surcharge loading and the structural loading at the pile top.

2. The present investigation could be extended to extensive examination of the effect of pile cap rigidity on the development of negative skin friction.

3. A parametric study could be performed with the use of present approach to investigate the physical factors influencing pile soil behavior.

4. Further studies are required to examine the effect of negative skin friction on battered piles.

5. The present model could be investigated further for piles socket into rocks.

6. The present model of negative skin friction analysis can be combined with a similar model developed for conventional pile capacity in order to establish a unified pile design procedure in consolidating soil.

7. The model developed for pile soil interaction in the present study may be investigated further to be used for other earth related structure involving soil structure interaction problems.

REFERENCES

1. Acar, Y. B., Avent, R. R. and Taha, M. R. (1994), "Downdrag on Friction Piles: A Case History," Proceedings of the Conference on Vertical and Horizontal Deformations of Foundations and Embankments, ASCE, College Station, Texas, pp. 986-999.

2. Alonso, E. E., Josa, A. and Ledsma, A. (1984), "Negative Skin Friction on Piles: A Simplified Analysis and Prediction Procedure," Geotechnique, Vol. 34, No. 3, pp. 341-357.

3. Bjerrum, L (1974), Problems of Soil Mechanics and Construction on Soft Clays," Norwegian Geotechnical Institute, Publication No. 110, Oslo.

4. Bjerrum, L., Johannessen, I. J. and Eide, O. (1969), "Reduction of Negative Skin Friction on Steel piles to Rock," Proc. of the 7th Int. Conf. on Soil Mechanics and Foundation Engineering, Mexico, Vol. 2, pp. 27-34.

5. Brackley, I. J. and Steffen, O. K. H. (1984), "Failure of a Piled Foundation," Proceedings of the 8th Conference for Africa on Soil Mechanics and Foundation Engineering, Harare, pp. 189-193

6. Brand, E. W. and Luangdilok, N. (1975), "A Long-Term Foundation Failure Caused by Downdrag on Piles," 4th Southeast Asian Conference on Soil Engineering, Kuala Lumpur, Malaysia, pp. 4.15-4.24.

7. Briaud, J. L., Jeong, S. and Bush, R. (1991), "Group Effect in the Case of Downdrag," Proceedings of the Geotechnical Engineering Congress, ASCE, Boulder, Colorado, pp. 505-518.

8. Budhu, M. (2000) "Soil Mechanics and Foundations", John Wiley & Sons, Inc., New York, 587p.

9. Burland, J. B. (1973), "Shaft Friction of Piles in Clay: A Simple Fundamental Approach," Ground Engineering, Foundation Publications Ltd., London, Vol. 6, No. 3, pp. 30-42.

10. Canadian Foundation Engineering Manual (1992), 3rd Edition, Canadian Geotechnical Society, Technical Committee on Foundations, 512p.

11. Caputo, V. and Viggiani, C. (1984), "Pile Foundation Analysis: A Simple Approach to Nonlinearity Effects," Rivista Italiana di Geotecnica, Vol. 18, No. 2, pp. 32-51.

12. Carrubba, P (1997), "Skin Friction on Large-Diameter Piles Socketed into Rock," Canadian Geotechnical Journal, Vol. 34, No. 2, pp. 230-240.

13. Castelli, F. and Maugeri, M. (2002), "Simplified Nonlinear Analysis for Settlement Prediction of Pile Groups," Journal of Geotechnical and Geoenvironmental Engineering, ASCE, Vol. 128, No. 1, pp. 76-84.

14. Chan, K. S., Karasudhi, P. and Lee, S. L. (1974), Force at a Point in the Interior of a Layered Elastic Half Space," International Journal of Solids and Structures, Vol. 10, pp. 1179-1199.

15. Chan, S. F. (1977), "Load Transfer Characteristics of an Instrumented Steel pile in a Fill Ground,' The 5th South Asian Conference on Soil Engineering, Bankok, Thailand, pp. 153-163.

16. Chow, Y.K., Chin, J. T. and Lee, S. L. (1990), "Negative Skin Friction on Pile Groups," International Journal for Numerical and Analytical Methods in Geomechanics, Vol. 14, No. 2, pp.75-91.

17. Chow, Y. K., Lim, C. H. and Karunaratne, G. P. (1996), "Numerical Modeling of Negative Skin Friction on Pile Groups," Computers and Geotechnics, Vol. 18, No. 3, pp. 201-224.

18. Clough, W. and Duncan, J. M. (1971), "Finite Element Analysis of Retaining Wall Behavior," Journal of the Soil Mechanics and Foundations Division, ASCE, Vol. 97, No. SM12, pp. 1657-1673.

19. Comodromos, E. M, Anagnostopoulos, C. T. and Georgiadis, M. K. (2003), Numerical Assessment of Axial Pile Group Response based on Load Test," Computers and Geotechnics, Vol. 30, No. 6, pp. 505-515.

20. Endo, M., Minou, A., Kawasaki, T. and Shibata, T. (1969), "Negative Skin Friction Acting on Steel Pipe Pile in Clay," Proc. of the 7th Int. Conf. on Soil Mechanics and Foundation Engineering, Mexico, Vol. 2, pp. 85-92.

21. Ergun, M. U. and Sonmez, D. (1995), "Negative Skin Friction from Surface Settlement Measurements in Model Group Tests," Canadian Geotechnical Journal, Vol. 32, No. 6, pp. 1075-1079.

22. Esmail, H. (1996), "Neutral Plane of Single Piles in Clay Subjected to Surcharge Loading," M.A.Sc. Thesis, Concordia University, Montreal, Quebec, Canada

23. Fellenius, B. H. (1989), "Unified Design of Piles and Pile Groups," Transportation Research Record, No. 1169, National Research Council, Washington, pp. 75-82.

24. Fellenius, B. H. (1999), "Piling Terminology," http://www.geoforum.com/info/pileinfo/terminology.asp

25. Fox, E. N. (1948), "The Mean Elastic Settlement of a Uniformly Loaded Area at a Depth below Ground Surface, Proc. of the 2nd Int. Conf. on Soil Mechanics and Foundation Engineering, Rotterdam, pp. 129-132.

26. Goh, A. T. C., Teh, C. I. and Wong, K. S. (1997), "Analysis of Piles Subjected to Embankment Induced Lateral Soil Movements," Journal of Geotechnical and Geoenvironmental Engineering, ASCE, Vol. 123, No. 9, pp. 792-801.

27. Guo, W. D. (2000), "Vertically Loaded Single Piles in Gibson Soil," Journal of Geotechnical and Geoenvironmental Engineering, ASCE, Vol. 126, No. 2, pp. 189-193.

28. Hanna, A.M., and Sharif A. (2006), "Drag force on a single pile in clay subjected to surcharge loading,"ASCE, International Journal of Geomechanics, Vol.6, No.2.

29. Hepworth, R. C. (1993), "Negative Skin Friction due to Wetting of Unsaturated Soil," Proceedings on Unsaturated Soil, ASCE National Convention, Dallas, Texas, pp. 44-53.

30. Hirayama, H. (1991), "Pile Group Settlement Interaction Considering Soil Non-Linearity," Computer Methods and Advances in Geomechanics, edited by G. Beer, J. R. Booker & J. P. Carter, A. A. Balkema, Rotterdam, Netherlands, Vol. 1, pp. 139-144.

31. Holtz, W. G. and Gibbs, H. J. (1979), "SPT and Relative Density of Coarse Sand-Discussion" Journal of Geotechnical Engineering, ASCE, Vol. 105, No. 3, pp. 439-441.

32. Imai, T. and Tonouchi, K. (1982), "Correlation of N value with S-wave Velocity and Shear Modulus," Proceedings of ESOPT - 2, Amsterdam, Vol. 1, pp. 67-72.

33. Indraratna B., Balasubramaniam A. S., Phamvan P. and Wong Y. K. (1992), "Development of Negative Skin Friction on Driven Piles in Soft Bangkok Clay," Canadian Geotechnical Journal, Vol. 29, No. 3 pp. 393-404.

34. Ito, T. and Matsui, T. (1976), "Negative Skin Friction Acting on Piles", Proc. of the 5th Int. Conf. on Soil Mechanics and Foundation Engineering, Budapest, pp. 297-311.

35. Jamiolkowski, M. Ladd, C. C., Germaine, J. T., and Lancellotta, R. (1985), "New Developments in Field and Laboratory Testing of Soils," Proc. of the 11th Int. Conf. on Soil Mechanics and Foundation Engineering, San Francisco, Vol. 1, pp. 57-153.

36. Jeong, S., Kim, S. and Briaud, J. L. (1997), "Analysis of Downdrag on Pile Groups by the Finite Element Method," Computers and Geotechnics, Vol. 21, No. 2, pp. 143-161.

37. Jeong, S., Lee, J. and Lee, C. J. (2004), "Slip Effect at the Pile-Soil Interface on Dragload," Computers and Geotechnics, Vol. 31, No. 2, pp. 115-126.

38. Kraft, L. M, Ray, R.P., and Kagawa, T. (1981), "Theoretical t-z Curves, Journal of Geotechnical Engineering, ASCE, Vol. 107, No. 11, pp. 1543-1561.

39. Ko, H. Y., Atkinson, R. H., Goble, G. G., and Ealy, C. D. (1984), "Centrifugal Modeling of Pile Foundations", Proceedings of a Symposium on Analysis and Design of Pile Foundations, edited by J. R. Meyer, ASCE, San Francisco, pp. 80-98.

40. Kulhawy, F. H. (1984), "Limiting Tip and Side Resistance: Fact or Fallacy?" Proceedings of a Symposium on Analysis and Design of Pile Foundations, edited by J. R. Meyer, ASCE, San Francisco, pp. 80-98.

41. Kuwabara, F. and Poulos, H. G. (1989), "Downdrag Forces in Group of Piles," Journal of Geotechnical Engineering, ASCE, Vol. 115, No. 6, pp. 806-818.

42. Ladd, C. C., Foote, R., Ishihara, K., Schlosser, F. and Poulos, H. G. (1977), "Stress Deformation and Strength Characteristics," Proc. of the 9th Int. Conf. on Soil Mechanics and Foundation Engineering, Tokyo, Vol. 2, pp. 421-494.

43. Lee, C. Z. and Ng, C.W.W (2004), "Development of Downdrag on Piles and Pile groups in Consolidating Soil," Journal of Geotechnical and Geoenvironmental Engineering, ASCE, Vol. 130, No. 9, pp. 905-914.

44. Lee, C. J., Bolton, M. D. and Al-Tabbaa, A. (2002), "Numerical Modeling of Group Effects on the Distribution of Dragloads in Pile Foundations," Geotechnique, Vol. 52, No. 5, pp. 325-335.

45. Lee, C. Y. (1993), "Pile Groups Under Negative Skin Friction," Journal of Geotechnical Engineering, ASCE, Vol. 119, No. 10, pp. 1587-1600.

46. Lee, K. M. and Xiao, Z. R. (2001), "A Simplified Nonlinear Approach for Pile Group Settlement Analysis in Multilayered Soils," Canadian Geotechnical Journal, Vol. 38, No. 10, pp. 1063-1080.

47. Leung, C. F., Radhakrishnan, R. and Tan, S. A. (1991), "Performance of Precast Driving Piles in Marine Clay," Journal of Geotechnical Engineering, ASCE, Vol. 117, No. 4, pp. 637-657.

48. Lim, C. H., Chow, Y. K., and Karunaratne, G. P. (1993), "Negative Skin Friction on Single Piles in a Layered Half-Space," International Journal for Numerical and Analytical Methods in Geomechanics, Vol. 17, pp.625-645.

49. Little, J. A. (1994), "Downdrag on Piles: Review and Recent Experimentation," Proceedings of the Conference on Vertical and Horizontal Deformations of Foundations and Embankments, ASCE, College Station, Texas, pp. 1805-1826.

50. Matyas, E. L. and Santamarina, J. C. (1994), "Negative Skin Friction and the Neutral Plane," Canadian Geotechnical Journal, Vol. 31, No. 4, pp. 591-597.

51. Maugeri, M and Castelli, F (1996), "Negative Skin Friction on Piles in Layered Soil Deposits – Discussion," Journal of Geotechnical Engineering, ASCE, Vol. 122, No. 12, pp. 1020-1021.

52. Mayne, P. W. and Kulhawy, F. H. (1982), "K_0-OCR Relationships in Soil", Journal of Geotechnical Engineering Division, ASCE, Vol. 108, No. GT6, pp. 851-872.

53. Mayne, P. W. and Mitchell, J. K. (1988), "Profiling of Overconsolidation Ratio in Clays by Field Vane", Canadian Geotechnical Journal, Vol. 25, No. 1, pp. 150-157.

54. Mesri, G. (1989), "A Re-evaluation of $s_{u(mob)} = 0.22\sigma_p'$ Using Laboratory Shear Tests", Canadian Geotechnical Journal, Vol. 26, No. 1, pp. 162-164.

55. Meyerhof, G. G. (1956), "Penetration Tests and Bearing Capacity of Cohesionless Soils," Journal of Geotechnical Engineering Division, ASCE, Vol. 82, No. GT1, pp. 1-19.

56. Mindlin, R. D., (1936), "Force at a Point in the Interior of a Semi-Infinite Solid," Physics, Vol. 7, pp. 195-202.

57. Poorooshasb, H. B., Alamgir, M., and Miura, N. (1996), "Negative Skin Friction on Rigid and Deformable Piles," Computers and Geotechnics, Vol. 18, No. 2, pp. 109-126.

58. Poulos, H. G. (1994), "Settlement Prediction for Driven Piles and Piles Groups," Proceedings of the Conference on Vertical and Horizontal Deformations of Foundations and Embankments, ASCE, College Station, Texas, pp. 1629-1649

59. Poulos, H. G. (1989), "Pile Behaviour – Theory and Application," Geotechnique, Vol. 39, No. 3, pp. 365-415.

60. Poulos, H.G. and Davis, E. H. (1980), "Pile Foundation Analysis and Design," John Wiley and Sons, New York.

61. Poulos, H. G. and Davis, E. H. (1975), "Prediction of Downdrag Forces in End-Bearing Piles," Journal of the Geotechnical Engineering Division, Vol. 101, No. 2, pp. 189-204.

62. Poulos, H. G. and Davis, E. H. (1972), "The Development of Negative Friction with Time in End-Bearing Piles," Australian Geomechanics Journal, Vol. C2, No. 1, pp. 11-20.

63. Poulos, H. G. and Mattes, N. S. (1969), "The Analysis of Downdrag in End-Bearing Piles," Proc. of the 7th Int. Conf. on Soil Mechanics and Foundation Engineering, Mexico, Vol. 2, pp. 203-209.

64. Shen, W. Y. and Teh, C. I. (2002), "A Variational Solution for Downdrag Force Analysis of Pile Groups," The International Journal of Geomechanics, ASCE, Vol. 2, No. 1, pp. 75-91.

65. Shibata, T., Sckiguchi, H. and Yukitomo, H. (1982), "Model Test and Analysis of Negative Skin Friction Acting on Piles," Soils and Foundations, Vol. 22, No. 2, pp. 29-39.

66. Teh, C. I. and Wong, K. S. (1995), "Analysis of Downdrag on Pile groups," Geotechnique, Vol. 45, No. 2, pp. 191-207.

67. Terzaghi, K. and Peck, R. B. (1948), "Soil Mechanics in Engineering Practice", 1st Edition, John Wiley and Sons, New York, pp. 469-477.

68. Timoshenko, S. P. and Goodier, J. N. (1970), "Theory of Elasticity", 3rd Edition, McGraw-Hill Book Company, New York, pp.398-409.

69. Walker, L. K. and Darvall, P. L. (1970), "Some Aspects of Dragdown on Piles," Proc. 2nd South-East Asian Conference on Soil Engineering, Singapore, pp. 121-137.

70. Wong, K. S. and Teh, C. I. (1995), "Negative Skin Friction on Piles in Layered Soil Deposits," Journal of Geotechnical Engineering, ASCE, Vol. 121, No. 6, pp. 457-465.

71. Zeevaert, L. (1959), "Reduction of Point Bearing Capacity of Piles Because of Negative Friction," Proc. of the 1st Pan-American Conf. on Soil Mechanics and Foundation Engineering, Mexico, Vol. 3, pp. 1145-1152.

APPENDIX

Computer Program PILES-NSF

Analysis of Negative Skin Friction on Piles and Pile Groups

(developed in mathematica programming code)

```
(* Program for NSF analysis
 for single or group piles *)

ClearAll[eL, ρ, l, k, ks, kp, sgmnt, n, i, j, Cf, jj, jjj, temp1,
  temp2, temp3, temp4, temp5, Kp, As, s, wp, wc, w, Δwp, kb, Ks, Kp,
  gs, fs, gb, Rhs, Ps, wp, df, fs, τ, τs, dfs, zlp, S, P, pu, cs];
<< Statistics`DescriptiveStatistics`
<< Graphics`MultipleListPlot`
<< Utilities`FilterOptions`
<< Graphics`Legend`
<< Graphics`Common`GraphicsCommon`
```

(* Input Data *)

```
n = 9; (* No. of piles *)
lp = 24; (* total pile length in m*)
r0 = 0.61 / 2; (* Outer radius in m *)
s = 5 * r0; (* Pile spacing *)
x = {0, s, 2 * s, 0, s, 2 * s, 0, s, 2 * s};
(* x coordinates of piles, may be left as it is for sigle pile *)
y = {0, 0, 0, s, s, s, 2 * s, 2 * s, 2 * s};
(* y coordinates of piles, may be left as it is for sigle pile*)
tp = 0.0095;
(* wall thickness in m of pile, put NA in case of solid pile *)
ec = NA; (* end condition, oe for open ended, NA for others *)
Epm = 200 * 10^9; (* Young's Modulus of Pile material *)
layer = 8; (* No. of intermediate soil layers*)
d = {0, 2, 5, 8, 11, 14, 18, 22, 24};
(* depth in m from piletop to the top of each successive layers *)
νst = 0.25; (* Poisson's ratio of intermediate layers *)
νs = {νst, νst, νst, νst, νst, νst, νst, νst};
(* each intermediate layer *)
gs = {39, 19, 22, 24, 26, 60, 66, 80} * 10^6;
(* Profile of shear modulus in the intermediate layers *)
fs = {45, 36, 39, 42, 45, 83, 99, 111} * 10^3;
(* Unit limiting shearing strength at shaft *)
νb = 0.3; (* Poison's ratio below pile toe*)
gb = 179 * 10^6; (* Shear modulus below pile toe *)
qb = 24 * 10^6;  (* Bearing capacity below pile toe*)
Sz = {25, 24, 21, 16, 11, 7, 4, 2, 0, 0} / 1000; (* Settlement Profile *)
```

(* General Calculations *)

```
Rf = 0.9;  (* Hyperbolic constant *)
m = layer + 2; (* No. of nodes per pile *)
meanνs = Mean[νs];
```

```
nNode = n * m; sNode = nNode - n;
temp1 = (j - 1) * n + jj; temp2 = (j - 1) * n + jjj;
vs = Join[{0}, vs];
gs = Join[{0}, gs];
fs = Join[{0}, fs];
If[n = 1, inc = 200, inc = 50];
z = Table[0, {i, m}]; l = Table[0, {i, m}]; As = Table[0, {i, m}];
S = Table[0, {i, nNode}]; eEs = Table[0, {i, m - 1}];
s = Table[0, {i, n}, {j, n}]; wc = Table[0, {i, nNode}];
wp = Table[0, {i, nNode}]; wg = Table[0, {i, nNode}];
w = Table[0, {i, nNode}]; P = Table[0, {i, nNode}];
ks = Table[0, {i, nNode}, {j, n}]; pf = Table[0, {i, m}];
Kp = Table[0, {i, nNode}, {j, nNode}]; Ks = Table[0, {i, nNode}, {j, nNode}];
Fs = Table[0, {i, nNode}, {j, nNode}]; Fs1 = Table[0, {i, sNode}, {j, sNode}];
t = Table[0, {i, m}, {j, n}];
Do[z[[i]] = (d[[i]] + d[[i - 1]]) / 2, {i, 2, m - 1}]; z[[1]] = 0;
z[[m]] = d[[m - 1]]; (* z is depth of nodes from the reference *)
Do[l[[i]] = d[[i]] - d[[i - 1]], {i, 2, m - 1}]; l = Delete[l, m];
As = 2 * π * r0 * l; Ap = π * r0^2; Ab = Ap; Ep = Epm;
If[tp =!= NA, Ap = Ap - π * (r0 - tp)^2; If[ec === oe, Ab = Ap]];
(* Area parameters of pile *)
Do[Do[If[i = j, s[[i, j]] = r0, s[[i, j]] =
    Sqrt[(x[[i]] - x[[j]])^2 + (y[[i]] - y[[j]])^2]], {j, n}], {i, n}];
If[n = 1, ClearAll[x, y]; x = {0}; y = {0}];
```

(* Pile Stiffness *)

```
Do[ kp = Ap * Ep / (z[[i + 1]] - z[[i]]);
  temp3 = (i - 1) * n + 1; temp4 = j; temp5 = n;
  Do[
   Kp[[temp4, temp4]] = Kp[[temp4, temp4]] + kp;
   Kp[[temp4 + temp5, temp4 + temp5]] =
    Kp[[temp4 + temp5, temp4 + temp5]] + kp;
   Kp[[temp4 + temp5, temp4]] = -kp;
   Kp[[temp4, temp4 + temp5]] = -kp,
   {j, temp3, temp3 + n - 1}], {i, m - 1}];
MatrixForm[Kp];
```

(* Initial soil stiffness and limiting frictional load vector *)

```
ρ = 0;
Do[ρ = ρ + gs[[i]] * l[[i]], {i, 2, m - 1}];
α = 1 / (1 + gs[[m - 1]] / gb);
ρ = ρ / lp / gs[[m - 1]];
rm = 2.5 * α * ρ * (1 - meanvs) * lp;
Do[pf[[i]] = fs[[i]] * As[[i]], {i, 2, m - 1}];
```

```
pf[[m]] = Ab * qb;
Do[Do[S[[temp1]] = Sz[[j]]; Do[If[j = m,
     If[jj = jjj, ks[[temp1, jjj]] = (1 / α) * 4 * gb * s[[jj, jjj]] / (1 - νb),
      ks[[temp1, jjj]] = (1 / α) * 2 * π * gb * s[[jj, jjj]] / (1 - νb)],
     ks[[temp1, jjj]] = 2 * π * gs[[j]] * l[[j]] / Log[rm / s[[jj, jjj]]] ],
    {jjj, n}], {jj, n}], {j, 2, m}];
MatrixForm[ks];
```

(* Iterative solution *)

```
Δwc = S / inc;
Do[

  (* Formulation of soil stiffness matrix *)

  wc = i * Δwc;
  Do[Do[Do[If[temp1 = temp2, Fs[[temp1, temp2]] = 1 / (ks[[temp1, jjj]] /
          (1 + Rf * ks[[temp1, jjj]] * Abs[w[[temp1]] / pf[[j]]]) ^ 2),
     Fs[[temp1, temp2]] = 1 / (ks[[temp1, jjj]])],
    {jjj, n}], {jj, n}], {j, 2, m}];
  Do[Do[Fs1[[jj, jjj]] = Fs[[jj + n, jjj + n]], {jjj, sNode}], {jj, sNode}];
  Fs1 = Inverse[Fs1];
  Do[Do[Ks[[jj + n, jjj + n]] = Fs1[[jj, jjj]], {jjj, sNode}], {jj, sNode}];

  (* Calculation of relative settlement *)

  Kg = Ks + Kp; Rhs = Ks.Δwc;
  Δwp = LinearSolve[Kg, Rhs];
  wp = wp + Δwp;
  MatrixForm[w];
  P = Kp.wp;
  Do[Do[If[P[[temp1]] > pf[[j]], P[[temp1]] = pf[[j]]], {jj, n}], {j, m}];
  Do[Do[wg[[temp1]] = 0; Do[If[temp1 ≠ temp2,
      wg[[temp1]] = wg[[temp1]] + Fs[[temp1, temp2]] * P[[temp2]]],
     {jjj, n}], {jj, n}], {j, 2, m}];
  w = wc - wp - wg,
  {i, inc}];
```

(* Processing Output *)

```
df = P;
ClearAll[Ks, Kp, Kg, Fs, Fs1, ks, ps, wbar, pbar, s, S, d, x, y, l];
df = Partition[df, n];
wp = Partition[wp, n]; wp = wp * 1000;
Do[Do[τ[[i, j]] = df[[i, j]] / As[[i]] / 1000, {j, n}], {i, 2, m - 1}];
Do[df[[i]] = df[[i]] + df[[i - 1]], {i, 2, m - 1}]; df = Chop[df / 1000];
zlp = -Delete[z / lp, {{1}, {m}}];
If[n = 9, centre = 5, centre = 13];
```

```
If[n ≠ 1,

 (* Group piles *)

 Print[
  " Results of group piles (3 x 3) with perfectly flexible pile cap"];
 Print["  z(m)    Dragload (kN) : Centre Pile, Side Pile, Corner Pile"];
 Print[MatrixForm[Simplify[z * 1.0]],
  "      "MatrixForm[Transpose[df][[centre]]],
  "      "MatrixForm[Transpose[df][[2]]],
  "      "MatrixForm[Transpose[df][[1]]]];
 Print["  z(m)    Shear Stress (kPa): Centre
    Pile, Side Pile, Corner Pile"];
 Print[MatrixForm[Simplify[z * 1.0]],
  "      "MatrixForm[Transpose[τ][[centre]]],
  "      "MatrixForm[Transpose[τ][[2]]],
  "      "MatrixForm[Transpose[τ][[1]]]];
 Print["  z(m)    Downdrag (mm): Centre Pile, Side Pile, Corner Pile"];
 Print[MatrixForm[Simplify[z * 1.0]],
  "       ", MatrixForm[Transpose[wp][[centre]]],
  "       ", MatrixForm[Transpose[wp][[2]]],
  "       ", MatrixForm[Transpose[wp][[1]]]];
 dfa = Transpose[df][[centre]]; dfa = Delete[dfa, {{1}, {m}}];
 dfga = Transpose[{dfa, zlp}];
 dfb = Transpose[df][[2]]; dfb = Delete[dfb, {{1}, {m}}];
 dfgb = Transpose[{dfb, zlp}];
 dfc = Transpose[df][[1]]; dfc = Delete[dfc, {{1}, {m}}];
 dfgc = Transpose[{dfc, zlp}];
 τa = Transpose[τ][[centre]]; τa = Delete[τa, {{1}, {m}}];
 τga = Transpose[{τa, zlp}];
 τb = Transpose[τ][[2]]; τb = Delete[τb, {{1}, {m}}];
 τgb = Transpose[{τb, zlp}];
 τc = Transpose[τ][[1]]; τc = Delete[τc, {{1}, {m}}];
 τgc = Transpose[{τc, zlp}];
 Print["Shearing Stress along Depth"];
 MultipleListPlot[τga, τgb, τgc, PlotLegend→
   {"Centre Pile", "Side Pile", "Corner Pile"}, PlotJoined→True];
 Print["Dragload along Depth"];
 MultipleListPlot[dfga, dfgb, dfgc, PlotLegend→
   {"Centre Pile", "Side Pile", "Corner Pile"}, PlotJoined→True],

 (* Single pile *)

 Print["Results of single pile"];
 Print["   z(m)     Dragload(kN)   Downdrag(mm)  Shear Stress(kPa)"];
 Print[MatrixForm[z * 1.0], "      ", MatrixForm[df],
  "      ", MatrixForm[wp], "      ", MatrixForm[τ]];
 MatrixForm[df];
 τ = Delete[Flatten[τ], {{1}, {m}}];
 τs = Transpose[Partition[Join[τ, zlp], m - 2]];
 df = Delete[Flatten[df], {{1}, {m}}];
```

```
dfs = Transpose[Partition[Join[df, zlp], m - 2]];
Print["Shearing Stress along Depth"];
MultipleListPlot[τs, PlotLegend → "τs", PlotJoined → True];
Print["Dragload along Depth"];
MultipleListPlot[dfs, PlotLegend → "dls", PlotJoined → True];
]
```

(* Output *)

Results of group piles (3 x 3) with perfectly flexible pile cap

z(m) Dragload (kN) : Centre Pile, Side Pile, Corner Pile

z(m)	Centre Pile	Side Pile	Corner Pile
0	0	0	0
1.	172.473	172.473	172.473
3.5	343.531	348.353	352.189
6.5	497.936	511.619	522.15
9.5	598.272	629.5	652.652
12.5	637.366	688.01	725.955
16.	651.151	709.582	757.758
20.	594.989	641.245	678.714
23.	510.225	534.393	554.638
24.	-515.056	-540.334	-561.68

z(m) Shear Stress (kPa): Centre Pile, Side Pile, Corner Pile

z(m)	Centre Pile	Side Pile	Corner Pile
0	0	0	0
1.	45.	45.	45.
3.5	29.7537	30.5924	31.2598
6.5	26.8572	28.3986	29.5629
9.5	17.4524	20.5041	22.6994
12.5	6.79999	10.1773	12.7504
16.	1.79841	2.81417	4.1488
20.	-7.32672	-8.91499	-10.3116
23.	-22.1156	-27.8787	-32.3727
24.	0	0	0

z(m) Downdrag (mm): Centre Pile, Side Pile, Corner Pile

z(m)	Centre Pile	Side Pile	Corner Pile
0	5.62332	5.73425	5.81785
1.	5.62332	5.73425	5.81785
3.5	5.49965	5.60981	5.69264
6.5	5.20809	5.31328	5.39198
9.5	4.78729	4.88011	4.94907
12.5	4.28252	4.34827	4.39693
16.	3.65544	3.67066	3.68119
20.	2.9234	2.87217	2.82772
23.	2.42138	2.3305	2.25376
24.	2.27768	2.17976	2.09706

Shearing Stress along Depth

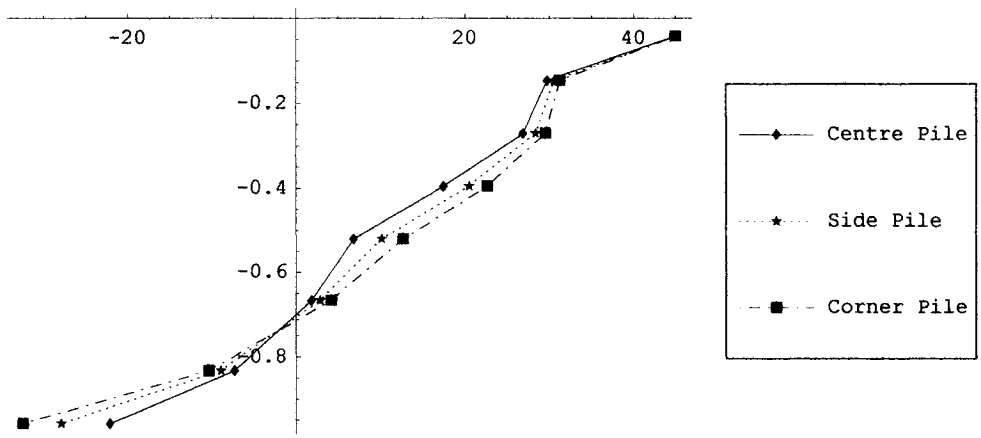

Dragload along Depth